

A Closer Look at Some Gas-Phase Depletions in the ISM:
 Trends for O, Ge and Kr vs. F_* , $f(\text{H}_2)$, and Starlight Intensity*

EDWARD B. JENKINS¹

¹*Princeton University Observatory
 Princeton, NJ 08544-1001*

ABSTRACT

In a survey of archived ultraviolet spectra of 100 stars recorded by the echelle spectrograph of the Space Telescope Imaging Spectrograph (STIS) on the Hubble Space Telescope (HST), we measure the strengths of the weak absorption features of O I, Ge II and Kr I in the interstellar medium. Our objective is to undertake an investigation that goes beyond earlier abundance studies to see how these elements are influenced independently by three different environmental properties: (1) values of a generalized atomic depletion factor F_* due to condensations onto dust grains (revealed here by the abundances of Mg and Mn relative to H), (2) the fraction of H atoms in the form of H_2 $f(\text{H}_2)$, and (3) the ambient intensity I of ultraviolet starlight relative to an average value in our part of the Galaxy I_0 . As expected, the gas-phase abundances of all three elements exhibit negative partial correlations with F_* . The abundances of free O atoms show significant positive partial correlations with $\log f(\text{H}_2)$ and $\log(I/I_0)$, while Ge and Kr exhibit negative partial correlations with $\log(I/I_0)$ at marginal levels of significance. After correcting for these trends, the abundances of O relative to H show no significant variations with location, except for the already-known radial gradient of light-element abundances in the Milky Way. A comparison of Ge and O abundances revealed no significant regional enhancements or deficiencies of neutron-capture elements relative to α -process ones.

Keywords: dust — ISM: abundances — ISM: atoms — ultraviolet: ISM

1. BACKGROUND

From studies of interstellar absorption lines in the UV spectra of stars in our region of the Galaxy, it is well established that interstellar dust sequesters into solid form much of the available interstellar gas atoms for elements heavier than helium, and these atomic depletions, some of which are profound for some elements, offer addi-

ebj@astro.princeton.edu

* Based on observations with the NASA/ESA Hubble Space Telescope obtained from the Data Archive at the Space Telescope Science Institute, which is operated by the Associations of Universities for Research in Astronomy, Incorporated, under NASA contract NAS5-26555. ©2019. The American Astronomical Society. All rights reserved.

tional insights on the elemental composition and relative amounts of the dust (Savage & Sembach 1996). In broadest terms, we know that the severity of element depletions is related to two factors: (1) elements that can form highly stable, refractory compounds experience the strongest depletions, and (2) depletions appear to increase for regions that have high gas densities, indicating that the growth and destruction of grains depend on the local gas environments.

To understand better variations in the amounts of dust grains and their composition, we consider a logarithmic depletion factor for any element X from the gas phase,

$$[X_{\text{gas}}/\text{H}] = \log \left(\frac{N(X)}{N(\text{H I}) + 2N(\text{H}_2)} \right)_{\text{obs}} - \log \left(\frac{X}{\text{H}} \right)_{\text{ref}}, \quad (1)$$

where $N(X)$ is the column density of the preferred ionization stage of element X , and the reference abundance ratio $(X/\text{H})_{\text{ref}}$ can apply to either B-type stars (Nieva & Przybilla 2012) or the Sun (Asplund et al. 2009).

In a study aimed at improving our understanding of such depletions, Jenkins (2009, hereafter J09) devised a unified interpretation for 17 different elements reported in more than 100 papers that covered 243 sight lines to different stars. His interpretation made use of an empirically determined principle that, from one region to the next, the logarithmic strengths of depletions of different elements followed one another in a linear fashion, and this behavior could be characterized with good accuracy in terms of a few simple coefficients. First, the overall severity of depletions for any sight line could be collectively characterized by a single scale factor, which he designated as F_* . According to this construction, any element X responds to changes in F_* in a manner that could be described by three coefficients unique to this element through the equation

$$[X_{\text{gas}}/\text{H}] = B_X + A_X(F_* - z_X), \quad (2)$$

where the constants B_X , A_X , and z_X are unique to each element X .¹ It follows that if all of the missing atoms are sequestered into solid form (or free molecules), their abundances relative to hydrogen are given by

$$(X_{\text{dust}}/\text{H}) = (X/\text{H})_{\text{ref}}(1 - 10^{[X_{\text{gas}}/\text{H}]}) . \quad (3)$$

Equations 2 and 3 assign absolute values for the depletions and dust abundances, but they rely on the reference abundances $\log(X/\text{H})_{\text{ref}}$ in Eq. 1 being correct. One can instead focus on differential changes as atoms accumulate in (or depart from) solid forms using the relationship

$$\begin{aligned} d(X_{\text{dust}}/\text{H})/dF_* &= -(\ln 10)(X/\text{H})_{\text{ref}}A_X 10^{B_X + A_X(F_* - z_X)} \\ &= -(\ln 10)A_X(X_{\text{gas}}/\text{H})_{F_*}, \end{aligned} \quad (4)$$

¹ The offset quantity z_X may seem superfluous for a linear equation that needs only two coefficients, but its use is intended to make the covariances in the errors for A_X and B_X equal to zero, which then simplifies the derivations of uncertainties of any relationships that make use of A_X and B_X .

which depends only on the how rapidly the depletions change with F_* (through the slope coefficient A_X) and the measured interstellar medium (ISM) abundance relative to hydrogen at a given value of F_* .

The present study is motivated by two puzzling conclusions that emerged from the depletion analysis reported in J09. The depletions of oxygen and krypton appeared to exceed what one might have expected, as will be outlined in the following subsections. We now hope to gain new insights by enlarging the sample of sight lines and studying how the abundances of O and Kr relate not only to F_* but also to other interstellar gas parameters such as the molecular hydrogen fraction $f(\text{H}_2) = 2N(\text{H}_2)/[2N(\text{H}_2) + N(\text{H I})]$ and the intensity of starlight in the ultraviolet. Another quantity that may seem relevant is the average volume density of hydrogen along a sight line $\langle n_{\text{H}} \rangle = N(\text{H})/d$, where d is the distance to the star. Many studies have shown that $\langle n_{\text{H}} \rangle$ correlates strongly with the strengths of depletions for those elements that are strongly depleted (Savage & Bohlin 1979 ; Harris et al. 1984 ; Murray et al. 1984 ; Gondhalekar 1985 ; Jenkins et al. 1986 ; Jenkins 1987 ; Welsh et al. 1997 ; Snow et al. 2002 ; Cartledge et al. 2004, 2006 ; Jensen & Snow 2007b, 2007a). We are not surprised to find that the quantities F_* and $\langle n_{\text{H}} \rangle$ are strongly correlated with each other (see Fig. 16 of J09). In making a choice between these two parameters, we regard F_* to be a more direct indicator of the maturity of the depletion process in any given sight line.

1.1. *The Problem with Oxygen*

Cartledge et al. (2004) found that $[\text{O}_{\text{gas}}/\text{H}]$ showed a weak but convincing downward trend with increasing values of $\langle n(\text{H}) \rangle$. From a qualitative perspective, this is not surprising since $\langle n(\text{H}) \rangle$ is strongly correlated with F_* , and the relative concentrations of oxygen-bearing compounds such as silicates and oxides should increase with greater values of F_* . However, as recognized by J09, quantitatively speaking the depletion of gas-phase oxygen is surprisingly strong. For instance, for a representative sight line with strong depletions (at $F_* = 1$), we can use the coefficients in J09 and Eq. 3 to arrive at a value $(\text{O}_{\text{dust}}/\text{H}) = 241$ parts per million (ppm) if $(\text{O}/\text{H})_{\text{ref}} = 575$ ppm is taken from B-star abundances (Nieva & Przybilla 2012).² This value for $(\text{O}_{\text{dust}}/\text{H})$ is substantially larger than 170 ppm taken from the corresponding sum of the dust abundances of 113 ppm for Mg, Si, and Fe multiplied by the largest plausible ratio of 1.5 for O for the most favorable combination of silicate and oxide compounds, MgSiO_3 plus Fe_2O_3 (Cardelli et al. 1996 ; Whittet 2010). The disparity between $(\text{O}_{\text{dust}}/\text{H}) = 241$ ppm and that consumed by silicates and oxides has created a challenge for explaining where some of the oxygen atoms are sequestered (Whittet 2010 ; Wang et al. 2015).

² The B-star reference abundance adopted here happens to be the same as the one adopted by J09, which was based on the present-day solar photospheric abundance $\log(\text{O}/\text{H})_{\odot} + 12 = 8.69$ recommended by Lodders (2003) plus her +0.07 dex correction for gravitational settling to arrive at a protosolar abundance. If such a correction were applied to some more recent measurements of the present-day solar photospheric O abundance of approximately 8.77 by Ayres et al. (2013) and Steffen et al. (2015), B_{O} would revert to a value of -0.225 , $(\text{O}/\text{H})_{\text{ref}} = 690$ ppm, and then an application of Eqs. 2 and 3 for $F_* = 1$ would yield $(\text{O}_{\text{dust}}/\text{H}) = 356$ ppm.

A contrasting view was presented by Voshchinnikov & Henning (2010). They claimed that a large fraction of their determinations of $(\text{O}_{\text{dust}}/\text{H})$ came out to be considerably lower than 170 ppm, and they argued that there was no problem in accounting for all of the O being incorporated into silicates. However, they adopted a value $(\text{O}/\text{H})_{\text{ref}} = 490$ ppm, and this reduced value affects both of the major terms on the right-hand side of Eq. 3 to create a prediction for a removal of only 155 ppm with the J09 coefficients at $F_* = 1$.

If one distrusts the reference abundances, one can resort to comparing the differential depletions of O and Si+Mg+Fe through the use of Eq. 4. At $F_* = 0$ the quantity $d(\text{O}_{\text{dust}}/\text{H})/dF_*$ divided by $d(\text{Mg}_{\text{dust}} + \text{Si}_{\text{dust}} + \text{Fe}_{\text{dust}}/\text{H})/dF_*$ equals 2.30, which to within the uncertainties is acceptable for O being incorporated into silicates and oxides. However, the ratio increases to 16 at $F_* = 1$, which indicates that in dense regions with strong depletions O must bind to some other element that has a high abundance (or to itself in the form of O_2). Clues on what processes may facilitate the removal of gas-phase O could emerge from a more comprehensive comparison of oxygen abundances with factors other than just F_* .

1.2. *The Problem with Krypton*

Superficially, one might expect krypton to be an element that is unlikely to show any depletions. It is a noble gas that is chemically inert because its outer valence shell of electrons is filled. Its van der Waals binding with neutral systems is extremely weak and easily disrupted. From these two perspectives, it may seem puzzling that the strengths of absorption features of this element’s dominant ionization state, Kr I, indicated an apparent, almost universal deficiency (~ 0.3 dex) of gas-phase Kr (Cardelli & Meyer 1997 ; Cartledge et al. 2003, 2008 ; Ritchey et al. 2018) when compared to its reference abundance relative to hydrogen. A link between Kr depletions and the relative concentrations of solid materials in the ISM was established later by J09, who found that Kr depletions appeared to become more severe with increasing values of F_* (i.e., $A_{\text{Kr}} = -0.166$, but with an uncertainty of 0.103). The statistical significance of this trend was improved in the more recent investigation by Ritchey et al. (2018) in their study of the interstellar abundances of r -process elements.

In a related development, there evolved an awareness that an acid-resistant residue of some primitive meteorites, known as phase Q,³ was shown to have significant concentrations of noble gases, with fractionations favoring the retention of heavier elements (Schelhaas et al. 1990 ; Amari et al. 2013) . Laboratory experiments designed to explore this issue indicated that noble gases can be made to bind to certain compounds found in meteoritic materials (Amberg et al. 1955 ; Yang & Anders 1982a, 1982b ; Yang et al. 1982 ; Wacker 1989 ; Marrocchi et al. 2005).

³ Q stands for quintessence, a designation originated by Lewis et al. (1975). This phase typically composes less than 0.04% of the mass of a meteorite.

There has also evolved a recognition that free noble gas atoms could bind to positive ions and charged molecular complexes (Holloway 1968 ; Wyatt et al. 1975). Within the contexts of the ISM and protoplanetary disks, the most prominent possibilities are the couplings with the partners H^+ , H_2^+ , and H_3^+ (Pauzat & Ellinger 2007 ; Pauzat et al. 2009 ; Theis et al. 2015). Indeed, emission and absorption features arising from interstellar ArH^+ have been detected in spectra recorded by instruments on the *Herschel* mission (Barlow et al. 2013 ; Schilke et al. 2014). Nevertheless, the concentrations of ArH^+ are small compared to the total abundances of Ar. Dissociative recombinations with free electrons are likely to strongly inhibit any accumulations of these complexes by amounts that could cause significant depletions of the atomic forms of noble gases. Electron fractions $n(e)/N(\text{H}_{\text{tot}}) \approx 3 \times 10^{-4}$ and typical destruction reaction rate constants of order $10^{-7} \text{cm}^3 \text{s}^{-1}$ (Mitchell 1990)⁴ make it doubtful that appreciable amounts of Kr can be bound in charged molecular complexes.

Two other considerations may be factored into the krypton abundance findings. One is that there might exist a real change in the overall abundance of Kr from one region to another, as proposed by Cartledge et al. (2008). The other possibility is that if the Kr and H are exposed to ionizing radiation with a sufficiently high energy to penetrate the mostly neutral hydrogen, the Kr could be more strongly ionized than H because its ionization cross section just above its threshold energy (14 eV) is much higher than that of H by about one order of magnitude (Sterling 2011). As a result, the apparent $(\text{Kr}_{\text{gas}}/\text{H})$ would be lowered, much as what one sees with the ratio of Ar I to O I in the low-density, partly ionized medium (Jenkins 2013).

2. INVESTIGATION STRATEGY

2.1. Basic Design

Ultraviolet spectra of stars observed using the echelle spectrographs of the Goddard High Resolution Spectrograph (GHRS) and the Space Telescope Imaging Spectrograph (STIS) on the *Hubble Space Telescope* (HST) have enabled observations for the investigation of interstellar atomic abundances, including those of O and Kr. There have been many publications of results for these two elements, and references to these works are listed in Table 1 of J09.⁵ Since the time of the latest of these publications, many new spectra have been recorded using the STIS echelle spectrograph in the medium- and high-resolution modes. The new spectra were acquired after the repair of STIS during the Fourth Servicing Mission (SM4) for *HST* in 2009, and they allow us to increase the number of samples. So that we can maintain a uniform approach for interpreting the absorption features, none of the previously reported measurements of column densities are incorporated in the present study; all of the outcomes given here are based on an original analysis using a set of rules applied in a consistent manner throughout all cases.

⁴ One exception is the rate for $\text{ArH}^+ + e \rightarrow \text{Ar} + \text{H}$, which is $< 10^{-9} \text{cm}^3 \text{s}^{-1}$ (Mitchell et al. 2005).

⁵ More recent measurements have been carried out by Ritchey et al. (2018).

A particularly large volume of the STIS echelle spectra cover the wavelength region from 1170 to 1372 Å, which includes transitions of O I, Mg II, Mn II, Kr I, and Ge II. These spectra are available from the *Mikulsky Archive for Space Telescopes* (MAST). Except for Kr, whose absorption is securely detected in only about half of the sight lines, the transitions for these elements are strong enough to measure with reasonable accuracy, but not so strong that saturation effects seriously compromise the derivations of column densities. The strongly depleted elements Mg and Mn allow us to determine F_* after their abundances are compared to those of atomic and molecular hydrogen. While O and Kr are the main focus of this investigation, we also consider abundances of Ge to check on whether or not enhancements or deficiencies of this element might signify variations in the total abundances of neutron capture elements from one location to the next, as suggested by Kr data analyzed by Cartledge et al. (2008). Ge is also a mildly depleted element whose correlation behaviors can be instructive when comparing them with those of O and Kr.

The remainder of this section and the one that follows describe how target stars and atomic transitions were selected and how the absorption features were analyzed. Tables 4 and 5 in Section 3 present the column density outcomes, and the more detailed measurement results appear in Table 7 in the appendix of this paper. Sections 4 and 5 describe the derivations of F_* and starlight intensity parameters, respectively. Section 6 describes some analyses of the depletion trends, followed by Section 7 that interprets them. Finally, Section 8 describes two investigations that attempted to reveal regional changes in abundances after correcting for the local environmental conditions that we identified earlier.

2.2. Selection of Target Stars

The first step to identify candidate spectral exposures was to collect all STIS E140H and E140M observations of stars listed as of 2016 in the Planned and Archived Exposures Catalog (PAEC) maintained by the Space Telescope Science Institute (STScI). By examining the quick-look preview displays in MAST and checking spectral types in the Simbad database, useful observations were identified that satisfied all of the following criteria:

1. The spectrum did not suffer from confusion arising from narrow stellar lines (E140M spectra are less tolerant for such confusion than those taken with E140H). The spectrum must also have had a respectable signal-to-noise ratio. (17 stars had no preview spectra available, so they were excluded in the selection process.)
2. The strengths of the two Mg II lines (see Fig. 1) are used to indicate that there is a sufficient amount of interstellar gas to make a meaningful determination of the fractional abundance of Kr. We do not exclude cases where the Kr I lines themselves are too weak to see, since the resulting upper limits for $N(\text{Kr I})$ could signify a large and interesting deficiency.

3. Stars of spectral type later than B3 were excluded, since the strong stellar Ly α feature prevents one from determining $N(\text{H I})$. Initially, stars with temperatures corresponding to the B2 and B3 were deemed acceptable if their $E(B-V)$ values were of order or greater than 0.2, since the interstellar H I absorption could dominate over the stellar feature. In later stages of selection, stars that had corrections for stellar features (described in Section 3.2) that were larger than the apparent value of $\log N(\text{H I}) - 0.5$ were excluded. Stars B1 and earlier are acceptable, but some luminous stars with strong N V P Cygni absorptions depressed the flux at 1236 Å to too low a level to see any Kr I absorption.
4. The star must have had a spectrum covering the region containing H₂ lines (at around 1100 Å and shortward) available from the MAST archive of observations by the *Far Ultraviolet Spectroscopic Explorer* (FUSE). However, a few exceptions are noted in Table 7.

The properties of the stars considered in this survey are summarized in Table 1. Except for the entries in Columns 10 and 11, which will be explained later, the meaning of the listed quantities should be self-evident. Stars with spectra in the archive that survived the initial screening but that were later rejected are listed in Table 2. Most of these rejections were based on our inability to obtain satisfactory corrections for the effects of the stellar Ly α absorption features.

Table 1. Stellar and Interstellar Medium Data

Target	Galactic Coordinates		d	Source ^a	z	Magnitudes		$E(B-V)$	Depletion	Starlight	Spectral
Star	ℓ	b	(kpc)	for d	(kpc)	B	V	(mag)	Strength F_* ^b	I/I_0 ^c	Type
(1)	(2)	(3)	(4)	(5)	(6)	(7)	(8)	(9)	(10)	(11)	(12)
BD+35 4258	77.19	−4.74	2.9	2	−0.2	9.42	9.46	0.22	0.38 ± 0.06	...	B0.5 Vn
BD+53 2820	101.24	−1.69	5.1	2	−0.1	10.02	9.96	0.28	0.44 ± 0.07	...	B0 IV:n
CPD-59 2603	287.59	−0.69	3.5	1	−0.0	8.93	8.75	0.43	0.51 ± 0.05	0.31	O7 Vf
CPD-59 4552	303.22	2.47	2.0	4	0.08	8.337	8.24	0.31	0.40 ± 0.05	...	B1 III
CPD-69 1743	303.71	−7.35	5.5	2	−0.7	9.43	9.46	0.19	0.40 ± 0.07	...	B0.5 III:n
HD108	117.93	1.25	3.8	1	0.08	7.58	7.40	0.42	0.53 ± 0.04	0.30	O6 pe
HD1383	119.02	−0.89	2.9	2	−0.0	7.89	7.63	0.37	0.48 ± 0.05	0.27	B1 II
HD3827	120.79	−23.2	1.8	4	−0.7	7.76	7.95	0.05	0.41 ± 0.07	0.16	B0.7 Vn
HD12323	132.91	−5.87	4.4	1	−0.4	8.87	8.92	0.23	0.51 ± 0.05	...	O9 V
HD13268	133.96	−4.99	2.1	1	−0.1	8.24	8.18	0.35	0.45 ± 0.07	...	O8 Vnn

Table 1 continued on next page

Table 1 (*continued*)

Target	Galactic Coordinates		d	Source ^a	z	Magnitudes		$E(B - V)$	Depletion	Starlight	Spectral
Star	ℓ	b	(kpc)	for d	(kpc)	B	V	(mag)	Strength F_* ^b	I/I_0 ^c	Type
(1)	(2)	(3)	(4)	(5)	(6)	(7)	(8)	(9)	(10)	(11)	(12)
HD13745	134.58	-4.96	3.2	1	-0.2	7.99	7.90	0.34	0.55 ± 0.05	...	O9.7 II _n
HD13841	134.38	-3.93	2.9	4	-0.2	7.60	7.37	0.33	0.58 ± 0.07	...	B1.5Ib
HD14818	135.62	-3.93	2.8	4	-0.1	6.56	6.26	0.37	0.39 ± 0.07	...	B2 Ia
HD15137	137.46	-7.58	3.5	1	-0.4	7.92	7.86	0.24	0.36 ± 0.06	0.32	O9.5 II-III _n
HD25443	143.68	7.35	1.1	4	0.14	6.998	6.76	0.44	0.72 ± 0.05	...	B0.5 III
HD35914	215.21	-24.2	5.4	4	-2.2	9.78	13.0	0.37	0.46 ± 0.06	...	O7fp
HD40893	180.09	4.34	3.1	2	0.23	9.05	8.99	0.31	0.58 ± 0.04	0.37	B0 IV
HD41161	164.97	12.89	1.4	1	0.31	6.658	6.76	0.19	0.35 ± 0.04	...	O8 V _n
HD46223	206.44	-2.07	2.1	4	-0.0	7.50	7.28	0.44	0.86 ± 0.03	...	O4 Vf
HD52266	219.13	-0.68	1.8	2	-0.0	7.22	7.23	0.22	0.56 ± 0.05	0.48	O9 IV _n
HD53975	225.68	-2.32	1.4	2	-0.0	6.40	6.50	0.16	0.38 ± 0.03	...	O7.5 V
HD63005	242.47	-0.93	5.4	1	-0.0	9.12	9.13	0.22	0.68 ± 0.04	...	O6 Vf
HD66788	245.43	2.05	4.3	1	0.15	9.35	9.43	0.20	0.55 ± 0.04	...	O9 V
HD69106	254.52	-1.33	1.5	1	-0.0	7.020	7.13	0.14	0.56 ± 0.04	0.45	B0.5 IV _{nn}
HD72648	262.23	-2.48	3.8	4	-0.1	7.75	7.62	0.21	0.83 ± 0.08	...	B1 Ib
HD75309	265.86	-1.90	2.9	1	-0.1	7.82	7.84	0.18	0.58 ± 0.04	0.46	B1 IIp
HD88115	285.32	-5.53	3.7	1	-0.3	8.26	8.31	0.12	0.39 ± 0.08	0.51	B1.5 I _{in}
HD89137	279.69	4.45	3.1	1	0.24	7.93	7.97	0.17	0.45 ± 0.04	...	O9.7 IIInp
HD90087	285.16	-2.13	2.8	1	-0.1	7.80	7.80	0.22	0.36 ± 0.07	...	O9 III _n
HD91824	285.70	0.07	3.0	2	0.00	8.09	8.15	0.22	0.33 ± 0.04	0.78	O7 V
HD91983	285.88	0.05	3.0	2	0.00	8.62	8.58	0.14	0.31 ± 0.05	0.51	B1 III
HD92554	287.60	-2.02	6.9	1	-0.2	9.60	9.50	0.34	0.15 ± 0.10	...	O9.5 II _n
HD93129	287.41	-0.57	2.8	1	-0.0	7.06	6.90	0.46	0.49 ± 0.05	...	O2 If
HD93205	287.57	-0.71	3.3	1	-0.0	7.80	7.75	0.44	0.33 ± 0.05	0.58	O3 Vf
HD93222	287.74	-1.02	3.6	1	-0.0	8.15	8.10	0.32	0.33 ± 0.04	0.82	O7 III _f
HD93843	288.24	-0.90	3.5	1	-0.0	7.29	7.33	0.24	0.50 ± 0.04	0.66	O5 III _f
HD94493	289.01	-1.18	3.4	1	-0.0	7.27	7.27	0.15	0.32 ± 0.05	0.49	B1 Ib
HD97175	294.53	-9.17	3.9	4	-0.6	8.79	8.87	0.16	0.49 ± 0.05	...	B0.5 III
HD99857	294.78	-4.94	3.5	1	-0.3	7.68	7.47	0.27	0.45 ± 0.05	0.55	B0.5 Ib
HD99890	291.75	4.43	3.5	1	0.27	8.23	8.31	0.15	0.16 ± 0.05	...	B0 III _n
HD99953	293.93	-2.13	3.0	4	-0.1	6.88	6.57	0.39	0.67 ± 0.06	...	B2 Ia
HD100199	293.94	-1.49	3.3	1	-0.0	8.147	8.17	0.19	0.41 ± 0.09	...	B0 III _{ne}
HD101190	294.78	-1.49	2.1	1	-0.0	7.37	7.33	0.30	0.51 ± 0.05	...	O6 Vf
HD103779	296.85	-1.02	4.3	2	-0.0	7.185	7.22	0.17	0.29 ± 0.05	0.33	B0.5 Iab
HD104705	297.45	-0.34	5.0	1	-0.0	7.78	7.83	0.17	0.40 ± 0.05	0.53	B0 Ib
HD108639	300.22	1.95	2.4	2	0.08	7.89	7.81	0.26	0.34 ± 0.04	0.55	B0.2 III
HD109399	301.71	-9.88	2.9	2	-0.5	7.67	7.67	0.19	0.44 ± 0.05	0.59	B0.7 II
HD111934	303.20	2.51	2.3	2	0.10	7.12	6.92	0.32	0.33 ± 0.10	0.63	B1.5 Ib
HD114886	305.52	-0.83	1.8	2	-0.0	6.98	6.89	0.32	0.47 ± 0.05	0.37	O9 III _n
HD115071	305.76	0.15	2.7	2	0.00	8.13	7.97	0.40	0.50 ± 0.06	0.74	B0.5 V _n
HD115455	306.06	0.22	2.6	1	0.01	8.17	7.97	0.40	0.41 ± 0.06	0.58	O7.5 III
HD116781	307.05	-0.07	2.2	1	-0.0	7.74	7.62	0.31	0.51 ± 0.04	0.47	B0 III _{ne}
HD116852	304.88	-16.1	4.5	2	-1.2	8.38	8.47	0.14	0.48 ± 0.04	0.80	O9 III

Table 1 continued on next page

Table 1 (*continued*)

Target	Galactic Coordinates		d	Source ^a	z	Magnitudes		$E(B - V)$	Depletion	Starlight	Spectral
Star	ℓ	b	(kpc)	for d	(kpc)	B	V	(mag)	Strength F_* ^b	I/I_0 ^c	Type
(1)	(2)	(3)	(4)	(5)	(6)	(7)	(8)	(9)	(10)	(11)	(12)
HD122879	312.26	1.79	3.3	1	0.10	6.64	6.50	0.29	0.51 ± 0.04	0.49	B0 Ia
HD124314	312.67	-0.42	1.4	1	-0.0	6.85	6.64	0.43	0.47 ± 0.05	0.58	O6 Vnf
HD124979	316.40	9.08	2.8	1	0.44	8.61	8.51	0.30	0.46 ± 0.07	...	O8 Vf
HD137595	336.72	18.86	0.50	2	0.16	7.52	7.49	0.18	0.85 ± 0.05	...	B3 Vn
HD144965	339.04	8.42	0.51	2	0.07	7.206	7.11	0.27	1.07 ± 0.09	0.76	B2 Vne
HD147888	353.65	17.71	0.12	2	0.03	7.05	6.74	0.42	1.15 ± 0.12	1.20	B3 V
HD148422	329.92	-5.60	10	1	-0.9	8.69	8.64	0.23	0.21 ± 0.09	...	B1 Ia
HD148937	336.37	-0.22	1.2	4	-0.0	7.12	6.71	0.52	0.56 ± 0.07	0.67	O6 fp
HD151805	343.20	1.59	6.0	1	0.17	9.01	9.01	0.19	0.54 ± 0.04	...	B1 Ib
HD152249	343.45	1.16	2.1	4	0.04	6.65	6.45	0.42	0.45 ± 0.06	...	O9 Iab
HD152424	343.36	0.89	2.1	4	0.03	6.69	6.27	0.57	0.66 ± 0.06	...	O9.2 Ia
HD152590	344.84	1.83	3.6	2	0.11	8.56	8.48	0.37	0.52 ± 0.05	0.77	O7 V
HD156359	328.68	-14.5	17	4	-4.2	9.52	9.72	0.06	0.24 ± 0.09	...	B0 Ia
HD163522	349.57	-9.09	9.9	2	-1.5	8.43	8.43	0.16	0.34 ± 0.08	...	B1 Ia
HD165246	6.40	-1.56	1.9	2	-0.0	7.70	7.60	0.33	0.78 ± 0.04	0.79	O8 Vn
HD167402	2.26	-6.39	7.0	3	-0.7	8.94	8.95	0.21	0.25 ± 0.07	...	B0 II/B0.5 Ib
HD168941	5.82	-6.31	7.8	2	-0.8	9.36	9.37	0.24	0.68 ± 0.06	...	O9.5 IIp
HD170740	21.06	-0.53	0.28	2	-0.0	5.96	5.72	0.38	0.87 ± 0.09	...	B2 IV-V
HD177989	17.81	-11.8	6.0	1	-1.2	9.22	9.34	0.11	0.66 ± 0.05	0.35	B0 III
HD178487	25.78	-8.56	5.7	1	-0.8	8.78	8.69	0.29	0.74 ± 0.07	...	B0.5 Ib
HD179407	24.02	-10.4	9.2	2	-1.6	9.44	9.44	0.23	0.63 ± 0.09	...	B0.5 Ib
HD185418	53.60	-2.17	1.2	1	-0.0	7.639	7.49	0.38	0.74 ± 0.04	0.23	B0.5 V
HD191877	61.57	-6.45	2.3	1	-0.2	6.217	6.27	0.14	0.53 ± 0.05	...	B1 Ib
HD192035	83.33	7.76	2.7	1	0.36	8.26	8.22	0.28	0.74 ± 0.07	...	B0 III-IVn
HD195455	20.27	-32.1	5.8	2	-3.0	9.02	9.20	0.07	0.39 ± 0.07	...	B0.5 III
HD195965	85.71	5.00	1.1	1	0.10	6.899	6.97	0.19	0.45 ± 0.05	0.32	B0 V
HD198478	85.75	1.49	1.3	2	0.03	5.28	4.86	0.43	0.75 ± 0.14	0.43	B3 Ia
HD198781	99.94	12.61	0.69	2	0.15	6.472	6.45	0.26	0.79 ± 0.05	0.37	B0.5 V
HD201345	78.44	-9.54	2.2	1	-0.3	7.611	7.76	0.14	0.34 ± 0.06	0.32	O9 V
HD202347	88.22	-2.08	1.0	1	-0.0	7.41	7.50	0.11	0.66 ± 0.08	0.20	B1.5 V
HD203374	100.51	8.62	0.34	2	0.05	6.908	6.67	0.43	0.66 ± 0.04	0.31	B2 Vne
HD206267	99.29	3.74	0.86	2	0.05	5.83	5.62	0.45	0.80 ± 0.05	0.30	O6.5 V
HD206773	99.80	3.62	0.82	2	0.05	7.10	6.87	0.39	0.60 ± 0.04	0.19	B0 V:nnep
HD207198	103.14	6.99	1.3	1	0.16	6.25	5.94	0.47	0.80 ± 0.05	0.20	O9.5 Ib-II
HD207308	103.11	6.82	1.2	2	0.14	7.74	7.49	0.44	0.82 ± 0.05	...	B0.7 III-IV(n)
HD207538	101.60	4.67	0.94	2	0.07	7.55	7.30	0.51	0.85 ± 0.05	...	O9.5 V
HD208440	104.03	6.44	1.1	2	0.12	7.93	7.91	0.27	0.65 ± 0.05	0.35	B1 V
HD209339	104.58	5.87	1.2	2	0.12	6.733	6.73	0.24	0.50 ± 0.05	0.34	B0 IV
HD210809	99.85	-3.13	4.3	1	-0.2	7.61	7.56	0.28	0.31 ± 0.06	0.29	O9 Iab
HD210839	103.83	2.61	1.1	1	0.05	5.29	5.05	0.49	0.78 ± 0.04	0.47	O6 Infp
HD218915	108.06	-6.89	5.0	1	-0.6	7.22	7.20	0.21	0.39 ± 0.06	0.33	O9.5 Iabe
HD219188	83.03	-50.1	2.1	2	-1.6	6.90	7.06	0.09	0.37 ± 0.06	0.01	B0.5 IIIIn
HD220057	112.13	0.21	0.77	2	0.00	6.948	6.94	0.17	0.69 ± 0.13	0.35	B3 IV

Table 1 continued on next page

Table 1 (*continued*)

Target	Galactic Coordinates		d	Source ^a	z	Magnitudes		$E(B - V)$	Depletion	Starlight	Spectral
Star	ℓ	b	(kpc)	for d	(kpc)	B	V	(mag)	Strength F_* ^b	I/I_0 ^c	Type
(1)	(2)	(3)	(4)	(5)	(6)	(7)	(8)	(9)	(10)	(11)	(12)
HD224151	115.44	−4.64	1.3	2	−0.1	6.21	6.00	0.34	0.49 ± 0.05	0.16	B0.5 II-III
HDE232522	130.70	−6.71	6.1	1	−0.7	8.65	8.70	0.14	0.41 ± 0.04	0.35	B1 II
HDE303308	287.59	−0.61	3.8	1	−0.0	8.30	8.17	0.33	0.42 ± 0.05	0.59	O3 Vf
HDE308813	294.79	−1.61	3.1	1	−0.0	9.30	9.32	0.26	0.52 ± 0.06	...	O9.5 V

^a(1) Bowen et al. (2008), (2) Jenkins (2009), (3) Savage et al. (2017), (4) this paper.

^bSee Section 4.

^cLogarithm of the intensity of starlight capable of ionizing neutral carbon for the foreground gas, relative to the Galactic average, as computed by Jenkins & Tripp (2011). See Section 5

Table 2. Rejected Stars

Star	Reason
BD+48 3437	Too many lines were difficult to measure.
HD23478	B3, $\log N(\text{H I})_{\text{stellar}} > \log N(\text{H I})_{\text{meas.}} - 0.5$
HD24190	B2 V and no photometric data available ^a
HD27778	B3V; $\log N(\text{H I})_{\text{stellar}} > \log N(\text{H I})_{\text{meas.}} - 0.5$
HD62542	B5V, but see note below ^b
HD72754	Too many lines were difficult to measure.
HD102065	Enormous stellar Ly α absorption, even though listed as a B2V star
HD114441	B2 V and no photometric data available ^a
HD117111	B2 V and no photometric data available ^a
HD153262	B0/3, so photometric data probably not useful ^a
HD203532	B3 IV; $\log N(\text{H I})_{\text{stellar}} > \log N(\text{H I})_{\text{meas.}} - 0.5$

^aPhotometric data are needed to compute $N(\text{H I})_{\text{stellar}}$ using the method of Diplas & Savage (1994).

^bThis case is unusual: Mg and Mn are very weak and hard to measure against bad stellar lines, but Ge and Kr show up as narrow and very believable absorptions. Abundances of Ge and Kr must be high relative to other elements, and their measurement outcomes are listed in Table 7. This sightline seems to be noteworthy, even though we could not include it in the general statistical analysis.

Table 3. Atomic Transitions

Atom and Ionization State ^a	λ (Å)	$\log f\lambda$	Source of the f -value	Revision in the Value of $\log f\lambda$ ^b
(1)	(2)	(3)	(4)	(5)
O I.....	1355.598 ^c	-2.805	(Morton 2003)	...
Mg II 1.....	1239.925	-0.106	(Morton 2003)	...
Mg II 2.....	1240.395	-0.355		
Mn II 1.....	1197.184	2.248	(Toner & Hibbert 2005)	-0.166
Mn II 2.....	1201.118	1.999		-0.164
Ge II.....	1237.059	3.033	(Heidarian et al. 2017)	-0.150
Kr I.....	1235.838	2.422	(Chan et al. 1992)	+0.020

^aThe Arabic numerals that follow some of the elements link the transitions to their measurements reported in Table 7.

^bAdopted value of $\log f\lambda$ minus the value reported in Morton (2000) or Morton (2003).

^cFour stars had wavelength coverages that did not include this transition.

2.3. Choices for Heavy Element Transitions

Table 3 lists the transitions, their wavelengths, and values of $\log f\lambda$ that were used to derive the column densities of the elements under study. For Mn, Kr, and Ge, Cashman et al. (2017) have offered updated f -values as suggested replacements to those listed in the very popular compilations of Morton (2000, 2003). Since the trends reported in J09 had all column densities modified so that they were consistent with the Morton listings, Column 5 of the table states the difference (revised $\log f\lambda$ – Morton’s $\log f\lambda$). The original sources for the f -values are listed in Column 4 of the table [except for those given in Morton (2003)]. Figure 1 illustrates the appearance of the Kr, Ge, and Mg lines in the spectrum of one star in our survey, HD 170740.

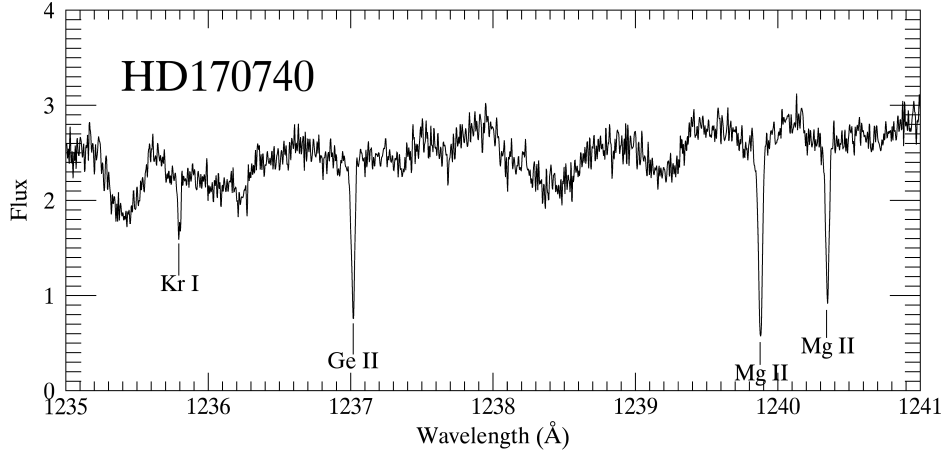


Figure 1. A STIS E140H exposure of the spectral region covering the transitions of Kr I, Ge II, and Mg II in the spectrum of HD 170740.

3. DERIVATIONS OF COLUMN DENSITIES

3.1. *Heavy Elements*

Prior to measuring the absorption features, velocity limits had to be defined. Unlike the clear, sharp absorptions that appear in Figure 1 for HD 170740, many other stars exhibited additional weak absorptions over large spans in velocity for the strongest feature of Mg II, as illustrated in Figure 2. Without reference to the Mg II profile, one would be inclined to measure the much weaker absorptions from other species over narrower velocity intervals. For instance, evaluations of Kr I and O I for HD 165246 might have included only the velocity interval from -13 to $+2 \text{ km s}^{-1}$, which would have missed very weak portions of the features that were buried in the noise and not apparent to the eye. For this reason, we adopted a strict policy of defining for all species the velocity endpoints v_1 and v_2 based on the Mg II feature at 1239.925 Å , regardless of whether or not the weaker lines showed absorptions at the most extreme velocities. Not only does this tactic prevent us from overlooking some absorption, but it also prevents a subtle downward bias in the definition of a continuum level (i.e., in some cases a localized depression of intensity in a region surrounding an obvious absorption feature could be mistakenly identified as a broad stellar absorption feature). Finally, it is important that we ensure an equitable pairing of the heavy elements to H I and H_2 , whose measures are independent of velocity. Overall, this rigid definition of the velocity endpoints usually weakens the significance of a determination that might otherwise seem by eye to be more confined and easy to measure, but we consider it to be a justifiable price to pay for avoiding a bias in the measurements. The velocity endpoints v_1 and v_2 are specified in the header for each target star in Table 7.

For each absorption feature, a column density was derived by integrating the apparent optical depths (AODs) (Savage & Sembach 1991) over the relevant velocity

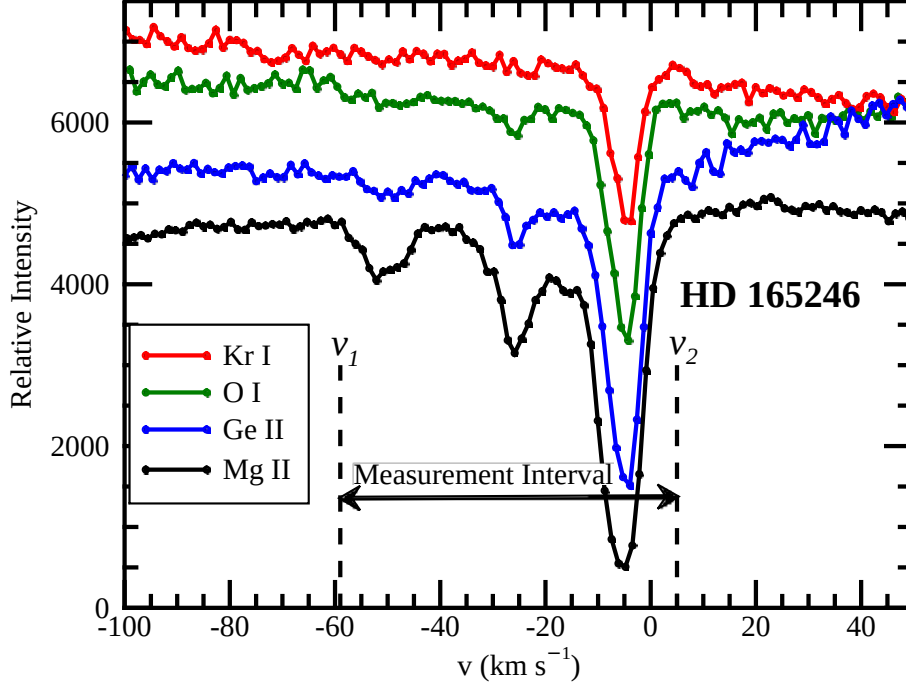


Figure 2. Absorption features in the E140H spectrum of HD 165246 for Kr I, O I, Ge II, and Mg II, which follow a sequence of increasing profile strengths. The dashed lines depict the velocity end points, $v_1 = -59 \text{ km s}^{-1}$ and $v_2 = +5 \text{ km s}^{-1}$ of the Mg II absorption.

interval. An apparent column density N_a is then given by the relation

$$N_a = \frac{m_e c}{\pi e^2 f \lambda} \int_{v_1}^{v_2} \tau_a(v) dv, \quad (5)$$

where the AOD $\tau_a(v) = \ln[(I_0(v)/I(v)]$, $I_0(v)$ is the continuum intensity, and $I(v)$ is the intensity within the absorption feature. The expression in front of the integral is equal to $3.77 \times 10^{14} \text{ cm}^{-2}$ if v is expressed in km s^{-1} and $f\lambda$ is in units of \AA (as shown in logarithmic form in Table 3).

For each feature, a continuum level $I_0(v)$ was defined using a Legendre polynomial of the lowest order that would give a reasonable fit to the spectrum outside of the interval spanned by v_1 and v_2 . Continuum placement errors can have a large influence in the uncertainties of weak lines. We evaluated the expected deviations produced by such errors by remeasuring the AODs at the lower and upper bounds for the continua, which were derived from the expected formal uncertainties in the polynomial coefficients of the fits as described by Sembach & Savage (1992). We multiplied these coefficient uncertainties by 2 in order to make approximate allowances for additional deviations that might arise from some freedom in assigning the most appropriate order for the polynomial. Final uncertainty estimates were defined in terms of uncertainties due to noise and those due to continuum fitting, both of which were combined in quadrature. Table 7 lists for the different transitions both equivalent width measurements and values of N_a , along with their respective 1σ uncertainties.

Table 7 reveals that there are many duplications in the column density derivations. For some targets, we had access to both high- and medium-resolution spectra (the E140H and E140M modes, respectively). For most but not all observations we could measure both a strong and a weak line of Mg II and Mn II. In making choices on which results to adopt for these two elements, the first level of priority was to favor the strong lines over the weaker ones, but with some exceptions described in the paragraph that follows. A secondary consideration (applied to all elements) was that measurements taken from the high-resolution spectra were favored over the medium-resolution ones.

In most instances, the column density outcomes for the two Mg II and Mn II lines agreed with each other to within their uncertainties. However, occasionally the weaker line yielded a value that was significantly larger than the stronger line. This condition indicates that some saturation of the strong line was occurring over a scale of velocity that was not resolved by the instrument, yielding an underestimate of the true opacity averaged over velocity. An example of this condition is shown for the Mg II doublet shown in Fig. 1 for the star HD 170740, where both the equivalent widths and AODs near the line bottom fall short of the 1.77:1 ratio of transition strengths. Here the AOD outcomes for the strong and weak line are $\log N(\text{Mg II}) = 15.75 \pm 0.02$ and 15.82 ± 0.03 , respectively. Adopting only the column density of the weaker line is not sufficient to overcome the error caused by saturation because even N_a for this line could fall short of the true value. A good approximation for deriving the true column density is to correct for the unresolved saturations by subjecting the AOD values at each velocity to a standard curve-of-growth analysis, according to the usual convention of interpreting equivalent widths for absorption features that are very poorly resolved. This approach is described and justified by Jenkins (1996). An application of this method to the Mg II lines of HD 170740 yields $\log N(\text{Mg II}) = 15.91 \pm 0.04$, which is measurably greater than the weak-line result. For all absorptions considered in this study none of the saturations were severe enough to invalidate this approach to correction. One can sense which cases needed the saturation corrections by consulting Table 7 and locating ion entries that have a “3” following them.

We considered a measurement to be marginal if the equivalent width outcome was less than the 2σ level of uncertainty from noise and continuum placement. For weak lines below this uncertainty threshold, we specified an upper limit for the column density based on a completely unsaturated line having a strength at the measurement value plus a 1σ positive excursion, but with an allowance for the fact that negative real line strengths are not allowed even though we occasionally obtained negative measurement outcomes caused by downward noise fluctuations (or a continuum placement that was too low). Details of how we calculated these 1σ upper limits are given in Appendix D of Bowen et al. (2008). Such a calculation avoids the absurd conclusion that an upper limit for a column density can be nearly zero or negative when the measurement yields an outcome that is $\leq -1\sigma$. It also yields a smooth transition to a conventional expression of a measured value plus its 1σ upper error

bar when this value is slightly larger than the twice its uncertainty. A substantial fraction of the Kr determinations (49 out of 100 stars) consisted of upper limits. For O and Ge, there were only 11 and 3 such upper limits, respectively.

The adopted column densities for the five elements considered in this study are listed for each star in Table 4.

Table 4. Element Measurement Outcomes^a

Star	$\log N(\text{O I})$	$\log N(\text{Mg II})$	$\log N(\text{Mn II})$	$\log N(\text{Ge II})$	$\log N(\text{Kr I})$
(1)	(2)	(3)	(4)	(5)	(6)
BD+35 4258	17.55 (+0.14, -0.21)	16.26 (+0.04, -0.03)	13.68±0.04	12.49±0.05	< 12.59
BD+53 2820	17.99 (+0.09, -0.11)	16.37 (+0.06, -0.04)	13.78±0.04	12.55 (+0.08, -0.09)	< 12.50
CPD-59 2603	18.02 (+0.05, -0.06)	16.31±0.01	13.91±0.04	12.66 (+0.04, -0.05)	< 12.66
CPD-59 4552	17.90 (+0.13, -0.19)	16.36±0.03	13.70±0.06	12.57 (+0.02, -0.03)	< 12.37
CPD-69 1743	< 17.59	16.20±0.04	13.45 (+0.06, -0.07)	12.26 (+0.09, -0.12)	< 12.55
HD108	18.09 (+0.06, -0.07)	16.30±0.02	13.69±0.05	12.66±0.03	< 12.51
HD1383	< 18.30	16.42±0.02	13.75±0.04	12.66±0.04	12.91 (+0.11, -0.15)
HD3827	< 17.25	15.48±0.03	13.23±0.05	< 11.95	< 12.01
HD12323	18.08 (+0.06, -0.07)	16.14±0.03	13.57 (+0.05, -0.06)	12.40 (+0.06, -0.07)	< 12.80
HD13268	18.10 (+0.08, -0.11)	16.44 (+0.06, -0.04)	13.80±0.03	12.54 (+0.09, -0.11)	< 12.47
HD13745	17.97 (+0.10, -0.14)	16.28±0.03	13.76 (+0.03, -0.04)	12.62 (+0.08, -0.10)	< 12.94
HD13841	< 18.29	16.31±0.02	13.76 (+0.10, -0.13)	12.75 (+0.04, -0.05)	< 13.13
HD14818	18.16 (+0.14, -0.21)	16.49±0.04	13.78 (+0.08, -0.10)	12.62 (+0.06, -0.08)	< 12.90
HD15137	17.88±0.05	16.22 (+0.02, -0.01)	13.59±0.02	12.48±0.06	12.74 (+0.11, -0.15)
HD25443	18.12 (+0.05, -0.06)	16.17±0.01	13.63 (+0.03, -0.04)	12.67±0.02	12.66 (+0.11, -0.16)
HD35914	...	16.12±0.03	13.31 (+0.08, -0.09)	12.52 (+0.06, -0.08)	< 12.48
HD40893	18.12±0.04	16.30±0.01	13.74±0.02	12.74±0.02	12.83 (+0.09, -0.11)
HD41161	17.84 (+0.05, -0.06)	16.08±0.01	13.44 (+0.01, -0.02)	12.41±0.03	< 12.46
HD46223	18.11 (+0.04, -0.05)	16.44±0.08	13.66 (+0.01, -0.02)	12.67±0.02	< 12.80
HD52266	17.89 (+0.08, -0.10)	16.07±0.01	13.70±0.03	12.45±0.02	12.55 (+0.17, -0.27)
HD53975	17.81 (+0.06, -0.07)	16.06±0.01	13.59±0.05	12.24 (+0.03, -0.04)	12.28 (+0.14, -0.21)
HD63005	17.89 (+0.07, -0.08)	15.98±0.02	13.56 (+0.06, -0.07)	12.51 (+0.05, -0.06)	< 12.76
HD66788	< 17.98	16.07±0.02	13.30 (+0.10, -0.12)	< 12.27	< 12.49
HD69106	17.61±0.05	15.89 (+0.02, -0.01)	13.36±0.01	12.24±0.02	12.23 (+0.03, -0.04)
HD72648	17.89 (+0.12, -0.16)	15.94±0.03	13.43 (+0.03, -0.04)	12.45±0.03	12.36 (+0.13, -0.19)
HD75309	17.72 (+0.09, -0.12)	15.94±0.01	13.43±0.02	12.43±0.03	12.08 (+0.16, -0.26)
HD88115	17.69 (+0.14, -0.21)	16.04±0.01	13.76 (+0.07, -0.05)	12.42±0.03	< 12.47
HD89137	17.70 (+0.08, -0.10)	16.02±0.01	13.71±0.04	12.29 (+0.03, -0.04)	< 12.77
HD90087	17.90 (+0.04, -0.05)	16.19±0.02	13.67±0.01	12.50±0.02	12.53 (+0.14, -0.22)
HD91824	< 17.70	16.20±0.02	13.61±0.02	12.48±0.02	12.47 (+0.08, -0.10)
HD91983	17.97 (+0.06, -0.08)	16.28 (+0.03, -0.02)	13.64 (+0.03, -0.04)	12.50±0.03	< 12.14
HD92554	17.89 (+0.15, -0.24)	16.48±0.03	13.80±0.03	12.67±0.05	< 12.31
HD93129	18.18 (+0.04, -0.05)	16.37±0.01	13.85±0.05	12.76±0.02	< 12.38
HD93205	...	16.40±0.02	14.07±0.02	12.65 (+0.03, -0.04)	< 12.68
HD93222	...	16.50±0.02	14.22±0.07	12.71±0.02	< 12.74
HD93843	17.93 (+0.09, -0.12)	16.25±0.01	13.88±0.01	12.55 (+0.02, -0.03)	< 12.35
HD94493	17.71 (+0.12, -0.16)	16.22±0.02	13.68±0.02	12.45 (+0.08, -0.09)	12.27 (+0.14, -0.21)

Table 4 continued on next page

Table 4 (*continued*)

Star	$\log N(\text{O I})$	$\log N(\text{Mg II})$	$\log N(\text{Mn II})$	$\log N(\text{Ge II})$	$\log N(\text{Kr I})$
(1)	(2)	(3)	(4)	(5)	(6)
HD97175	17.87 (+0.09, -0.12)	15.93±0.02	13.62±0.09	12.20 (+0.06, -0.07)	12.54 (+0.11, -0.15)
HD99857	17.90 (+0.09, -0.11)	16.26±0.02	13.70±0.02	12.54±0.03	12.58 (+0.09, -0.11)
HD99890	17.92 (+0.09, -0.12)	16.19±0.01	13.63±0.01	12.41±0.03	12.23 (+0.14, -0.22)
HD99953	18.07 (+0.11, -0.14)	16.24±0.02	13.78 (+0.04, -0.05)	12.73±0.02	< 12.75
HD100199	17.92 (+0.10, -0.13)	16.23±0.04	13.61±0.03	12.61 (+0.05, -0.06)	< 12.57
HD101190	18.00 (+0.06, -0.07)	16.29±0.04	13.64±0.03	12.49±0.03	12.45 (+0.17, -0.28)
HD103779	17.80 (+0.11, -0.16)	16.27±0.02	13.62 (+0.03, -0.04)	12.44 (+0.05, -0.06)	12.62 (+0.10, -0.13)
HD104705	17.84 (+0.07, -0.08)	16.15±0.01	13.67±0.02	12.56 (+0.07, -0.08)	12.24 (+0.16, -0.26)
HD108639	18.11 (+0.04, -0.05)	16.41±0.02	13.97±0.05	12.66±0.02	12.49 (+0.07, -0.08)
HD109399	17.69 (+0.12, -0.17)	16.09±0.02	13.54 (+0.02, -0.03)	12.34 (+0.05, -0.06)	12.38 (+0.16, -0.25)
HD111934	17.96 (+0.14, -0.22)	16.45 (+0.05, -0.04)	13.82 (+0.06, -0.07)	12.67±0.02	< 12.84
HD114886	18.05 (+0.11, -0.14)	16.28 (+0.01, -0.02)	13.76±0.02	12.72±0.02	12.49 (+0.16, -0.26)
HD115071	18.20 (+0.05, -0.06)	16.36±0.02	13.96±0.04	12.74±0.01	12.56 (+0.08, -0.10)
HD115455	18.24 (+0.09, -0.12)	16.44 (+0.03, -0.02)	13.77±0.04	12.70±0.02	< 13.03
HD116781	18.01 (+0.07, -0.09)	16.11 (+0.01, -0.02)	13.65±0.02	12.49±0.04	< 12.52
HD116852	17.74 (+0.10, -0.13)	15.90±0.01	13.59±0.03	12.17±0.04	< 12.33
HD122879	18.04±0.05	16.20±0.01	13.73±0.01	12.62±0.02	12.55 (+0.06, -0.07)
HD124314	18.21±0.02	16.37 (+0.02, -0.01)	13.93±0.03	12.74±0.02	12.87 (+0.06, -0.07)
HD124979	17.94 (+0.08, -0.10)	16.30±0.01	13.88±0.02	12.67±0.04	< 12.60
HD137595	17.91 (+0.05, -0.06)	15.74±0.02	13.56±0.05	12.28±0.04	12.23 (+0.09, -0.11)
HD144965	17.89 (+0.06, -0.08)	15.57±0.02	13.10 (+0.05, -0.06)	12.22±0.04	12.38 (+0.08, -0.10)
HD147888	18.21±0.02	16.00 (+0.03, -0.02)	13.77 (+0.06, -0.04)	12.85±0.07	12.66 (+0.08, -0.03)
HD148422	< 18.23	16.47±0.06	13.88 (+0.10, -0.12)	< 12.54	< 12.59
HD148937	18.40±0.03	16.40±0.02	14.12±0.07	12.87±0.02	< 12.64
HD151805	18.06 (+0.08, -0.09)	16.22±0.02	13.85±0.04	12.69±0.03	12.62 (+0.13, -0.19)
HD152249	18.09 (+0.08, -0.09)	16.35±0.02	13.75 (+0.20, -0.05)	12.70±0.02	12.68 (+0.14, -0.21)
HD152424	18.21 (+0.08, -0.09)	16.31±0.01	13.96±0.03	12.81 (+0.03, -0.04)	12.78 (+0.17, -0.27)
HD152590	18.08 (+0.12, -0.16)	16.30±0.02	13.72 (+0.04, -0.05)	12.60±0.01	12.64 (+0.12, -0.16)
HD156359	< 17.79	15.92±0.05	13.17 (+0.14, -0.21)	12.02 (+0.15, -0.24)	< 12.69
HD163522	< 18.00	16.18±0.03	13.50 (+0.14, -0.21)	12.50 (+0.06, -0.07)	< 12.96
HD165246	18.01 (+0.04, -0.05)	16.05±0.01	13.80±0.03	12.55 (+0.05, -0.06)	12.34 (+0.07, -0.08)
HD167402	< 18.04	16.34±0.06	13.72 (+0.08, -0.10)	12.51 (+0.10, -0.12)	< 12.76
HD168941	17.84 (+0.08, -0.10)	15.92±0.04	13.51 (+0.06, -0.08)	12.50 (+0.06, -0.08)	< 12.62
HD170740	18.01 (+0.05, -0.06)	15.91±0.04	13.29 (+0.06, -0.07)	12.36±0.04	12.43 (+0.14, -0.20)
HD177989	17.75±0.05	15.84±0.01	13.44±0.01	12.24±0.03	12.24 (+0.07, -0.09)
HD178487	< 17.83	15.97±0.04	13.59 (+0.10, -0.13)	12.38 (+0.11, -0.15)	< 12.69
HD179407	17.82 (+0.15, -0.24)	15.98 (+0.07, -0.09)	13.60 (+0.06, -0.08)	12.46 (+0.13, -0.19)	< 12.78
HD185418	18.00±0.03	16.03 (+0.02, -0.01)	13.72±0.03	12.49±0.01	12.61±0.03
HD191877	17.80 (+0.07, -0.09)	15.92±0.01	13.46±0.02	12.31±0.04	12.02 (+0.13, -0.19)
HD192035	18.01 (+0.05, -0.06)	16.07 (+0.05, -0.04)	13.40 (+0.05, -0.06)	12.49±0.04	< 12.51
HD195455	17.62 (+0.10, -0.14)	15.58±0.02	13.10 (+0.05, -0.06)	11.70 (+0.11, -0.14)	12.33 (+0.14, -0.21)
HD195965	17.74 (+0.05, -0.06)	16.00 (+0.03, -0.02)	13.43 (+0.05, -0.06)	12.35±0.03	< 11.76
HD198478	18.19 (+0.11, -0.15)	16.13±0.05	13.83 (+0.09, -0.08)	12.68 (+0.03, -0.04)	< 12.56
HD198781	17.87 (+0.04, -0.05)	15.74±0.01	13.35±0.02	12.34±0.02	12.42 (+0.07, -0.08)
HD201345	17.72 (+0.06, -0.07)	16.02±0.02	13.47±0.01	12.44 (+0.04, -0.05)	12.00 (+0.11, -0.15)

Table 4 continued on next page

Table 4 (*continued*)

Star	$\log N(\text{O I})$	$\log N(\text{Mg II})$	$\log N(\text{Mn II})$	$\log N(\text{Ge II})$	$\log N(\text{Kr I})$
(1)	(2)	(3)	(4)	(5)	(6)
HD202347	17.43 (+0.14, −0.22)	15.63±0.02	13.18 (+0.06, −0.07)	12.16±0.04	12.38 (+0.07, −0.09)
HD203374	17.87±0.05	16.09±0.01	13.62±0.02	12.59±0.02	12.50 (+0.05, −0.06)
HD206267	18.10±0.03	16.04±0.02	13.62±0.02	12.58±0.03	12.59 (+0.08, −0.10)
HD206773	17.89±0.03	15.98±0.01	13.53 (+0.01, −0.02)	12.45±0.03	12.49 (+0.10, −0.12)
HD207198	18.15±0.03	16.06±0.01	13.66±0.02	12.61±0.02	12.67 (+0.07, −0.09)
HD207308	17.97 (+0.08, −0.10)	16.01±0.04	13.55±0.04	12.51±0.03	12.33 (+0.16, −0.25)
HD207538	18.17 (+0.04, −0.05)	16.02±0.02	13.56 (+0.09, −0.12)	12.58 (+0.05, −0.06)	< 12.70
HD208440	17.98±0.04	16.04±0.01	13.69±0.04	12.51±0.02	12.34 (+0.10, −0.12)
HD209339	17.82±0.05	16.11 (+0.03, −0.02)	13.73±0.05	12.49±0.02	12.41 (+0.07, −0.09)
HD210809	17.88 (+0.08, −0.10)	16.39±0.03	13.96±0.06	12.59±0.04	< 12.44
HD210839	18.17±0.03	16.04±0.01	13.59±0.02	12.64±0.03	< 12.45
HD218915	17.72 (+0.11, −0.15)	16.22±0.02	13.60±0.03	12.43±0.05	< 12.53
HD219188	17.30 (+0.08, −0.10)	15.72±0.02	13.10±0.02	12.02±0.04	11.95 (+0.10, −0.13)
HD220057	17.76 (+0.05, −0.06)	15.80 (+0.04, −0.02)	13.44±0.05	12.22±0.03	12.26 (+0.09, −0.12)
HD224151	18.06 (+0.07, −0.09)	16.30±0.01	13.75±0.03	12.65±0.04	< 12.71
HDE232522	18.02 (+0.13, −0.19)	16.15 (+0.01, −0.02)	13.61±0.04	12.45±0.03	< 12.40
HDE303308	...	16.39±0.02	14.13±0.01	12.70±0.03	12.53 (+0.14, −0.22)
HDE308813	17.81 (+0.12, −0.16)	16.12 (+0.03, −0.04)	13.62 (+0.04, −0.05)	12.53±0.04	12.74 (+0.12, −0.17)

^a Values of N are expressed in units of cm^{-2} . All uncertainties in this table represent possible deviations at a level of 1σ .

3.2. Atomic and Molecular Hydrogen

All spectra considered here cover the Ly α transition of H I at 1215.67Å. The Ly α absorptions are so broad and well resolved that one may reconstruct how a spectrum would appear without this feature by multiplying it by $\exp(+\tau)$ for a line with damping wings, as has been done in the past by Jenkins (1971), Bohlin (1975), Savage et al. (1977), and Diplas & Savage (1994), and then inspect which choice of $N(\text{H I})$ yields the most reasonable-looking outcome. Error limits are defined in terms of where the reconstructions appeared by eye to be unreasonable, i.e., showing deviations that produced appreciable emission or absorption on either side of the line core. These limits are judged to be at about the 1.5σ confidence level and will be treated as such in later analyses.

For some of the stars with spectral types cooler than B1, one may expect that the stellar Ly α absorption is strong enough to produce a spurious increase in the inferred value for $N(\text{H I})$ in the foreground. If this stellar contamination is not too large, a corrected value for the hydrogen column density can be derived by subtracting an effective $N(\text{H I})$ based on a prediction for the strength of the stellar contribution. J09 described a means for making such corrections, which followed an original prescription of Diplas & Savage (1994). Cases where such stellar corrections were warranted are

listed in Table 7 and are identified with the designation “H I sc”. The result for the original profile fit is shown just above it (without the “sc”).

For determinations of the molecular hydrogen abundances, we relied on spectra downloaded from the *FUSE* Virtual Observatory (VO)⁶ maintained by MAST. Most of the H₂ in the ISM is in the two lowest states of rotational excitation $J = 0$ and 1 in this molecule’s ground vibrational state (Jensen et al. 2010). Hence, we can ignore the higher J levels since their contributions to the total amount of hydrogen $N(\text{H I}) + 2N(\text{H}_2)$ are negligible. A process similar to the one invoked for interpreting the Ly α absorption can be used to derive $N(J = 0)$ and $N(J = 1)$, but the implementation is more complex because one must simultaneously explore values of several free parameters that can affect the outcomes. For instance, most of the intrinsic profile strengths and shapes depend not only on the column density but also on the velocity dispersion of the molecular gas. Beyond this, one must account for the influence of such instrumental parameters as the line spread function of the *FUSE* spectrograph and errors in the wavelength scale, both of which are not known with much accuracy. The synthesis of intrinsic H₂ absorptions is greatly facilitated by invoking the optical depth profiles of the Lyman band systems provided by McCandliss (2003). An iterative exploration of the different free parameters ultimately revealed the best nulling of the absorptions by the R and P branches of the 4-0, 2-0, 1-0 and 0-0 Lyman bands. The weak 1-0 and 0-0 bands were usually the most useful in constraining the column densities. As with the flux reconstructions for Ly α absorptions, the acceptable ranges for H₂ column densities were governed by the lack of appreciable emission or absorption after the corrections were implemented.

Table 5 lists for each star the logarithms of the atomic and molecular hydrogen column densities (in units of cm⁻²). The table also lists in the last three columns the total hydrogen column densities $\log N(\text{H}_{\text{tot}}) = \log[2N(\text{H}_2) + N(\text{H I})]$, the $J = 0$ to 1 rotational temperature $T_{01} = 74 \text{ K}/[\log N(J = 0) - \log N(J = 1) + 0.954]$, and $\log f(\text{H}_2) = \log[2N(\text{H}_2)/N(\text{H}_{\text{tot}})]$. Uncertainty limits in the logarithms of the H₂ and H I column densities are usually asymmetrical. To derive proper offsets and uncertainties for the relevant sums, which are needed for calculations of the total $N(\text{H}_2)$, $N(\text{H}_{\text{tot}})$, T_{01} , and $f(\text{H}_2)$, we implemented the error combination method of Model 2 of Barlow (2003), which makes use of the fact that the means, variances, and unnormalized skewness of distorted Gaussians are additive after convolution.

The only numbers in Table 5 that will be incorporated into the study of depletions are $\log N(\text{H}_{\text{tot}})$ (in Column 6) and $\log f(\text{H}_2)$ (Column 8). Other quantities are listed in case they are of potential use to other investigations. While T_{01} might be a relevant physical quantity to explore for correlations, in fact trials to see whether had any influence on depletions failed to reveal any meaningful relationships.

⁶ <http://archive.stsci.edu/pub/vospectra/fuse2/>

Table 5. H₂ and H I Measurement Outcomes^a

Star	log $N(\text{H}_2)$			log $N(\text{H I})$	log $N(\text{H}_{\text{tot}})$ (Total H)	T_{01}	log $f(\text{H}_2)$
	$J = 0$	$J = 1$	Total				
(1)	(2)	(3)	(4)	(5)	(6)	(7)	(8)
BD+35 4258	19.09 ^{+0.14} _{-0.19}	19.45 ^{+0.13} _{-0.18}	19.61 ^{+0.11} _{-0.13}	21.24 ^{+0.03} _{-0.07}	21.26 ^{+0.03} _{-0.07}	124 ⁺⁸³ ₋₃₅	-1.34 ^{+0.12} _{-0.14}
BD+53 2820	19.70 ^{+0.11} _{-0.26}	19.89 ± 0.15	20.10 ^{+0.11} _{-0.13}	21.35 ^{+0.05} _{-0.07}	21.40 ^{+0.05} _{-0.06}	100 ⁺⁵⁸ ₋₂₄	-0.99 ^{+0.12} _{-0.14}
CPD-59 2603	19.51 ^{+0.25} _{-0.08}	19.82 ± 0.11	20.02 ^{+0.12} _{-0.10}	21.43 ^{+0.04} _{-0.05}	21.46 ^{+0.04} _{-0.05}	112 ⁺⁴¹ ₋₃₁	-1.14 ^{+0.13} _{-0.10}
CPD-59 4552	20.13 ^{+0.11} _{-0.09}	20.15 ^{+0.10} _{-0.14}	20.45 ± 0.08	21.28 ^{+0.05} _{-0.06}	21.39 ^{+0.04} _{-0.05}	78 ⁺¹⁶ ₋₁₁	-0.64 ± 0.09
CPD-69 1743	19.58 ^{+0.23} _{-0.16}	19.49 ^{+0.13} _{-0.21}	19.85 ^{+0.15} _{-0.13}	21.16 ^{+0.04} _{-0.09}	21.20 ^{+0.04} _{-0.08}	68 ⁺²² ₋₁₃	-1.04 ^{+0.17} _{-0.14}
HD108	20.17 ^{+0.12} _{-0.07}	20.10 ± 0.09	20.45 ^{+0.08} _{-0.06}	21.38 ± 0.05	21.47 ± 0.04	72 ⁺¹¹ ₋₈	-0.72 ^{+0.09} _{-0.08}
HD1383	20.05 ± 0.11	20.28 ^{+0.09} _{-0.10}	20.49 ± 0.07	21.46 ^{+0.05} _{-0.06}	21.54 ^{+0.04} _{-0.05}	103 ⁺²⁶ ₋₁₇	-0.75 ^{+0.08} _{-0.09}
HD3827	17.71 ^{+0.18} _{-0.50}	18.24 ± 0.30	18.35 ^{+0.25} _{-0.23}	20.55 ^{+0.07} _{-0.05}	20.56 ^{+0.07} _{-0.05}	203 ^{+∞} ₋₁₁₃	-1.92 ^{+0.25} _{-0.24}
HD12323	19.87 ^{+0.12} _{-0.15}	20.04 ^{+0.09} _{-0.17}	20.26 ^{+0.08} _{-0.11}	21.19 ^{+0.04} _{-0.05}	21.28 ± 0.04	93 ⁺³⁰ ₋₁₈	-0.72 ^{+0.09} _{-0.12}
HD13268	20.03 ± 0.13	20.24 ± 0.10	20.46 ± 0.08	21.34 ± 0.07	21.44 ± 0.06	99 ⁺²⁹ ₋₁₈	-0.68 ± 0.10
HD13745	20.25 ± 0.07	20.20 ^{+0.12} _{-0.14}	20.53 ± 0.07	21.34 ± 0.05	21.46 ± 0.04	74 ⁺¹² ₋₁₀	-0.63 ± 0.08
HD13841	20.28 ^{+0.08} _{-0.10}	20.23 ± 0.18	20.56 ± 0.10	21.44 ^{+0.06} _{-0.12}	21.54 ^{+0.05} _{-0.09}	74 ⁺¹⁹ ₋₁₃	-0.66 ^{+0.14} _{-0.12}
HD14818	20.22 ± 0.18	20.19 ^{+0.11} _{-0.08}	20.52 ^{+0.11} _{-0.10}	21.40 ± 0.07	21.51 ± 0.06	77 ⁺¹⁹ ₋₁₄	-0.68 ^{+0.13} _{-0.12}
HD15137	19.81 ^{+0.08} _{-0.11}	20.03 ^{+0.11} _{-0.21}	20.23 ^{+0.08} _{-0.12}	21.24 ^{+0.08} _{-0.06}	21.32 ^{+0.07} _{-0.05}	101 ⁺²⁹ ₋₂₄	-0.80 ^{+0.10} _{-0.14}
HD25443	20.62 ^{+0.07} _{-0.10}	20.61 ± 0.13	20.92 ± 0.08	21.29 ^{+0.06} _{-0.05}	21.56 ± 0.05	78 ⁺¹⁵ ₋₁₁	-0.34 ± 0.09
HD35914	19.54 ± 0.07	19.06 ± 0.14	19.67 ± 0.06	21.18 ^{+0.07} _{-0.04}	21.21 ^{+0.07} _{-0.04}	52 ⁺⁶ ₋₅	-1.24 ^{+0.08} _{-0.09}
HD40893	20.28 ^{+0.02} _{-0.04}	20.30 ^{+0.05} _{-0.06}	20.59 ± 0.03	21.46 ^{+0.04} _{-0.06}	21.56 ^{+0.03} _{-0.05}	79 ± 5	-0.67 ^{+0.06} _{-0.05}
HD41161	19.60 ± 0.12	19.76 ^{+0.12} _{-0.11}	19.99 ^{+0.09} _{-0.08}	21.09 ± 0.05	21.16 ± 0.04	94 ⁺²⁵ ₋₁₆	-0.86 ± 0.10
HD46223	20.37 ^{+0.04} _{-0.09}	20.37 ^{+0.10} _{-0.06}	20.67 ^{+0.06} _{-0.05}	21.46 ^{+0.04} _{-0.02}	21.59 ^{+0.03} _{-0.02}	80 ⁺¹¹ ₋₈	-0.62 ^{+0.07} _{-0.06}
HD52266	19.68 ± 0.09	19.70 ^{+0.13} _{-0.12}	20.00 ± 0.08	21.22 ^{+0.04} _{-0.05}	21.27 ^{+0.04} _{-0.05}	79 ⁺¹⁶ ₋₁₁	-0.97 ± 0.09
HD53975	18.75 ^{+0.16} _{-0.19}	18.90 ^{+0.11} _{-0.07}	19.15 ± 0.09	21.08 ^{+0.04} _{-0.02}	21.09 ^{+0.04} _{-0.02}	94 ⁺³¹ ₋₁₉	-1.65 ± 0.10
HD63005	19.78 ^{+0.14} _{-0.21}	19.92 ^{+0.10} _{-0.04}	20.17 ± 0.09	21.24 ^{+0.03} _{-0.06}	21.31 ^{+0.03} _{-0.05}	94 ⁺³¹ ₋₁₈	-0.83 ± 0.10
HD66788	19.31 ^{+0.21} _{-0.03}	19.43 ^{+0.17} _{-0.12}	19.72 ^{+0.14} _{-0.10}	21.23 ^{+0.04} _{-0.02}	21.26 ^{+0.04} _{-0.02}	85 ⁺³⁰ ₋₁₇	-1.24 ^{+0.14} _{-0.11}
HD69106	19.40 ± 0.10	19.49 ± 0.10	19.75 ± 0.07	21.07 ± 0.04	21.11 ± 0.04	86 ⁺¹⁷ ₋₁₂	-1.06 ± 0.08
HD72648	20.30 ± 0.19	20.45 ± 0.20	20.70 ± 0.15	21.19 ^{+0.07} _{-0.06}	21.41 ± 0.07	92 ⁺⁴⁸ ₋₂₃	-0.42 ± 0.16
HD75309	19.77 ^{+0.10} _{-0.09}	19.93 ^{+0.08} _{-0.15}	20.16 ^{+0.06} _{-0.09}	21.10 ^{+0.03} _{-0.06}	21.19 ^{+0.03} _{-0.05}	91 ⁺²⁰ ₋₁₅	-0.72 ^{+0.08} _{-0.10}
HD88115	18.81 ± 0.18	19.02 ± 0.18	19.25 ± 0.14	21.03 ^{+0.06} _{-0.09}	21.04 ^{+0.06} _{-0.09}	99 ⁺⁵³ ₋₂₆	-1.49 ^{+0.16} _{-0.15}
HD89137	19.62 ^{+0.14} _{-0.08}	19.75 ^{+0.12} _{-0.07}	20.02 ^{+0.09} _{-0.07}	21.03 ^{+0.07} _{-0.02}	21.11 ^{+0.06} _{-0.02}	91 ⁺²⁰ ₋₁₅	-0.81 ^{+0.10} _{-0.09}
HD90087	19.53 ^{+0.11} _{-0.06}	19.61 ± 0.10	19.88 ± 0.07	21.19 ^{+0.05} _{-0.09}	21.23 ^{+0.05} _{-0.08}	83 ⁺¹⁵ ₋₁₁	-1.04 ^{+0.11} _{-0.09}
HD91824	19.59 ± 0.13	19.43 ^{+0.07} _{-0.21}	19.81 ^{+0.09} _{-0.11}	21.12 ± 0.04	21.16 ± 0.04	65 ⁺¹³ ₋₁₀	-1.05 ^{+0.10} _{-0.11}
HD91983	19.86 ^{+0.11} _{-0.06}	19.74 ^{+0.03} _{-0.13}	20.10 ± 0.07	21.15 ^{+0.06} _{-0.05}	21.22 ^{+0.05} _{-0.04}	66 ⁺⁹ ₋₇	-0.82 ± 0.08
HD92554	18.97 ^{+0.11} _{-0.07}	18.90 ^{+0.08} _{-0.21}	19.24 ^{+0.07} _{-0.10}	21.34 ^{+0.09} _{-0.11}	21.35 ^{+0.09} _{-0.11}	70 ⁺¹² ₋₁₁	-1.81 ± 0.13
HD93129	19.85 ^{+0.09} _{-0.05}	19.94 ^{+0.10} _{-0.07}	20.21 ^{+0.07} _{-0.05}	21.47 ^{+0.07} _{-0.04}	21.52 ^{+0.06} _{-0.04}	86 ⁺¹⁴ ₋₁₀	-1.01 ± 0.08
HD93205	19.34 ± 0.17	19.47 ^{+0.15} _{-0.10}	19.73 ^{+0.12} _{-0.10}	21.36 ± 0.05	21.38 ± 0.05	92 ⁺³² ₋₂₀	-1.35 ^{+0.13} _{-0.12}
HD93222	19.49 ^{+0.13} _{-0.10}	19.43 ^{+0.13} _{-0.18}	19.77 ^{+0.09} _{-0.10}	21.47 ^{+0.03} _{-0.04}	21.49 ^{+0.03} _{-0.04}	72 ⁺¹⁶ ₋₁₁	-1.41 ± 0.10
HD93843	19.14 ^{+0.17} _{-0.12}	19.42 ± 0.13	19.62 ± 0.10	21.30 ^{+0.05} _{-0.04}	21.32 ^{+0.05} _{-0.04}	108 ⁺⁴² ₋₂₄	-1.40 ± 0.11
HD94493	19.78 ± 0.07	19.80 ^{+0.09} _{-0.17}	20.09 ^{+0.06} _{-0.09}	21.10 ^{+0.06} _{-0.05}	21.18 ^{+0.05} _{-0.04}	79 ⁺¹³ ₋₁₂	-0.79 ^{+0.08} _{-0.10}

Table 5 continued on next page

Table 5 (*continued*)

Star	log $N(\text{H}_2)$			log $N(\text{H I})$	log $N(\text{H}_{\text{tot}})$ (Total H)	T_{01}	log $f(\text{H}_2)$
	$J = 0$	$J = 1$	Total				
(1)	(2)	(3)	(4)	(5)	(6)	(7)	(8)
HD97175	$19.80^{+0.12}_{-0.09}$	$19.75^{+0.14}_{-0.07}$	$20.10^{+0.09}_{-0.07}$	$20.96^{+0.06}_{-0.05}$	$21.07^{+0.05}_{-0.04}$	74^{+14}_{-10}	$-0.67^{+0.10}_{-0.09}$
HD99857	19.97 ± 0.07	$20.02^{+0.06}_{-0.18}$	$20.30^{+0.05}_{-0.09}$	$21.27^{+0.07}_{-0.03}$	$21.35^{+0.06}_{-0.03}$	80 ± 12	$-0.77^{+0.07}_{-0.11}$
HD99890	$19.18^{+0.14}_{-0.09}$	19.30 ± 0.12	19.56 ± 0.09	$21.12^{+0.05}_{-0.07}$	$21.14^{+0.05}_{-0.07}$	88^{+23}_{-15}	$-1.27^{+0.11}_{-0.10}$
HD99953	20.39 ± 0.17	$20.12^{+0.22}_{-0.20}$	20.60 ± 0.14	21.45 ± 0.07	21.56 ± 0.06	61^{+17}_{-11}	-0.66 ± 0.15
HD100199	19.81 ± 0.09	$19.87^{+0.13}_{-0.08}$	$20.15^{+0.08}_{-0.07}$	$21.18^{+0.06}_{-0.13}$	$21.26^{+0.05}_{-0.11}$	84^{+16}_{-11}	$-0.79^{+0.13}_{-0.09}$
HD101190	$20.22^{+0.05}_{-0.13}$	$20.03^{+0.04}_{-0.10}$	$20.43^{+0.04}_{-0.08}$	$21.24^{+0.03}_{-0.06}$	$21.35^{+0.03}_{-0.05}$	64^{+10}_{-6}	$-0.62^{+0.07}_{-0.09}$
HD103779	19.46 ± 0.15	19.68 ± 0.08	19.90 ± 0.08	21.17 ± 0.05	21.21 ± 0.05	101^{+32}_{-19}	-1.02 ± 0.09
HD104705	$19.67^{+0.09}_{-0.10}$	$19.76^{+0.09}_{-0.17}$	$20.02^{+0.07}_{-0.10}$	$21.15^{+0.06}_{-0.05}$	$21.21^{+0.05}_{-0.04}$	85^{+18}_{-14}	$-0.90^{+0.08}_{-0.11}$
HD108639	19.68 ± 0.14	$19.72^{+0.13}_{-0.19}$	$20.01^{+0.10}_{-0.11}$	$21.36^{+0.04}_{-0.03}$	$21.40^{+0.04}_{-0.03}$	80^{+24}_{-15}	$-1.09^{+0.10}_{-0.12}$
HD109399	19.76 ± 0.12	19.62 ± 0.12	20.01 ± 0.09	$21.11^{+0.05}_{-0.06}$	$21.17^{+0.04}_{-0.05}$	67^{+12}_{-9}	-0.86 ± 0.10
HD111934	20.11 ± 0.21	$19.98^{+0.17}_{-0.13}$	$20.37^{+0.15}_{-0.14}$	$21.32^{+0.06}_{-0.14}$	$21.41^{+0.06}_{-0.11}$	69^{+21}_{-14}	$-0.72^{+0.18}_{-0.16}$
HD114886	19.90 ± 0.11	$20.07^{+0.08}_{-0.12}$	$20.30^{+0.07}_{-0.08}$	$21.34^{+0.06}_{-0.05}$	$21.41^{+0.05}_{-0.04}$	92^{+21}_{-14}	$-0.82^{+0.08}_{-0.09}$
HD115071	$20.37^{+0.04}_{-0.11}$	$20.29^{+0.10}_{-0.14}$	$20.63^{+0.06}_{-0.08}$	$21.39^{+0.04}_{-0.09}$	$21.51^{+0.04}_{-0.07}$	73^{+11}_{-10}	-0.58 ± 0.09
HD115455	20.24 ± 0.06	$20.24^{+0.12}_{-0.07}$	$20.55^{+0.07}_{-0.05}$	$21.38^{+0.05}_{-0.09}$	$21.49^{+0.04}_{-0.07}$	78^{+12}_{-8}	$-0.63^{+0.10}_{-0.07}$
HD116781	$19.66^{+0.09}_{-0.11}$	19.86 ± 0.12	$20.08^{+0.09}_{-0.08}$	21.21 ± 0.05	21.27 ± 0.04	99^{+27}_{-18}	-0.89 ± 0.10
HD116852	$19.48^{+0.15}_{-0.11}$	19.40 ± 0.09	$19.75^{+0.09}_{-0.07}$	20.96 ± 0.04	21.01 ± 0.04	71^{+12}_{-10}	$-0.96^{+0.10}_{-0.08}$
HD122879	$19.88^{+0.11}_{-0.08}$	20.12 ± 0.09	$20.33^{+0.07}_{-0.06}$	$21.31^{+0.06}_{-0.05}$	$21.39^{+0.05}_{-0.04}$	103^{+22}_{-16}	-0.77 ± 0.08
HD124314	20.13 ± 0.09	$20.06^{+0.16}_{-0.14}$	$20.41^{+0.09}_{-0.08}$	$21.41^{+0.06}_{-0.04}$	$21.49^{+0.05}_{-0.04}$	72^{+15}_{-10}	-0.79 ± 0.10
HD124979	20.08 ± 0.07	$20.12^{+0.05}_{-0.15}$	$20.39^{+0.05}_{-0.08}$	21.27 ± 0.09	21.37 ± 0.07	79 ± 10	$-0.69^{+0.09}_{-0.11}$
HD137595	$20.26^{+0.09}_{-0.07}$	20.31 ± 0.08	20.59 ± 0.06	$20.97^{+0.06}_{-0.08}$	$21.24^{+0.04}_{-0.05}$	81^{+12}_{-9}	$-0.34^{+0.08}_{-0.07}$
HD144965	$20.47^{+0.04}_{-0.05}$	$20.39^{+0.13}_{-0.06}$	$20.74^{+0.07}_{-0.04}$	$20.97^{+0.09}_{-0.30}$	$21.31^{+0.06}_{-0.12}$	72^{+10}_{-6}	$-0.25^{+0.13}_{-0.08}$
HD147888	$20.36^{+0.05}_{-0.08}$	19.73 ± 0.13	$20.45^{+0.05}_{-0.07}$	$21.68^{+0.08}_{-0.19}$	$21.73^{+0.07}_{-0.17}$	47^{+5}_{-4}	$-0.97^{+0.18}_{-0.11}$
HD148422	19.92 ± 0.13	$19.71^{+0.19}_{-0.10}$	$20.15^{+0.11}_{-0.10}$	$21.24^{+0.09}_{-0.06}$	$21.31^{+0.08}_{-0.05}$	65^{+14}_{-9}	$-0.87^{+0.12}_{-0.13}$
HD148937	$20.40^{+0.08}_{-0.04}$	20.35 ± 0.09	$20.68^{+0.06}_{-0.05}$	$21.48^{+0.06}_{-0.11}$	$21.60^{+0.05}_{-0.08}$	73^{+9}_{-7}	$-0.61^{+0.10}_{-0.08}$
HD151805	$20.15^{+0.08}_{-0.11}$	$19.91^{+0.14}_{-0.19}$	$20.35^{+0.07}_{-0.09}$	21.33 ± 0.05	21.41 ± 0.04	62^{+11}_{-9}	$-0.76^{+0.09}_{-0.10}$
HD152249	20.02 ± 0.11	19.90 ± 0.14	20.28 ± 0.09	21.38 ± 0.07	21.45 ± 0.06	69^{+14}_{-10}	-0.87 ± 0.11
HD152424	20.27 ± 0.06	$20.41^{+0.06}_{-0.19}$	$20.65^{+0.05}_{-0.11}$	$21.48^{+0.06}_{-0.07}$	$21.59^{+0.05}_{-0.06}$	90^{+14}_{-17}	$-0.65^{+0.08}_{-0.12}$
HD152590	20.21 ± 0.12	$20.08^{+0.17}_{-0.15}$	20.47 ± 0.10	$21.37^{+0.07}_{-0.03}$	$21.47^{+0.06}_{-0.03}$	69^{+16}_{-11}	-0.72 ± 0.11
HD156359	17.74 ± 0.27	17.70 ± 0.30	$18.07^{+0.21}_{-0.23}$	$20.80^{+0.10}_{-0.06}$	$20.80^{+0.10}_{-0.06}$	75^{+51}_{-22}	$-2.45^{+0.22}_{-0.25}$
HD163522	$19.26^{+0.26}_{-0.11}$	19.36 ± 0.25	$19.66^{+0.19}_{-0.18}$	$21.14^{+0.08}_{-0.07}$	$21.17^{+0.08}_{-0.07}$	82^{+52}_{-21}	-1.21 ± 0.20
HD165246	19.78 ± 0.12	$19.87^{+0.09}_{-0.06}$	$20.14^{+0.07}_{-0.06}$	$21.41^{+0.03}_{-0.04}$	$21.46^{+0.03}_{-0.04}$	87^{+16}_{-13}	$-1.01^{+0.08}_{-0.07}$
HD167402	$19.80^{+0.14}_{-0.07}$	19.69 ± 0.11	$20.06^{+0.10}_{-0.07}$	$21.13^{+0.05}_{-0.04}$	21.20 ± 0.04	69^{+12}_{-9}	$-0.84^{+0.10}_{-0.08}$
HD168941	19.84 ± 0.07	$19.76^{+0.14}_{-0.11}$	$20.11^{+0.08}_{-0.07}$	$21.18^{+0.05}_{-0.07}$	$21.25^{+0.04}_{-0.06}$	72^{+13}_{-8}	$-0.84^{+0.10}_{-0.08}$
HD170740	$20.67^{+0.08}_{-0.17}$	20.40 ± 0.15	$20.86^{+0.08}_{-0.12}$	$21.09^{+0.06}_{-0.17}$	$21.41^{+0.06}_{-0.10}$	62^{+12}_{-9}	$-0.25^{+0.13}_{-0.14}$
HD177989	19.99 ± 0.12	$19.61^{+0.24}_{-0.22}$	20.16 ± 0.12	$20.99^{+0.05}_{-0.06}$	21.11 ± 0.05	56^{+14}_{-9}	-0.64 ± 0.13
HD178487	20.25 ± 0.11	20.14 ± 0.15	20.51 ± 0.09	$21.22^{+0.04}_{-0.10}$	$21.36^{+0.04}_{-0.08}$	70^{+15}_{-10}	$-0.54^{+0.12}_{-0.11}$
HD179407	19.97 ± 0.14	$19.90^{+0.08}_{-0.19}$	$20.23^{+0.09}_{-0.11}$	$21.20^{+0.06}_{-0.10}$	$21.28^{+0.05}_{-0.08}$	70^{+17}_{-12}	-0.75 ± 0.12
HD185418	$20.34^{+0.11}_{-0.07}$	20.47 ± 0.08	$20.72^{+0.07}_{-0.06}$	$21.19^{+0.05}_{-0.04}$	$21.42^{+0.04}_{-0.03}$	89^{+15}_{-12}	-0.40 ± 0.07

Table 5 continued on next page

Table 5 (*continued*)

Star	log $N(\text{H}_2)$			log $N(\text{H I})$	log $N(\text{H}_{\text{tot}})$ (Total H)	T_{01}	log $f(\text{H}_2)$
	$J = 0$	$J = 1$	Total				
(1)	(2)	(3)	(4)	(5)	(6)	(7)	(8)
HD191877	19.73 ^{+0.27} _{-0.10}	19.68 ^{+0.03} _{-0.17}	20.00 ^{+0.17} _{-0.10}	21.03 ± 0.05	21.11 ± 0.05	68 ⁺¹⁹ ₋₁₂	-0.81 ^{+0.17} _{-0.11}
HD192035	20.40 ^{+0.07} _{-0.03}	20.18 ^{+0.17} _{-0.03}	20.63 ^{+0.09} _{-0.05}	21.20 ^{+0.04} _{-0.10}	21.39 ^{+0.04} _{-0.07}	63 ⁺¹² ₋₄	-0.44 ^{+0.11} _{-0.07}
HD195455	17.96 ^{+0.12} _{-0.31}	18.24 ^{+0.26} _{-0.21}	18.42 ^{+0.19} _{-0.16}	20.61 ^{+0.04} _{-0.09}	20.62 ^{+0.04} _{-0.09}	122 ⁺¹⁴⁶ ₋₄₄	-1.87 ^{+0.21} _{-0.17}
HD195965	19.99 ^{+0.11} _{-0.12}	19.95 ^{+0.10} _{-0.11}	20.28 ± 0.08	20.92 ± 0.05	21.09 ± 0.04	74 ⁺¹⁴ ₋₁₀	-0.51 ± 0.09
HD198478	20.43 ^{+0.33} _{-0.19}	20.21 ^{+0.53} _{-0.23}	20.76 ^{+0.33} _{-0.35}	21.32 ^{+0.12} _{-0.13}	21.53 ^{+0.13} _{-0.12}	63 ⁺⁶³ ₋₁₇	-0.48 ^{+0.35} _{-0.37}
HD198781	20.27 ^{+0.08} _{-0.07}	20.04 ^{+0.16} _{-0.28}	20.48 ^{+0.08} _{-0.10}	20.93 ^{+0.07} _{-0.03}	21.17 ± 0.05	61 ⁺¹² ₋₁₁	-0.40 ^{+0.10} _{-0.11}
HD201345	18.83 ^{+0.06} _{-0.20}	19.22 ± 0.16	19.36 ± 0.12	21.00 ^{+0.05} _{-0.06}	21.02 ^{+0.05} _{-0.06}	141 ⁺¹⁰⁰ ₋₄₃	-1.35 ^{+0.14} _{-0.13}
HD202347	19.62 ^{+0.17} _{-0.15}	19.71 ^{+0.09} _{-0.11}	19.98 ^{+0.10} _{-0.09}	20.83 ^{+0.08} _{-0.10}	20.94 ^{+0.07} _{-0.08}	85 ⁺²⁴ ₋₁₅	-0.66 ^{+0.12} _{-0.11}
HD203374	20.36 ^{+0.09} _{-0.05}	20.35 ^{+0.10} _{-0.06}	20.67 ^{+0.07} _{-0.05}	21.20 ^{+0.05} _{-0.04}	21.41 ^{+0.04} _{-0.03}	76 ⁺¹⁰ ₋₇	-0.44 ^{+0.07} _{-0.06}
HD206267	20.59 ^{+0.10} _{-0.06}	20.47 ^{+0.14} _{-0.12}	20.85 ^{+0.08} _{-0.07}	21.22 ^{+0.06} _{-0.04}	21.49 ^{+0.05} _{-0.04}	69 ⁺¹³ ₋₈	-0.35 ^{+0.09} _{-0.08}
HD206773	20.01 ^{+0.09} _{-0.03}	20.18 ^{+0.07} _{-0.15}	20.41 ^{+0.06} _{-0.09}	21.09 ^{+0.07} _{-0.03}	21.24 ^{+0.05} _{-0.03}	91 ⁺¹⁸ ₋₁₃	-0.54 ^{+0.07} _{-0.10}
HD207198	20.59 ± 0.05	20.34 ^{+0.10} _{-0.08}	20.79 ± 0.05	21.28 ^{+0.07} _{-0.09}	21.50 ^{+0.05} _{-0.06}	61 ⁺⁶ ₋₅	-0.41 ± 0.07
HD207308	20.66 ^{+0.07} _{-0.09}	20.23 ± 0.12	20.80 ^{+0.06} _{-0.07}	21.20 ^{+0.06} _{-0.05}	21.46 ± 0.04	54 ⁺⁶ ₋₅	-0.36 ^{+0.07} _{-0.08}
HD207538	20.60 ^{+0.07} _{-0.08}	20.49 ± 0.11	20.85 ± 0.06	21.27 ^{+0.06} _{-0.07}	21.52 ^{+0.04} _{-0.05}	70 ⁺¹⁰ ₋₈	-0.36 ± 0.08
HD208440	20.04 ^{+0.15} _{-0.10}	19.87 ^{+0.16} _{-0.12}	20.28 ^{+0.11} _{-0.09}	21.24 ^{+0.06} _{-0.04}	21.33 ^{+0.05} _{-0.04}	66 ⁺¹⁴ ₋₁₀	-0.75 ^{+0.12} _{-0.11}
HD209339	19.78 ^{+0.07} _{-0.17}	19.89 ^{+0.08} _{-0.18}	20.13 ^{+0.06} _{-0.11}	21.20 ± 0.04	21.27 ± 0.04	87 ⁺²⁶ ₋₁₇	-0.84 ^{+0.08} _{-0.12}
HD210809	19.54 ± 0.09	19.75 ^{+0.17} _{-0.14}	19.97 ^{+0.12} _{-0.09}	21.31 ^{+0.06} _{-0.05}	21.35 ^{+0.06} _{-0.05}	100 ⁺³⁴ ₋₁₉	-1.08 ^{+0.13} _{-0.11}
HD210839	20.54 ± 0.06	20.46 ± 0.09	20.80 ± 0.05	21.24 ± 0.05	21.48 ± 0.04	72 ⁺⁹ ₋₇	-0.38 ^{+0.06} _{-0.07}
HD218915	19.79 ^{+0.12} _{-0.10}	19.91 ^{+0.06} _{-0.07}	20.16 ± 0.06	21.20 ^{+0.07} _{-0.06}	21.27 ^{+0.06} _{-0.05}	88 ⁺¹⁵ ₋₁₂	-0.81 ± 0.08
HD219188	18.82 ^{+0.21} _{-0.07}	19.20 ^{+0.12} _{-0.09}	19.38 ^{+0.11} _{-0.09}	20.72 ^{+0.07} _{-0.05}	20.76 ^{+0.06} _{-0.05}	126 ⁺⁴⁹ ₋₃₄	-1.09 ^{+0.12} _{-0.11}
HD220057	20.06 ^{+0.12} _{-0.06}	19.84 ^{+0.11} _{-0.14}	20.27 ^{+0.09} _{-0.07}	20.95 ^{+0.14} _{-0.23}	21.11 ^{+0.10} _{-0.15}	62 ⁺¹⁰ ₋₇	-0.52 ^{+0.17} _{-0.13}
HD224151	20.21 ^{+0.03} _{-0.08}	20.31 ^{+0.09} _{-0.19}	20.55 ^{+0.06} _{-0.10}	21.35 ^{+0.05} _{-0.08}	21.47 ^{+0.04} _{-0.06}	88 ⁺¹³ ₋₁₈	-0.61 ^{+0.09} _{-0.11}
HDE232522	19.88 ^{+0.13} _{-0.11}	19.90 ^{+0.03} _{-0.17}	20.18 ^{+0.08} _{-0.10}	21.12 ^{+0.04} _{-0.05}	21.21 ± 0.04	76 ⁺¹⁸ ₋₁₂	-0.73 ^{+0.09} _{-0.11}
HDE303308	19.81 ± 0.08	19.97 ^{+0.07} _{-0.11}	20.20 ^{+0.05} _{-0.07}	21.41 ^{+0.03} _{-0.08}	21.46 ^{+0.03} _{-0.07}	92 ⁺¹⁶ ₋₁₂	-0.95 ^{+0.09} _{-0.08}
HDE308813	19.95 ^{+0.08} _{-0.12}	19.88 ^{+0.10} _{-0.05}	20.23 ± 0.07	21.20 ^{+0.06} _{-0.04}	21.28 ^{+0.05} _{-0.04}	74 ⁺¹¹ ₋₉	-0.76 ^{+0.08} _{-0.09}

^a Values of N are expressed in units of cm^{-2} . All uncertainties in this table represent possible deviations at a level estimated to be 1.5σ . The outcomes in columns 4, 6, 7 and 8 have small offsets from the linear combinations of quantities expressed in other columns in recognition of shifts that are required when quantities with asymmetric errors are utilized, as described in Section 3.2.

4. DERIVATIONS OF F_*

As indicated in Section 2.1, comparisons of the column densities of the strongly depleted elements Mg and Mn to those of H_{tot} indicate the overall strengths of depletions F_* for the different sight lines. For either element, we evaluate the equation

$$F_* = \frac{[X_{\text{gas}}/\text{H}] - B_X}{A_X} + z_X, \quad (6)$$

where X denotes either Mg or Mn and the coefficients A_X , B_X , and z_X are listed in Table 4 of J09.⁷ Column 10 of Table 1 lists weighted means of the F_* values derived from these two elements. Special care must be exercised in deriving the values and uncertainties of these means, since both of the individual contributions rely in part on a single quantity $N(\text{H}_{\text{tot}})$. Our derivations of weighted means for F_* made use of a special treatment that accounted for the errors that were common to both measurements (Robinson 2016 pp. 91-95).

5. STARLIGHT INTENSITIES

Ultraviolet and visible photons from stars have a major influence on the physical state and chemistry of gas in H I regions. They photoionize many of the heavy elements and thus produce free electrons, they irradiate dust grains that then eject photoelectrons (which are then a source of heating), they may liberate loosely bound atoms from grains via photodesorption, and they photodissociate molecular hydrogen and other molecular species. For these reasons, photons may have either direct or indirect influences on the atomic species being investigated in this study. In many instances, the gas can be exposed to a strongly elevated radiation field because a large fraction of the interstellar matter can reside in a dense gas complex that once formed the target star and its neighbors. Conversely, much of the gas near the star may be completely ionized or blown away by stellar winds, and thus most of the neutral material along the sight line could be in some random location well removed from the UV-bright stars. For these reasons, we consider the intensity of the radiation field a useful parameter to include in our investigation of depletions.

About half of the targets in our survey were included in the study of interstellar thermal pressures by Jenkins & Tripp (2011). They evaluated the characteristic starlight intensities for the gas in the sight lines by studying the balance between neutral and singly ionized carbon atoms and then applying an interpretation based on the competition between the photoionizations and the recombinations with free electrons and dust grains. They tabulated their calculated values for the intensities of starlight I at energies above the ionization potential of neutral carbon (11.26 eV) in terms of $\log(I/I_0)$, where I_0 is the average intensity at our location in the Milky Way determined by Mathis et al. (1983). Values of $\log(I/I_0)$ from Jenkins & Tripp (2011) are listed in Column 10 of Table 1. All of the values listed here are positive, which reinforces the concept that in each case most of the gas is near the target star and is thus subjected to a stronger-than-usual radiation field.

⁷ B_{Mn} was increased by 0.16 dex to compensate for the reduction in the adopted value of $\log f\lambda$ for this element; see Column 5 of Table 3.

spanning large distances across other spiral arms in the Galaxy. Ritchey et al. (2018) recognized the importance of using a strong absorption feature (in their case, the 1355 Å line of O I) to define the velocity limits and gave specific examples where their results gave larger values of $N(\text{Kr I})$ than previous determinations that were based purely on the appearance of the weak line being measured.

Out of the 51 cases where Kr absorption was detected, there are 28 of them that have positive 1σ error bars for $\log(\text{Kr}/\text{H}_{\text{tot}})$ that are below our adopted protosolar $\log(\text{Kr}/\text{H})$. For the upper limits, 24 out of 49 are below the protosolar value at the 1σ level of confidence. If the interstellar values of (Kr/H) were indeed equal to the protosolar value and all of the apparent deficiencies of Kr were due only to measurement errors, we would have expected to find a grand total of only 16 such examples. However, it should be noted that the disparity between $(28 + 24)$ and 16 decreases markedly if one claims that $\log(\text{Kr}/\text{H})_{\text{ref}}$ drops below -8.71 because many of the upper error bars are just slightly below the dashed line in Figure 3. As an added assurance that the lowest outcomes for measured detections and upper limits for $\log(\text{Kr}/\text{H}_{\text{tot}})$ were real, the spectra were reinspected to see whether any anomalies in the observations might have been present. No anomalies were apparent for these cases.

We cannot claim that there is any evidence that (Kr/H) might occasionally be above the protosolar value, since there are only four detections that have their lower error bars above this level. These cases could simply be accidental deviations. However, the existence of such outcomes plus others at the high end of the distribution gives us confidence that an appropriate reference abundance is probably not much lower than our adopted value of $\log(\text{Kr}/\text{H})_{\text{ref}} = -8.71$.

6.2. Partial Correlations of Depletions with F_* and $\log f(H_2)$

We begin our study of depletions by comparing them with two variable parameters, F_* and $\log f(H_2)$, that have been determined for all of the sight lines that were available. Later (Section 6.3 below), we will expand the parameters to include $\log(I/I_0)$, but for a smaller number of examples, i.e., only for target stars that are in common with those in the investigation by Jenkins & Tripp (2011).

If the quantities F_* and $\log f(H_2)$ were very strongly correlated with each other for the different sight lines, it would be impossible to identify which of the two parameters was responsible for any depletion trend. Fortunately, even though F_* has some relationship with molecular fractions (see Figure 16 of J09), the correlation is weak enough that we can resolve which parameter is influential on depletions (or if they both have an influence). We do this by determining partial correlations, which address the question, if we could hold one of the parameters to a constant value, do variations in the other one drive the depletion in one direction or another?

We propose a simple linear relationship

$$[X_{\text{gas}}/\text{H}] = B_2\{X\} + A_2\{X, F_*\} \left(F_* - z_2\{X, F_*\} \right)$$

$$+ A_2\{X, \log f(\text{H}_2)\} \left(\log f(\text{H}_2) - z_2\{X, \log f(\text{H}_2)\} \right) \quad (7)$$

that describes how, on average, the depletions of element X are influenced by either F_* or $\log f(\text{H}_2)$. (The subscript 2 for the coefficients indicates that there are two free environmental parameters. Later, we will consider three simultaneous parameters and attach a subscript 3 to these same coefficients. Note that the assignments B , A , and z are consistent with the coefficients in Eq. 2 for trends with just F_* .) As was the case for the z term in Eq. 2, the two z constants in Eq. 7 are set to the average value of the associated parameters in our sample so that the errors in B and A have a near-zero covariance. This elimination of the covariances makes it simpler to understand the uncertainties for other applications that make use of B and A .

Our task of performing a multiparameter regression must accommodate two complicating factors. One is that we must include those determinations that happen to be upper limits instead of positive detections. The proportions of upper limits for measurements of O and Ge are low (11% and 3%, respectively), but the upper limit fraction for Kr is 49%. The other complication is that the errors in measuring $N(\text{H}_{\text{tot}})$ have a simultaneous influence on the two independent variables F_* and $\log f(\text{H}_2)$ and also the dependent variable $\log(X/\text{H})$. Hence, the off-diagonal elements of the covariance matrices are nonzero, and this effect can either strengthen or weaken an inferred correlation and lead to a bias in the slope coefficients $A_2\{X, F_*\}$ and $A_2\{X, \log f(\text{H}_2)\}$ (Kelly 2007). To cope with these two complications, we employ the analysis package `mlinmix_err` developed by Kelly (2007)⁸, which employs a Bayesian approach to linear regression. One drawback of this routine is that it does not accommodate asymmetric errors, so we must convert the errors to a symmetric form equal to $(\sigma^+ + \sigma^-)/2$ for all measured quantities. The output that shows the joint probability distributions for the constants $B_2\{X\}$, $A_2\{X, F_*\}$, and $A_2\{X, \log f(\text{H}_2)\}$ is obtained from a Gibbs sampler that performs random draws from the posterior distribution in a Markov chain Monte Carlo (MCMC) method.

The upper portion of Table 6 shows the numerical values for $B_2\{X\}$, $A_2\{X, F_*\}$, and $A_2\{X, \log f(\text{H}_2)\}$ for the three elements, along with their uncertainties. The preferred values were obtained from the medians of the marginalized probability functions, and the uncertainties were computed by matching the cumulative distributions of these probabilities to that of a Gaussian at the $\pm 1\sigma$ points. The joint probability distributions are shown in 2-dimensional form in Figures 4 and 5, along with the marginalized outcomes shown as simple graphs.

While the slope coefficients $A_2\{\text{O}, F_*\}$ and $A_2\{\text{Kr}, F_*\}$ are negative, as expected from earlier studies (J09, Ritchey et al. 2018), their significance levels are poor. However, the negative trend for $[\text{Ge}_{\text{gas}}/\text{H}]$ against F_* is clearly established. All three elements appear to show no dependence on $\log f(\text{H}_2)$, which is consistent with the findings of Meyer et al. (1994); (1998) and André et al. (2003) for O and Cartledge

⁸ This software is available at <https://idlastro.gsfc.nasa.gov/ftp/pro/math/>.

et al. (2008) for Kr. The elongations and backward slants of the shapes of the joint distributions of F_* and $\log f(\text{H}_2)$ for all three elements arise from the mild correlation of the two independent variables for the stars that were sampled. (If such correlations happened to be stronger, the elongations of the distributions would be even more severe.)

The effects of measurement error covariances are important, and they appear to have been neglected in previous studies. As an experiment, if we perform a test run where we ignore the covariances by artificially setting them to zero and leave the diagonal error terms as they were, we find that that $A_2\{\text{O}, F_*\} = -0.20 (+0.09, -0.08)$, and $A_2\{\text{Kr}, F_*\} = -0.32 (+0.19, -0.17)$. After comparing these outcomes with their counterparts in Table 6, it is clear that they are stronger and have a higher level of significance above zero. When the real depletion trend is intrinsically strong, neglecting the covariances is not so important: the value $A_2\{\text{Ge}, F_*\} = -0.39 \pm 0.06$, which is just slightly stronger than the outcome where the covariances were included.

Table 6. Depletion Coefficients

Coefficient	$X = \text{O}$	$X = \text{Ge}$	$X = \text{Kr}$
$(X/\text{H})_{\text{ref}}^a$	8.76 ^{b,c}	3.69 ^c	3.29 ^c
$B_2\{X\}^d$	-0.13 ± 0.11	-0.49 ± 0.006	$-0.16 (+0.023, -0.027)$
$A_2\{X, F_*\}$	$-0.09 (+0.10, -0.09)$	-0.30 ± 0.06	$-0.14 (+0.22, -0.19)$
$z_2\{X, F_*\}$	0.538	0.531	0.531
$A_2\{X, \log f(\text{H}_2)\}$	0.00 ± 0.05	-0.03 ± 0.03	$0.01 (+0.11, -0.12)$
$z_2\{X, \log f(\text{H}_2)\}$	-0.826	-0.843	-0.843
$B_3\{X\}^d$	-0.14 ± 0.14	-0.49 ± 0.008	-0.13 ± 0.034
$A_3\{X, F_*\}$	-0.28 ± 0.13	$-0.24 (+0.09, -0.08)$	$-0.16 (+0.23, -0.21)$
$z_3\{X, F_*\}$	0.543	0.531	0.531
$A_3\{X, \log f(\text{H}_2)\}$	0.18 ± 0.08	-0.06 ± 0.05	$0.11 (+0.14, -0.16)$
$z_3\{X, \log f(\text{H}_2)\}$	-0.801	-0.825	-0.825
$A_3\{X, \log(I/I_0)\}$	0.18 ± 0.08	-0.04 ± 0.06	-0.16 ± 0.16
$z_3\{X, \log(I/I_0)\}$	0.449	0.460	0.460

^aAdopted protosolar abundances on a logarithmic scale where $\text{H} = 12$.

^bSee the discussion in Section 1.1.

^cProtosolar abundances generated from the solar photospheric abundances compiled by Asplund et al. (2009) plus a 0.04 dex correction that they suggested for gravitational settling.

^dThe uncertainties listed for the B coefficients apply only to those associated with the determinations of ISM abundances (X_{gas}/H) in this paper. They do not include uncertainties in the reference abundances.

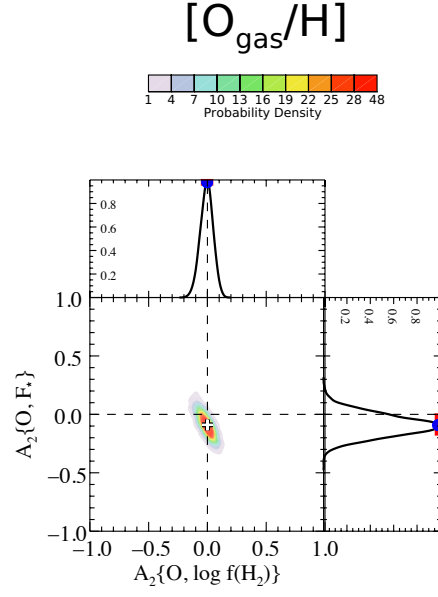


Figure 4. The relative joint probabilities of the slope coefficients $A_2\{O, F_*\}$ and $A_2\{O, \log f(\text{H}_2)\}$ (color display) and their marginalized distributions (plots with curves). At the tops of the distribution plots, the preferred values and ranges inside $\pm 1\sigma$ limits are shown with a blue circle and red bar, respectively.

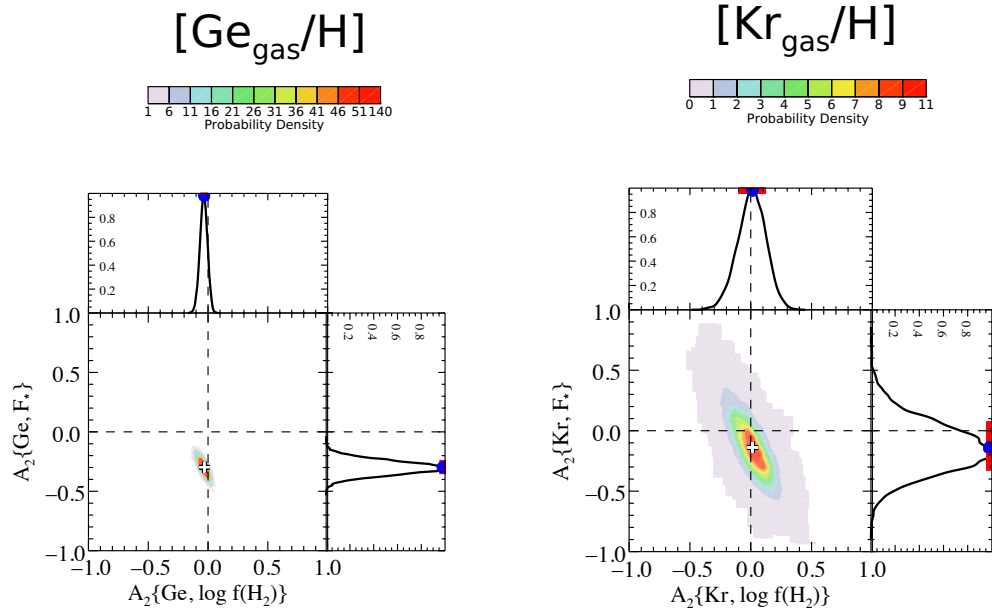


Figure 5. Same displays as that shown in Fig. 4, except for the elements Ge and Kr.

6.3. Trends That Include Starlight Intensities

We now move on to investigate the possible influence of a third physical variable, $\log(I/I_0)$ presented in Section 5, but for a reduced number of sight lines. Using the same construction as that employed for Eq. 7, we state that

$$\begin{aligned} [X_{\text{gas}}/\text{H}] = & B_3\{X\} + A_3\{X, F_*\} \left(F_* - z_3\{X, F_*\} \right) \\ & + A_3\{X, \log f(\text{H}_2)\} \left(\log f(\text{H}_2) - z_3\{X, \log f(\text{H}_2)\} \right) \\ & + A_3\{X, \log(I/I_0)\} \left(\log(I/I_0) - z_3\{X, \log(I/I_0)\} \right) \end{aligned} \quad (8)$$

The lower portion of Table 6 lists the solutions for the coefficients in Eq. 8, and Figs. 6, 7 and 8 show the probability distributions in the same style as those presented in the previous section (Figs. 4 and 5) .

The recognition that there may be three possible influences on the element depletions has resulted in some important changes in the outcomes. The strength of the trend of the depletion of O with F_* now appears to be stronger than before, and its significance has improved even though the sample size is smaller and the error in the coefficient is slightly larger. Evidently, our consideration of an extra parameter, the starlight intensity, has revealed trends that were otherwise hidden by its influence on the gas-phase abundances. It is interesting to note, however, that the value for

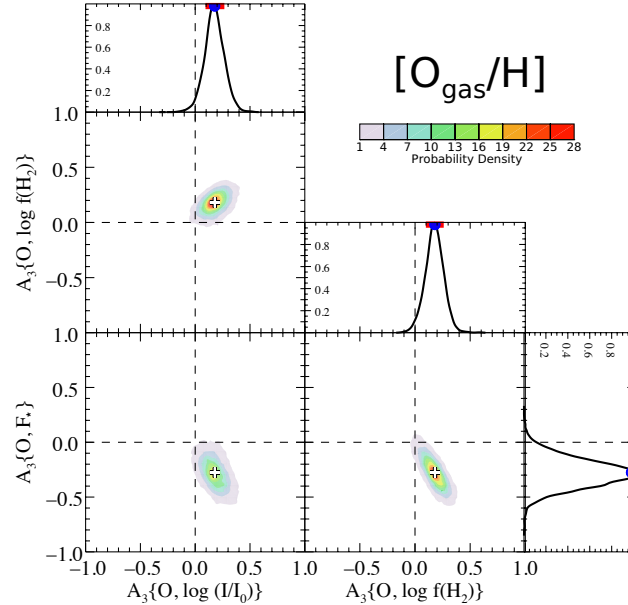


Figure 6. Relative joint probabilities of the slope coefficients $A_3\{O, F_*\}$, $A_3\{O, \log f(\text{H}_2)\}$, and $A_3\{O, \log(I/I_0)\}$, (color displays). Each panel depicts the distribution of the probabilities for two coefficients as they would appear in projection over the distribution of the third, unspecified coefficient. The plots on the sides showing the curves indicate the probability distributions for a single coefficient marginalized over the distributions of the other two quantities. At the tops of the distribution plots, the preferred values and ranges inside $\pm 1\sigma$ limits are shown with a blue circle and red bar, respectively.

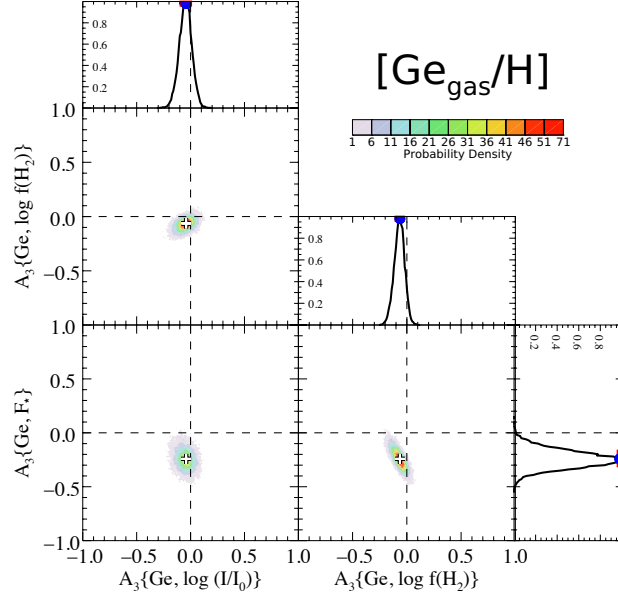


Figure 7. Same display as that shown in Fig. 6, except for the element Ge.

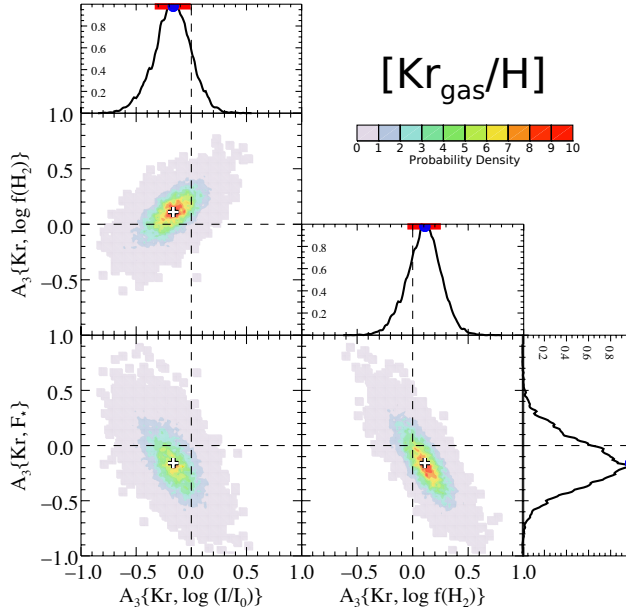


Figure 8. Same display as that shown in Fig. 6, except for the element Kr.

$A_3\{\text{O}, F_*\} = -0.28 \pm 0.13$ found here is roughly consistent with $A_{\text{O}} = -0.225 \pm 0.053$ derived by J09, which was based on a dependence on F_* alone (but for a larger sample size and a somewhat different selection of stars). As we found earlier, the negative slope of the major axis of the probability cloud projected on the $A_3\{\text{O}, \log f(\text{H}_2)\} - A_3\{\text{O}, F_*\}$ plane arises from the mild correlation between $\log f(\text{H}_2)$ and F_* . A positive slope seen for the cloud on the $A_3\{\text{O}, \log(I/I_0)\} - A_3\{\text{O}, \log f(\text{H}_2)\}$ plane arises from a weak anticorrelation between the molecular abundances and starlight

intensity. These two effects are simply a consequence of the conditions that exist in our sample.

An important outcome is the fact that the oxygen A_3 slope coefficients for both the molecular fractions and starlight intensities exhibit significant positive values. If we multiply the best values for the A_3 coefficients for O by the spans over which their accompanying parameters vary in our sample, we find that both F_* and $\log(H_2)$ each account for depletion changes of about ± 0.15 dex. For $\log(I/I_0)$ the changes amount to about ± 0.07 dex. Typical uncertainties in $\log(O_{\text{gas}}/H)$ range from 0.05 to 0.20 dex, but 70% of the cases are below 0.10 dex. One can appreciate that the effects of any of the three environmental conditions on typical single cases are usually difficult to identify with much confidence.

The distribution for $A_3\{\text{Kr}, F_*\}$ seems to be almost the same as that for $A_2\{\text{Kr}, F_*\}$. All three of the A_3 coefficients for Kr differ from zero, but only at about or slightly less than the 1σ level of significance. The result for $A_3\{\text{Kr}, F_*\}$ is not as definitive as the determination of A_{Kr} in the study by Ritchey et al. (2018), who found that this coefficient differed from zero at the 2.8σ significance level. However, the preferred value of $A_3\{\text{Kr}, F_*\}$ is identical to the value of A_{Kr} listed in J09 and not far from that of Ritchey et al. (2018). Our general finding for the strength of the depletions, as indicated by $B_3\{\text{Kr}\}$, is less than all previous determinations. We attribute the apparent weaker depletions of Kr to two important differences in analysis methodologies. First, as discussed in Section 3.1, our adoption of generously wide velocity limits from the appearance of strong lines often increased the outcomes for the values of the column densities (and also their uncertainties because more noise and stretches of continuum had to be incorporated into the measurements). Second, as pointed out in Section 6.2, any neglect of error covariances can produce misleading results. This brought about a need to construct a probability distribution for the depletion trends with F_* that acknowledged and corrected for the effect that errors in $N(H_{\text{tot}})$ induce a spurious strengthening of the trend (i.e., any erroneous increase in $N(H_{\text{tot}})$ creates an increase in F_* at the same time that it lowers the inferred $[\text{Kr}_{\text{gas}}/H]$, which then strengthens a negative correlation). Larger uncertainties may also arise from the fact that we are examining the dependence of depletions on more than one parameter.

The negative trend for $[\text{Ge}_{\text{gas}}/H]$ against F_* is still significant, although its magnitude has decreased slightly from that expressed by the A_2 coefficient, and it seems much less steep than the relationships $A_{\text{Ge}} = -0.615 \pm 0.083$ and -0.371 ± 0.081 found by J09 and Ritchey et al. (2018), respectively. It is probable that the diminished response to F_* compared to the findings of the previous studies arises from the effects discussed above for Kr. The magnitudes of the behaviors of $[\text{Ge}_{\text{gas}}/H]$ against $\log f(H_2)$ and $\log(I/I_0)$ are similar to those of $[\text{O}_{\text{gas}}/H]$, but with a reversal of sign.

7. INTERPRETATION

The consideration of partial correlations of the abundances of free O, Ge, and Kr atoms with two environmental conditions other than F_* should provide clues on secondary processes that may either enhance or reduce the atomic depletions. At this stage, we can offer speculations about the meanings of these other trends, which might encourage future investigators to follow up on specific approaches, either theoretical or observational. In the following subsections, we explore factors beyond F_* derived from comparing Mg and Mn to H, which we acknowledge to be an important factor for driving the depletions of the elements O, Ge, and Kr.

7.1. Influences on $[O_{\text{gas}}/H]$

One might expect that as $f(\text{H}_2)$ increases we would see less O in atomic form because higher molecular hydrogen fractions could be more favorable for creating a chain of reactions that could involve other molecules, some of which could contain oxygen. The near-zero outcome for $A_2\{\text{O}, \log f(\text{H}_2)\}$ indicates that this concept is overly simplistic and probably not important. Instead, after we test for the independent actions of $f(\text{H}_2)$ and starlight intensity I , a subtler picture emerges, where $[O_{\text{gas}}/H]$ shows positive correlations with both of these environmental conditions.

We first address a possible reason why $A_3\{\text{O}, \log f(\text{H}_2)\}$ is significantly above zero. We know that a concentration of molecular hydrogen is governed mostly by a balance between the local rate of formation on dust grains and the photodissociation of the free molecules by starlight. Moreover, the formation rate in any given volume should be proportional to the product of the local densities of atomic hydrogen and dust grains. Since F_* is well correlated with local hydrogen densities, as well as the proportion of elements in the form of dust, we can assert that to first order it can be used as a measure of the H_2 formation rate. This concept, along with the principle that partial correlations are intended to indicate what should happen if we vary one parameter while the others are held constant, can lead to an intriguing conjecture based on the following thought experiment. If we had the ability to peg the destruction rate (proportional to I) to a constant value, and we could do likewise for F_* , from the arguments just presented we would simplistically expect to find $f(\text{H}_2)$ to remain constant. By virtue of our detecting changes in $[O_{\text{gas}}/H]$ with residual deviations in $f(\text{H}_2)$, we discover that there must be variations in the H_2 concentrations caused by some factors (or a single factor) other than F_* or I , and the gas-phase O-to-H ratio seems to respond to such factors. Possible secondary effects could include variations in grain composition or size at fixed values of F_* , which might influence the production rate of H_2 (Snow 1983). In turn, changes in these grain properties could partly influence the concentration of free O atoms for any fixed value of dissociating radiation intensity and dust-to-gas mass ratio. For instance, we could speculate that a dust population that is more strongly dominated by relatively small grains may produce more H_2 , given the increased average surface-to-volume ratio, but these same

grains may more effectively lose any embedded H_2O ice via photodesorption (Cruz-Diaz et al. 2018), and the free water molecules would subsequently be broken up by photodissociation. One might check this proposal by learning more about the extinction properties of dust on the sight lines to see if grain sizes really matter, but that examination is a complex undertaking that is beyond the scope of this study.

Two possibilities may explain the positive value for $A_3\{\text{O}, \log(I/I_0)\}$. One is simply a different approach to the argument presented earlier about the positive outcome for $A_3\{\text{O}, \log f(\text{H}_2)\}$. If F_* and $f(\text{H}_2)$ could be held constant, one would expect that I would need to increase to compensate for any greater efficiency of H_2 production by some differing grain population, and, as proposed before, those same grains could have secondary properties that would make them less able to sequester O atoms. An alternative (or additional) means for explaining the increase in the free oxygen atoms for an increase in I may simply be an enhanced liberation of O arising from the more rapid photodesorption and subsequent photodissociation of H_2O ice that may have resided on the surfaces of dust grains. However, this proposal is disfavored by the observed lack of infrared ice-band features in sight lines with extinctions as low as those in our sample, unless, of course, many of the grains are so large that they are completely opaque in the infrared (Poteet et al. 2015).

7.2. Influences on $[Kr_{\text{gas}}/H]$

We return to the topics discussed in Section 1.2 that addressed possible causes for the depletions of Kr in the ISM. The level of significance of the three A_3 coefficients determined in this study for Kr is not high. Nevertheless, it is useful to explore the possible interpretations of these coefficients if the inferred values are indeed real.

We had dismissed the possibility that positively charged radicals in the gas phase could play an important role in depleting Kr, but from the meteoritic studies and laboratory experiments there were indications that heavier noble gases could bind to solid materials in space. Of special relevance to Kr depletions studied here are the experiments conducted by Nichols et al. (1992) that indicated that enhanced adsorption with stronger binding than a Van der Waals attraction could occur if a surface was irradiated by energetic protons, which create free radicals and broken bonds capable of maintaining strong chemical attractions for the noble gas atoms (Hohenberg et al. 2002).⁹ Ionizing radiation may also be able to create such enhanced binding sites on the surfaces of materials. These findings may account for our observation that Kr depletions not only depend on the presence of solids, as indicated by the negative value of $A_3\{\text{Kr}, F_*\}$, but they also respond to increased levels of UV irradiation that can create more chemically active binding sites, as suggested by the negative value of $A_3\{\text{Kr}, \log(I/I_0)\}$. An alternative explanation for a negative outcome for $A_3\{\text{Kr}, \log(I/I_0)\}$ is that there is a stronger tendency for Kr to be photoionized rela-

⁹ These authors and others often refer to this type of binding as “anomalous adsorption.”

tive to H in low-density regions where some infiltration of Kr-ionizing radiation may occur.

We still face the challenge of interpreting the positive outcome for $A_3\{\text{Kr}, \log f(\text{H}_2)\}$. We speculate that this dependence, if real, may arise from the more effective neutralization of the active sites by gases that have richer concentrations of molecules.

8. REGIONAL VARIATIONS

Now that we have characterized the responses of $[\text{O}_{\text{gas}}/\text{H}]$ and $[\text{Ge}_{\text{gas}}/\text{H}]$ with respect to certain environmental parameters, we can touch on the topic of possible changes in the abundances of these two elements with location. In doing so, it can be instructive to discount the effects of F_* and $f(\text{H}_2)$, so that the shifts attributable only to location are more apparent. In principle, we could also compensate for the influence of I/I_0 , but doing so would significantly limit the number of available samples. We do not address changes in $[\text{Kr}_{\text{gas}}/\text{H}]$ because a high proportion of the measurements are upper limits.

It is important to acknowledge that two considerations might disfavor our being able to detect meaningful changes in abundances with location. First, Roy & Kunth (1995) pointed out that there are a number of hydrodynamical processes that should efficiently mix the interstellar gases at many different distance scales, although hydrodynamical simulations by de Avillez & Mac Low (2002) indicate that the characteristic decay rate for localized chemical inhomogeneities may be as long as tens of megayears. From an observational standpoint, we note that Esteban & García-Rojas (2018) found that the abundances of O relative to H in H II regions in our Galaxy deviate by less than ± 0.05 dex (which is of order their measurement uncertainties) from a best fit to an overall abundance gradient with galactocentric distance. Nevertheless, while mixing effects may be important, we must acknowledge the possibility that infalling, low-metallicity gas impacting the Galactic plane could create temporary dilutions of the existing material in specific regions. The second consideration that may reduce abundance contrasts is that most of our measurements sample gas that is likely to be distributed over many kiloparsecs, which would tend to wash out any fluctuations that we may be looking for. While this could apply in most cases, there may still be instances where much of the material that is sensed happens to be concentrated in the progenitorial star-forming clouds in the immediate vicinity of the target stars.

8.1. *Changes in Corrected $[\text{O}_{\text{gas}}/\text{H}]$ with Location*

From the investigation presented in Section 6.2, we found that $A_2\{\text{O}, \log f(\text{H}_2)\} = 0.00 \pm 0.05$, which indicates that no correction for $\log f(\text{H}_2)$ is needed (unless we were to include $\log(I/I_0)$ as a relevant parameter). However, we do need to compensate for changes in F_* . Thus, we can define a quantity

$$\begin{aligned} \Delta(\text{O}/\text{H}) = & \log N(\text{O I}) - \log N(\text{H}_{\text{tot}}) - (\text{O}/\text{H})_{\text{ref}} + 12 - B_2\{\text{O}\} \\ & - A_2\{\text{O}, F_*\} \left(F_* - z_2\{\text{O}, F_*\} \right), \end{aligned} \quad (9)$$

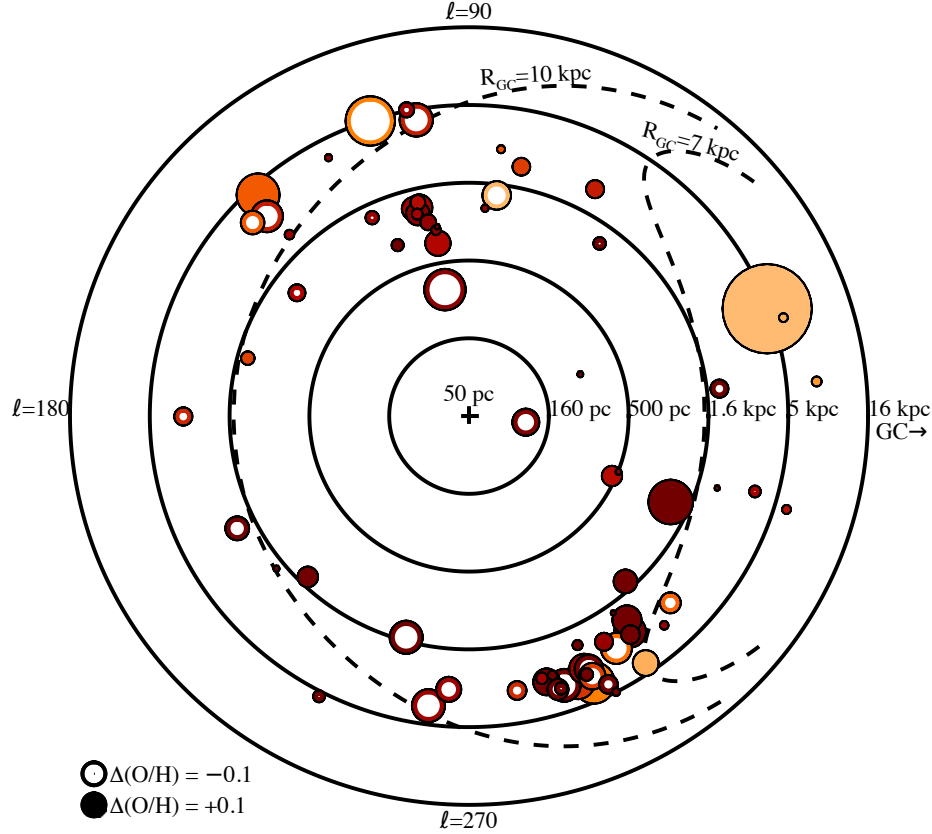


Figure 9. Depiction of the results for $\Delta(\text{O}/\text{H})$ at the locations of 75 targets projected on the plane of the Galaxy, but with distances from the Sun laid out in concentric rings having equal logarithmic intervals. The diameter of each circle that represents a target is proportional to the absolute value of $\Delta(\text{O}/\text{H})$, with solid interiors depicting positive values and open ones depicting negative values. The colors of the symbols (or their borders) represent distances from the Galactic plane, ranging from dark brown for $z \sim 0$ to orange for targets at large distances either above or below the plane. Distances from the Galactic center R_{GC} are indicated by the dashed lines.

which indicates residual deviations from the average behavior of oxygen gas-phase abundances.

Figure 9 depicts the results for $\Delta(\text{O}/\text{H})$ for 75 sight lines that have uncertainties in this quantity that are less than 0.15 dex. This choice for the cutoff in uncertainties was governed by a desire to have a balance between a respectably large number of samples and yet show results that were not too unreliable. Unfortunately, there are too few targets at small distances to test the assertions by Meyer et al. (1994, 1998), André et al. (2003) and Cartledge et al. (2004) that the interstellar gases within about 800 pc of the Sun may have been diluted by the infall of low-metallicity, extragalactic gas near our location.¹⁰ Another prospect for detecting dilution by the infall of high-

¹⁰ The other studies made use of observations taken with the GHRS on HST, which could tolerate the high count rates for the spectra of nearby, bright stars. The permissible upper limits on count rate for the detectors on STIS are low enough to force the selection of rather distant O- and B-type stars, except for a few observations that used neutral density filters.

velocity, metal-poor gas might have been Complex C (Richter et al. 2001 ; Tripp et al. 2003), which extends down to the Galactic plane at longitudes $40^\circ < \ell < 80^\circ$. Unfortunately, the distance to Complex C is about 10 ± 2.5 kpc (Thom et al. 2007 ; Wakker et al. 2007), which is not covered by our sample.

With one exception (HD 12323 located at $r, \ell = [4.37 \text{ kpc}, 133^\circ]$ with $\Delta(\text{O}/\text{H}) = +0.17 \pm 0.07$ dex), the measurements for stars with galactocentric distances $R_{\text{GC}} > 10$ kpc seem to be deficient in oxygen, with $\Delta(\text{O}/\text{H}) \sim -0.05$ to -0.2 dex. A majority of the stars near or inside the $R_{\text{GC}} = 7$ kpc boundary show an excess of oxygen. This behavior is consistent with the abundance gradients $-0.07 \text{ dex kpc}^{-1}$ for light elements in early B-type main-sequence stars found by Rolleston et al. (2000) and $-0.051 \text{ dex kpc}^{-1}$ for $R_{\text{GC}} > 7$ kpc determined for H II regions by Esteban & García-Rojas (2018). $\Delta(\text{O}/\text{H})$ could also be influenced in part by possible systematic differences in starlight intensity and molecular fractions with galactocentric distance. The outstanding case in the diagram for an overabundance of O, ($\Delta(\text{O}/\text{H}) = 0.37 \pm 0.13$ dex) located at $r, \ell = [4.9 \text{ kpc}, 20.3^\circ]$, corresponds to the sight line toward the star HD 195455, which is at $z = -3.0$ kpc below the Galactic plane.

8.2. Changes in Corrected $[Ge_{\text{gas}}/O_{\text{gas}}]$ with Location

To check on possible local enhancements of neutron-capture elements relative to α -process ones, we can use Ge and O as proxies and examine the distribution with location of the quantity

$$\begin{aligned} \Delta(\text{Ge}/\text{O}) = & \log N(\text{Ge II}) - \log N(\text{O I}) - (\text{Ge}/\text{H})_{\text{ref}} + (\text{O}/\text{H})_{\text{ref}} - B_2\{\text{Ge}\} + B_2\{\text{O}\} \\ & - A_2\{\text{Ge}, F_*\} \left(F_* - z_2\{\text{Ge}, F_*\} \right) + A_2\{\text{O}, F_*\} \left(F_* - z_2\{\text{O}, F_*\} \right) \\ & - A_2\{\text{Ge}, \log f(\text{H}_2)\} \left(\log f(\text{H}_2) - z_2\{\text{Ge}, \log f(\text{H}_2)\} \right), \end{aligned} \quad (10)$$

which again represents abundances that have been corrected for the general trends in F_* and $\log f(\text{H}_2)$. One advantage of this measure is that the outcomes are not sensitive to errors in $N(\text{H}_{\text{tot}})$, as is the case for $\Delta(\text{O}/\text{H})$. Moreover, the influences of measurement errors in either F_* or $\log f(\text{H}_2)$ are reduced in proportion to the respective differences in the A_2 coefficients for the two elements. A depiction of the values of $\Delta(\text{Ge}/\text{O})$ vs. location is given in Figure 10. Changes in $\Delta(\text{Ge}/\text{O})$ seem to show no coherent patterns beyond what one would expect to find from chance, and in particular there does not seem to be a duplication of the pattern for the Kr/H vs. distance trend shown by Cartledge et al. (2008). There appears to be an approximate anticorrelation in the outcomes shown in Figures 9 and 10; this is simply a consequence of the fact that $\log N(\text{O I})$ appears in both expressions shown in Eqs. 9 and 10, but with opposite sign. Random changes in $\log N(\text{O I})$ due to either measurement errors or real variations will contribute to this anticorrelation.

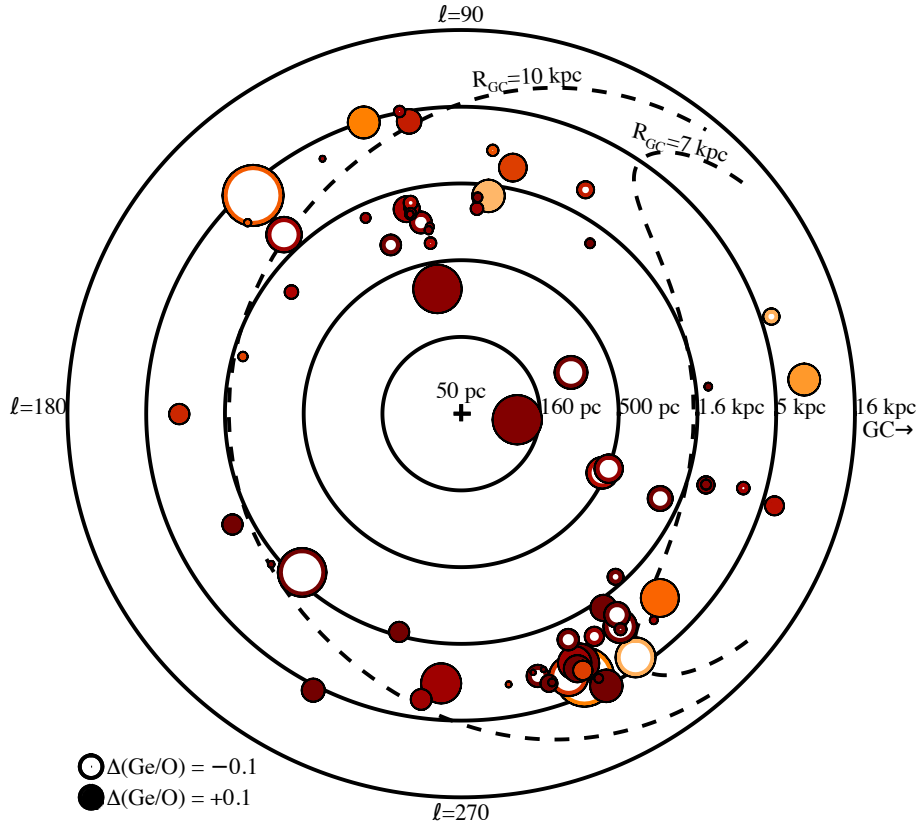


Figure 10. Diagram indicating 72 values of $\Delta(\text{Ge}/\text{O})$, using the same representation as in Figure 9. As with the choices for examples in Figure 9, determinations with uncertainties greater than 0.15 dex were rejected.

9. SUMMARY

The aim of this investigation was to probe to greater depth the various factors that can influence the interstellar gas-phase abundances of the elements O, Ge, and Kr relative to hydrogen in both atomic and molecular forms. These three elements were selected because they have weak (and thus unsaturated) absorption features in a wavelength region that is covered by many medium- and high-resolution echelle STIS spectra in the public archive. In addition, the depletions of O and Kr below their stellar reference abundance levels are of special interest. For instance, O seems more depleted than one would expect from the formation of silicates and oxides (as outlined by J09), and we would expect Kr to show virtually no depletion because it is chemically inert. A more definitive investigation that addressed different responses of such depletions was anticipated to yield more insights on these puzzling cases.

One hundred stars were found to satisfy the criteria that the interstellar features of these elements could be measured with reasonable accuracy, although many cases revealed only upper limits, but ones that were still meaningful. The profiles of Ly α absorption reveal the column densities of H I, and Lyman band absorptions of H₂ recorded by *FUSE* indicate the column densities of this molecule in its two lowest

rotational states. Two different transitions of both Mn II and Mg II were used to derive column densities of these two elements, which, after comparisons against total hydrogen densities (both atomic and molecular), were employed to derive a measure of the generalized strength of depletions of atoms onto dust grains, as characterized by the parameter F_* defined by J09. In addition to F_* , two other environmental parameters of interest in this study are the fraction of H atoms in molecular form $f(\text{H}_2)$, and the local intensity of UV starlight I determined for about half of our stars by Jenkins & Tripp (2011). Initially, the rotation temperatures of the $J = 0$ and 1 levels of H_2 were thought to be of interest, but attempts to discover meaningful relationships with this parameter failed to show any significant effects.

All line measurements were performed using a uniform protocol for determining the outcomes and their uncertainties. For instance, the velocity intervals over which all of the spectral intensities were sampled were strictly defined by the limits of absorption for the strongest and most easily measurable features, those of the Mg II doublet at 1240 Å. In most cases this conservative definition of velocity endpoints seemed wider than the apparent span of a weak line, such as that for O I or Kr I, with the consequence that both the measurement uncertainties and the column density outcomes were increased. Nevertheless, these increased velocity spans guaranteed a more complete pairing with all of the hydrogen gas (for which velocity limits were unavailable) and may explain why the overall krypton-to-hydrogen and germanium-to-hydrogen ratios generally came out to be slightly larger in the present work than in previous surveys.

The study of partial correlations of atomic abundances relative to hydrogen (atomic plus molecular) was divided into two parts. One part included all of the stars but was limited to exploring relationships with only F_* and $\log f(\text{H}_2)$. The other part expanded the parameter list to include the starlight intensity $\log(I/I_0)$ (where I_0 is an average value for our region of the Galaxy), but the sample size was about half as large. One important feature in our derivation of the dependencies of the abundances against the parameters was a recognition of error covariances, which tended to change the coefficient values and their estimated uncertainties. For O and Kr, including the covariances, as opposed to ignoring them, resulted in a reduction of the magnitudes of the coefficients and an increase in their expected uncertainties. For Ge, recognizing covariances had little effect. Another feature in the analysis was that we incorporated upper limits for the column densities into the coefficient derivations instead of simply ignoring them.

All three elements show atomic abundances that decrease with increasing F_* , which is in accord with previous studies. In the investigation where $\log(I/I_0)$ was not considered, there seemed to be no changes with $\log f(\text{H}_2)$ for any of the elements. However, when this extra parameter was included, the negative trend of O with F_* seemed to strengthen, and significant positive correlations with $\log f(\text{H}_2)$ and $\log(I/I_0)$ emerged. Speculations on the possible causes of these relationships are

discussed in Section 7.1. Trends of Kr depletions onto solids might be explained by variations in the ability of grain surfaces to provide enhanced absorption sites, as suggested in Section 7.2.

Finally, attempts were made to look for regional variations in abundance ratios in two forms: O/H and Ge/O. A special feature of this investigation was that these two ratios were expressed in the forms of residual deviations away from the general trends that were found for F_* and $\log f(\text{H}_2)$. The only variation that seemed to go beyond just chance fluctuations was a tendency for the corrected O/H to decrease with galactocentric distance, which is in accord with many previous studies of elemental abundances in our Galaxy.

This research was supported by an archival research grant nr. HST-AR-14570.001-A provided by NASA through the Space Telescope Science Institute (STScI), which is operated by the Associations of Universities for Research in Astronomy, Incorporated, under NASA contract NAS5-26555. All of the spectroscopic data analyzed in this paper were obtained from the *Mikulski Archive for Space Telescopes* (MAST) maintained by the STScI. Specific observations can be accessed via the following collections on MAST: STIS E140H data: <https://doi.org/10.17909/t9-dre3-6g69> ; STIS E140M data: <https://doi.org/10.17909/t9-0mtk-2a73> ; FUSE data: <https://doi.org/10.17909/t9-537q-4w41>. The author is grateful to Sarah Weissman at the STScI for her assistance in creating the DOIs. This research has made use of the SIMBAD database, operated at CDS, Strasbourg, France. For some theoretical insights, the author benefited from useful discussions with Bruce Draine.

Facilities: HST (STIS), FUSE

Software: mlinmix_err (Kelly 2007)

REFERENCES

- Amari, S., Matsuda, J.-i., Stroud, R. M., & Chisholm, M. F. 2013, *ApJ*, 778, 37
- Amberg, C. H., Spencer, W. B., & Beebe, R. A. 1955, *CaJCh*, 33, 305
- André, M., Oliveira, C., Howk, J. C., et al. 2003, *ApJ*, 591, 1000
- Asplund, M., Grevesse, N., Sauval, A. J., & Scott, P. 2009, *ARA&A*, 47, 481
- Ayres, T. R., Lyons, J. R., Ludwig, H. G., Caffau, E., & Wedemeyer-Böhm, S. 2013, *ApJ*, 765, 46
- Barlow, M. J., Swinyard, B. M., Owen, P. J., et al. 2013, *Sci*, 342, 1343
- Barlow, R. 2003, *ArXiv Physics e-prints*.0306138
- Bohlin, R. C. 1975, *ApJ*, 200, 402
- Bowen, D. V., Jenkins, E. B., Tripp, T. M., et al. 2008, *ApJS*, 176, 59
- Cardelli, J. A., Meyer, D. M., Jura, M., & Savage, B. D. 1996, *ApJ*, 467, 334
- Cardelli, J. A., & Meyer, D. M. 1997, *ApJ*, 477, L57
- Cartledge, S. I. B., Meyer, D. M., & Lauroesch, J. T. 2003, *ApJ*, 597, 408
- Cartledge, S. I. B., Lauroesch, J. T., Meyer, D. M., & Sofia, U. J. 2004, *ApJ*, 613, 1037
- . 2006, *ApJ*, 641, 327
- Cartledge, S. I. B., Lauroesch, J. T., Meyer, D. M., Sofia, U. J., & Clayton, G. C. 2008, *ApJ*, 687, 1043
- Cashman, F. H., Kulkarni, V. P., Kisieliu, R., Ferland, G. J., & Bogdanovich, P. 2017, *ApJS*, 230, 8
- Chan, W. F., Cooper, G., Guo, X., Burton, G. R., & Brion, C. E. 1992, *PhRvA*, 46, 149
- Cruz-Diaz, G. A., Martín-Doménech, R., Moreno, E., Muñoz Caro, G. M., & Chen, Y.-J. 2018, *MNRAS*, 474, 3080
- de Avillez, M. A., & Mac Low, M. M. 2002, *ApJ*, 581, 1047
- Diplas, A., & Savage, B. D. 1994, *ApJS*, 93, 211
- Esteban, C., & García-Rojas, J. 2018, *MNRAS*, 478, 2315

- Gondhalekar, P. M. 1985, *ApJ*, 293, 230
- Harris, A. W., Gry, C., & Bromage, G. E. 1984, *ApJ*, 284, 157
- Heidarian, N., Irving, R. E., Federman, S. R., et al. 2017, *JPhB*, 50, 155007
- Hohenberg, C. M., Thonnard, N., & Meshik, A. 2002, *Meteoritics and Planetary Science*, 37, 257
- Holloway, J. 1968, *Noble-Gas Chemistry* (London: Methuen Publishing)
- Jenkins, E. B. 1971, *ApJ*, 169, 25
- Jenkins, E. B., Savage, B. D., & Spitzer, L. 1986, *ApJ*, 301, 355
- Jenkins, E. B. 1996, *ApJ*, 471, 292
- . 2009, *ApJ*, 700, 1299
- Jenkins, E. B., & Tripp, T. M. 2011, *ApJ*, 734, 65
- Jenkins, E. B. 2013, *ApJ*, 764, 25
- . 1987, in *Interstellar Processes*, eds. D. J. Hollenbach, & H. A. Thronson, Jr. (Dordrecht: Reidel), 533-559
- Jensen, A. G., & Snow, T. P. 2007a, *ApJ*, 669, 401
- . 2007b, *ApJ*, 669, 378
- Jensen, A. G., Snow, T. P., Sonneborn, G., & Rachford, B. L. 2010, *ApJ*, 711, 1236
- Kelly, B. C. 2007, *ApJ*, 665, 1489
- Lewis, R. S., Srinivasan, B., & Anders, E. 1975, *Sci*, 190, 1251
- Lodders, K. 2003, *ApJ*, 591, 1220
- Marrocchi, Y., Razafitianamaharavo, A., Michot, L. J., & Marty, B. 2005, *GeCoA*, 69, 2419
- Mathis, J. S., Mezger, P. G., & Panagia, N. 1983, *A&A*, 128, 212
- McCandliss, S. R. 2003, *PASP*, 115, 651
- Meyer, D. M., Jura, M., Hawkins, I., & Cardelli, J. A. 1994, *ApJ*, 437, L59
- Meyer, D. M., Jura, M., & Cardelli, J. A. 1998, *ApJ*, 493, 222
- Mitchell, J. B. A. 1990, *PhR*, 186, 215
- Mitchell, J. B. A., Novotny, O., LeGarrec, J. L., et al. 2005, *JPhB*, 38, L175
- Morton, D. C. 2000, *ApJS*, 130, 403
- Morton, D. C. 2003, *ApJS*, 149, 205
- Murray, M. J., Dufton, P. L., Hibbert, A., & York, D. G. 1984, *ApJ*, 282, 481
- Nichols, R. H., Jr., Nuth, J. A., III, Hohenberg, C. M., Olinger, C. T., & Moore, M. H. 1992, *Metic*, 27, 555
- Nieva, M. F., & Przybilla, N. 2012, *A&A*, 539, 143N
- Pauzat, F., & Ellinger, Y. 2007, *JChPh*, 127, 014308
- Pauzat, F., Ellinger, Y., Pilmé, J., & Mousis, O. 2009, *JChPh*, 130, 174313
- Poteet, C. A., Whittet, D. C. B., & Draine, B. T. 2015, *ApJ*, 801, 110
- Richter, P., Sembach, K. R., Wakker, B. P., et al. 2001, *ApJ*, 559, 318
- Ritchey, A. M., Federman, S. R., & Lambert, D. L. 2018, *ApJS*, 236, 36
- Robinson, E. L. 2016, *Data Analysis for Scientists and Engineers* (Princeton: Princeton U. Press)
- Rolleston, W. R. J., Smartt, S. J., Dufton, P. L., & Ryans, R. S. I. 2000, *A&A*, 363, 537
- Roy, J. R., & Kunth, D. 1995, *A&A*, 294, 432
- Savage, B. D., Bohlin, R. C., Drake, J. F., & Budich, W. 1977, *ApJ*, 216, 291
- Savage, B. D., & Bohlin, R. C. 1979, *ApJ*, 229, 136
- Savage, B. D., & Sembach, K. R. 1991, *ApJ*, 379, 245
- . 1996, *ARA&A*, 34, 279
- Savage, B. D., Kim, T.-S., Fox, A. J., et al. 2017, *ApJS*, 232, 25
- Schelhaas, N., Ott, U., & Begemann, F. 1990, *GeCoA*, 54, 2869
- Schilke, P., Neufeld, D. A., Müller, H. S. P., et al. 2014, *A&A*, 566, A29
- Sembach, K. R., & Savage, B. D. 1992, *ApJS*, 83, 147
- Snow, T. P. 1983, *ApJ*, 269, L57
- Snow, T. P., Rachford, B. L., & Figoski, L. 2002, *ApJ*, 573, 662
- Steffen, M., Prakashavičius, D., Caffau, E., et al. 2015, *A&A*, 583, A57
- Sterling, N. C. 2011, *A&A*, 533, A62
- Theis, R. A., Morgan, W. J., & Fortenberry, R. C. 2015, *MNRAS*, 446, 195
- Thom, C., Peek, J. E. G., Putman, M. E., et al. 2007, *ApJ*, 684, 364
- Toner, A., & Hibbert, A. 2005, *MNRAS*, 361, 673
- Tripp, T. M., Wakker, B. P., Jenkins, E. B., et al. 2003, *AJ*, 125, 3122
- Voshchinnikov, N. V., & Henning, T. 2010, *A&A*, 517, A45
- Wacker, J. F. 1989, *GeCoA*, 53, 1421
- Wakker, B. P., York, D. G., Howk, J. C., et al. 2007, *ApJ*, 670, L113
- Wang, S., Li, A., & Jiang, B. W. 2015, *MNRAS*, 454, 569
- Welsh, B. Y., Sasseen, T., Craig, N., Jelinsky, S., & Albert, C. E. 1997, *ApJS*, 112, 507
- Whittet, D. C. B. 2010, *ApJ*, 710, 1009
- Wyatt, J. R., Strattan, L. W., Snyder, S. C., & Hierl, P. M. 1975, *JChPh*, 62, 2555
- Yang, J., & Anders, E. 1982a, *GeCoA*, 46, 861
- Yang, J., Lewis, R. S., & Anders, E. 1982, *GeCoA*, 46, 841
- Yang, J., & Anders, E. 1982b, *GeCoA*, 46, 877

APPENDIX

A. BASIC MEASUREMENT OUTCOMES

Table 7 lists for each star the results of analyzing the interstellar absorption features of H I, O I, Mg II, Mn II, Ge II, and Kr I, based on the analysis methods discussed in Section 3. Measurements of H₂ are not included in this table but do appear in Table 5.

Table 7. STIS Measurement Outcomes^a

Line ^b	W_λ (mÅ)	$\log N_a(\text{cm}^{-2})^c$
BD+35 4258 M -42 to 13 km s^{-1}		
H I	...	21.24 (+0.03, -0.07)
O I	6.3 ± 2.6	17.55 (+0.14, -0.21)
Mg II 1	71.3 ± 3.1	16.07 ± 0.02
Mg II 2	58.9 ± 3.8	16.18 ± 0.03
Mg II 3	...	16.26 (+0.04, -0.03)
Mn II 1	66.9 ± 6.2	13.68 ± 0.04
Mn II 2	45.9 ± 11.2	13.71 (+0.10, -0.13)
Ge II	32.6 ± 3.8	12.49 ± 0.05
Kr I	6.4 ± 4.7	< 12.59
BD+53 2820 M -58 to 4 km s^{-1}		
H I	...	21.35 (+0.05, -0.07)
O I	16.9 ± 4.0	17.99 (+0.09, -0.11)
Mg II 1	89.1 ± 5.4	16.14 ± 0.03
Mg II 2	72.4 ± 6.0	16.26 ± 0.04
Mg II 3	...	16.37 (+0.06, -0.04)
Mn II 1	82.4 ± 6.7	13.78 ± 0.04
Mn II 2	46.9 ± 15.5	13.79 (+0.11, -0.16)
Ge II	37.3 ± 6.9	12.55 (+0.08, -0.09)
Kr I	-9.1 ± 9.5	< 12.50
CPD-59 2603 H -50 to 19 km s^{-1}		
H I	...	21.43 (+0.04, -0.05)
Mg II 1	113.5 ± 2.0	16.31 ± 0.01
Mg II 2	76.9 ± 4.3	16.33 (+0.02, -0.03)
Mn II 2	62.2 ± 5.7	13.91 ± 0.04
Ge II	43.4 ± 4.6	12.66 (+0.04, -0.05)
Kr I	7.9 ± 5.0	< 12.66

Table 7 continued on next page

Table 7 (*continued*)

Line ^b	W_λ (mÅ)	$\log N_a(\text{cm}^{-2})^c$
CPD-59 2603 M -50 to 23 km s^{-1}		
H I	...	21.44 (+0.02, -0.08)
O I	18.7 ± 2.4	18.02 (+0.05, -0.06)
Mg II 1	118.4 ± 7.1	16.28 ± 0.03
Mg II 2	79.8 ± 4.2	16.31 (+0.02, -0.03)
Mn II 2	61.4 ± 5.2	13.87 ± 0.04
Ge II	35.5 ± 3.8	12.53 (+0.04, -0.05)
CPD-59 4552 H -39 to 18 km s^{-1}		
H I	...	21.28 (+0.05, -0.06)
O I	13.8 ± 5.0	17.90 (+0.13, -0.19)
Mg II 1	91.6 ± 3.1	16.23 (+0.01, -0.02)
Mg II 2	63.0 ± 3.2	16.26 ± 0.02
Mg II 3	...	16.36 ± 0.03
Mn II 1	66.4 ± 9.2	13.70 ± 0.06
Mn II 2	38.8 ± 13.0	13.68 (+0.12, -0.16)
Ge II	35.9 ± 2.1	12.57 (+0.02, -0.03)
Kr I	1.6 ± 4.1	< 12.37
CPD-69 1743 M -49 to 24 km s^{-1}		
H I	...	21.16 (+0.04, -0.09)
O I	4.4 ± 2.8	< 17.59
Mg II 1	72.7 ± 4.4	16.01 ± 0.03
Mg II 2	50.9 ± 3.8	16.08 (+0.03, -0.04)
Mg II 3	...	16.20 ± 0.04
Mn II 1	45.6 ± 6.9	13.45 (+0.06, -0.07)
Ge II	19.2 ± 4.8	12.26 (+0.09, -0.12)
Kr I	-3.5 ± 8.5	< 12.55

Table 7 continued on next page

Table 7 (*continued*)

Line ^b	W_λ (mÅ)	$\log N_a(\text{cm}^{-2})^c$
HD108 H -52 to 9 km s^{-1}		
H I	...	21.38 ± 0.05
O I	21.0 ± 3.2	$18.09 (+0.06, -0.07)$
Mg II 1	83.0 ± 2.2	16.21 ± 0.01
Mg II 2	61.7 ± 2.3	16.24 ± 0.02
Mg II 3	...	16.30 ± 0.02
Mn II 1	63.2 ± 7.3	13.69 ± 0.05
Mn II 2	36.5 ± 7.3	$13.64 (+0.07, -0.09)$
Ge II	43.0 ± 2.6	12.66 ± 0.03
Kr I	5.4 ± 3.8	< 12.51
HD108 M -52 to 9 km s^{-1}		
H I	...	$21.38 (+0.06, -0.09)$
O I	24.5 ± 10.0	$18.15 (+0.15, -0.23)$
Mg II 1	73.2 ± 3.5	16.09 ± 0.02
Mg II 2	57.3 ± 2.9	$16.18 (+0.02, -0.03)$
Mg II 3	...	16.28 ± 0.04
Mn II 1	59.2 ± 11.7	$13.62 (+0.08, -0.10)$
Mn II 2	30.5 ± 21.2	< 13.70
Ge II	45.1 ± 4.3	$12.66 (+0.04, -0.05)$
Kr I	-0.7 ± 7.7	< 12.56
HD1383 H -72 to 5 km s^{-1}		
H I	...	$21.46 (+0.05, -0.06)$
O I	24.0 ± 13.1	< 18.30
Mg II 1	121.9 ± 3.0	16.31 ± 0.01
Mg II 2	87.2 ± 4.1	16.36 ± 0.02
Mg II 3	...	16.42 ± 0.02
Mn II 1	77.3 ± 7.8	13.75 ± 0.04
Ge II	44.9 ± 4.2	12.66 ± 0.04
Kr I	22.0 ± 6.5	$12.91 (+0.11, -0.15)$

Table 7 continued on next page

Table 7 (*continued*)

Line ^b	W_λ (mÅ)	$\log N_a(\text{cm}^{-2})^c$
HD1383 M -72 to 5 km s^{-1}		
H I	...	$21.46 (+0.04, -0.05)$
O I	21.5 ± 6.7	$18.08 (+0.12, -0.16)$
Mg II 1	111.6 ± 4.4	16.22 ± 0.02
Mg II 2	82.3 ± 5.7	16.31 ± 0.03
Mg II 3	...	16.40 ± 0.04
Mn II 1	105.8 ± 8.7	13.85 ± 0.04
Ge II	62.6 ± 8.0	12.78 ± 0.06
Kr I	-6.7 ± 13.5	< 12.73
HD3827 H -60 to 8 km s^{-1}		
H I	...	$20.55 (+0.07, -0.05)$
O I	-0.3 ± 2.5	< 17.25
Mg II 1	24.1 ± 1.7	15.48 ± 0.03
Mg II 2	13.2 ± 1.7	$15.45 (+0.05, -0.06)$
Mn II 1	30.0 ± 3.3	13.23 ± 0.05
Mn II 2	7.6 ± 3.8	$12.88 (+0.17, -0.29)$
Ge II	6.5 ± 3.9	< 11.95
Kr I	1.2 ± 1.5	< 12.01
HD12323 M -57 to 10 km s^{-1}		
H I	...	$21.19 (+0.04, -0.05)$
O I	21.1 ± 3.1	$18.08 (+0.06, -0.07)$
Mg II 1	66.0 ± 5.3	16.02 ± 0.03
Mg II 2	47.2 ± 3.2	16.08 ± 0.03
Mg II 3	...	16.14 ± 0.03
Mn II 1	57.1 ± 7.2	$13.57 (+0.05, -0.06)$
Mn II 2	32.0 ± 6.7	$13.53 (+0.08, -0.10)$
Ge II	26.5 ± 4.0	$12.40 (+0.06, -0.07)$
Kr I	10.6 ± 7.4	< 12.80

Table 7 continued on next page

Table 7 (*continued*)

Line ^b	W_λ (mÅ)	$\log N_a(\text{cm}^{-2})^c$
HD13268 M -77 to 8 km s^{-1}		
H I	...	21.34 ± 0.07
O I	22.3 ± 4.8	$18.10 (+0.08, -0.11)$
Mg II 1	104.2 ± 4.4	16.23 ± 0.02
Mg II 2	83.8 ± 4.0	16.32 ± 0.02
Mg II 3	...	$16.44 (+0.06, -0.04)$
Mn II 1	93.8 ± 5.8	13.80 ± 0.03
Mn II 2	55.5 ± 8.1	$13.79 (+0.06, -0.07)$
Ge II	35.1 ± 8.2	$12.54 (+0.09, -0.11)$
Kr I	-19.8 ± 11.4	< 12.47
HD13745 M -66 to 10 km s^{-1}		
H I	...	21.34 ± 0.05
O I	16.7 ± 4.5	$17.97 (+0.10, -0.14)$
Mg II 1	97.2 ± 4.9	16.17 ± 0.02
Mg II 2	67.6 ± 4.6	16.22 ± 0.03
Mg II 3	...	16.28 ± 0.03
Mn II 1	85.1 ± 6.6	$13.76 (+0.03, -0.04)$
Mn II 2	44.3 ± 14.9	$13.70 (+0.12, -0.17)$
Ge II	43.1 ± 9.0	$12.62 (+0.08, -0.10)$
Kr I	-0.6 ± 18.0	< 12.94
HD13841 H -87 to 8 km s^{-1}		
H I	...	$21.44 (+0.06, -0.12)$
O I	21.2 ± 14.6	< 18.29
Mg II 1	125.9 ± 4.8	16.31 ± 0.02
Mg II 2	76.0 ± 5.0	16.28 ± 0.03
Mn II 1	81.6 ± 22.2	$13.76 (+0.10, -0.13)$
Ge II	57.1 ± 6.1	$12.75 (+0.04, -0.05)$
Kr I	18.1 ± 18.7	< 13.13

Table 7 continued on next page

Table 7 (*continued*)

Line ^b	W_λ (mÅ)	$\log N_a(\text{cm}^{-2})^c$
HD14818 H -72 to 9 km s^{-1}		
H I	...	21.40 ± 0.07
O I	24.5 ± 9.8	$18.16 (+0.14, -0.21)$
Mg II 1	103.5 ± 4.6	16.28 ± 0.02
Mg II 2	89.1 ± 5.7	16.39 ± 0.03
Mg II 3	...	16.49 ± 0.04
Mn II 1	81.7 ± 16.6	$13.78 (+0.08, -0.10)$
Mn II 2	51.5 ± 10.1	$13.77 (+0.07, -0.09)$
Ge II	39.9 ± 6.9	$12.62 (+0.06, -0.08)$
Kr I	13.0 ± 9.4	< 12.90
HD15137 H -31 to 7 km s^{-1}		
H I	...	$21.24 (+0.08, -0.06)$
O I	13.1 ± 1.5	17.88 ± 0.05
Mg II 1	70.9 ± 1.0	16.13 ± 0.01
Mg II 2	51.8 ± 1.1	16.17 ± 0.01
Mg II 3	...	$16.22 (+0.02, -0.01)$
Mn II 1	52.8 ± 1.8	13.59 ± 0.02
Mn II 2	38.2 ± 3.8	$13.64 (+0.04, -0.05)$
Ge II	29.1 ± 4.1	12.48 ± 0.06
Kr I	14.9 ± 4.2	$12.74 (+0.11, -0.15)$
HD25443 H -24 to 13 km s^{-1}		
H I	...	$21.29 (+0.06, -0.05)$
O I	21.5 ± 2.9	$18.12 (+0.05, -0.06)$
Mg II 1	72.4 ± 1.7	16.17 ± 0.01
Mg II 2	50.3 ± 1.8	16.17 ± 0.02
Mn II 1	54.2 ± 4.1	$13.63 (+0.03, -0.04)$
Ge II	41.7 ± 2.2	12.67 ± 0.02
Kr I	12.1 ± 3.7	$12.66 (+0.11, -0.16)$

Table 7 continued on next page

Table 7 (*continued*)

Line ^b	W_λ (mÅ)	$\log N_a(\text{cm}^{-2})^c$
HD35914 H 13 to 57 km s ⁻¹		
H I	...	21.18 (+0.07, -0.04)
Mg II 1	54.9 ± 2.0	15.98 ± 0.02
Mg II 2	41.5 ± 2.5	16.04 ± 0.03
Mg II 3	...	16.12 ± 0.03
Mn II 1	28.1 ± 6.4	13.31 (+0.08, -0.09)
Ge II	31.5 ± 5.2	12.52 (+0.06, -0.08)
Kr I	1.9 ± 5.3	< 12.48
HD36486 ^d M 12 to 32 km s ⁻¹		
H I	...	20.19 (+0.07, -0.06)
O I	0.9 ± 1.5	< 17.16
Mg II 1	10.8 ± 2.3	15.15 (+0.08, -0.10)
Mn II 1	5.2 ± 2.9	< 12.64
Ge II	3.0 ± 1.8	< 11.61
Kr I	-0.4 ± 2.2	< 12.00
HD37021 ^d H 5 to 32 km s ⁻¹		
H I	...	21.68 (+0.02, -0.05)
O I	18.2 ± 1.2	18.09 ± 0.03
Mg II 1	33.9 ± 0.4	15.78 ± 0.01
Mg II 2	26.7 ± 0.5	15.87 ± 0.01
Mg II 3	...	15.98 (+0.03, -0.02)
Mn II 1	37.5 ± 0.7	13.59 ± 0.01
Mn II 2	31.1 ± 0.9	13.69 ± 0.01
Mn II 3	...	13.86 ± 0.05
Ge II	22.2 ± 0.4	12.42 ± 0.01
Kr I	9.0 ± 0.5	12.55 ± 0.02
HD37061 ^d H 13 to 35 km s ⁻¹		
H I	...	21.73 ± 0.04
O I	23.3 ± 0.8	18.26 ± 0.01
Mg II 1	26.1 ± 0.5	15.70 ± 0.01
Mg II 2	22.6 ± 0.7	15.82 ± 0.01
Mg II 3	...	15.94 ± 0.02
Mn II 1	30.2 ± 0.6	13.48 ± 0.01
Mn II 2	27.2 ± 0.9	13.65 ± 0.02

Table 7 continued on next page

Table 7 (*continued*)

Line ^b	W_λ (mÅ)	$\log N_a(\text{cm}^{-2})^c$
Mn II 3	...	13.87 ± 0.06
Ge II	24.2 ± 0.5	12.51 ± 0.01
Kr I	11.5 ± 0.5	12.69 ± 0.02
HD37468 ^d H -4 to 33 km s^{-1}		
H I	...	$20.65 (+0.03, -0.05)$
O I	4.5 ± 1.5	$17.39 (+0.13, -0.18)$
Mg II 1	18.1 ± 0.5	15.42 ± 0.01
Mg II 2	10.8 ± 0.8	15.41 ± 0.03
Mn II 1	9.4 ± 1.1	$12.76 (+0.04, -0.05)$
Mn II 2	10.9 ± 1.2	13.04 ± 0.05
Mn II 3	...	13.12 ± 0.07
Ge II	6.4 ± 0.7	11.77 ± 0.05
Kr I	2.8 ± 0.7	$12.00 (+0.09, -0.12)$
HD37468 M -6 to 34 km s^{-1}		
H I	...	$20.66 (+0.04, -0.05)$
O I	3.2 ± 1.5	$17.24 (+0.17, -0.27)$
Mg II 1	23.8 ± 1.6	15.50 ± 0.03
Mg II 2	13.1 ± 1.4	$15.47 (+0.04, -0.05)$
Mn II 1	10.6 ± 2.2	$12.78 (+0.08, -0.10)$
Mn II 2	8.0 ± 3.4	$12.90 (+0.15, -0.24)$
Ge II	5.7 ± 1.0	$11.71 (+0.07, -0.08)$
Kr I	0.7 ± 1.3	< 11.90
HD40893 H -19 to 52 km s^{-1}		
H I	...	$21.46 (+0.04, -0.06)$
O I	21.9 ± 2.1	18.12 ± 0.04
Mg II 1	96.9 ± 2.3	16.30 ± 0.01
Mg II 2	68.2 ± 2.7	16.31 ± 0.02
Mn II 1	70.7 ± 3.4	13.74 ± 0.02
Mn II 2	43.3 ± 4.5	13.72 ± 0.04
Ge II	50.8 ± 2.8	12.74 ± 0.02
Kr I	18.0 ± 4.0	$12.83 (+0.09, -0.11)$

Table 7 continued on next page

Table 7 (*continued*)

Line ^b	W_λ (mÅ)	$\log N_a(\text{cm}^{-2})^c$
HD41161 H -21 to 21 km s^{-1}		
H I	...	21.09 ± 0.05
O I	12.2 ± 1.5	$17.84 (+0.05, -0.06)$
Mg II 1	69.7 ± 1.0	16.08 ± 0.01
Mg II 2	45.3 ± 1.1	16.07 ± 0.01
Mn II 1	42.9 ± 1.4	$13.44 (+0.01, -0.02)$
Mn II 2	22.5 ± 1.9	$13.38 (+0.03, -0.04)$
Ge II	26.4 ± 1.9	12.41 ± 0.03
Kr I	4.1 ± 3.9	< 12.46
HD43818 ^d H -8 to 35 km s^{-1}		
H I	...	21.53 ± 0.06
O I	28.9 ± 2.0	18.27 ± 0.03
Mg II 1	98.7 ± 1.3	16.47 ± 0.02
Mg II 2	75.2 ± 1.3	16.45 ± 0.01
Mn II 1	66.8 ± 3.9	13.77 ± 0.03
Ge II	46.9 ± 5.4	12.78 ± 0.05
Kr I	31.5 ± 6.7	$13.11 (+0.08, -0.11)$
HD46223 M -5 to 42 km s^{-1}		
H I	...	$21.46 (+0.04, -0.02)$
O I	21.4 ± 2.3	$18.11 (+0.04, -0.05)$
Mg II 1	68.5 ± 1.5	16.10 ± 0.01
Mg II 2	56.8 ± 1.3	16.23 ± 0.01
Mg II 3	...	16.44 ± 0.08
Mn II 1	60.2 ± 2.0	$13.66 (+0.01, -0.02)$
Mn II 2	40.5 ± 3.6	13.68 ± 0.04
Ge II	43.0 ± 1.8	12.67 ± 0.02
Kr I	11.5 ± 6.5	< 12.80

Table 7 continued on next page

Table 7 (*continued*)

Line ^b	W_λ (mÅ)	$\log N_a(\text{cm}^{-2})^c$
HD52266 H 4 to 51 km s ⁻¹		
H I	...	21.22 (+0.04, -0.05)
O I	13.1 ± 2.8	17.89 (+0.08, -0.10)
Mg II 1	62.1 ± 0.6	16.07 ± 0.01
Mg II 2	39.2 ± 0.7	16.06 ± 0.01
Mn II 1	47.9 ± 0.9	13.55 ± 0.01
Mn II 2	34.0 ± 1.8	13.61 ± 0.02
Mn II 3	...	13.70 ± 0.03
Ge II	26.0 ± 1.2	12.45 ± 0.02
Kr I	9.7 ± 4.6	12.55 (+0.17, -0.27)
HD53975 H -7 to 46 km s ⁻¹		
H I	...	21.08 (+0.04, -0.02)
O I	11.5 ± 1.6	17.81 (+0.06, -0.07)
Mg II 1	67.3 ± 1.2	16.06 ± 0.01
Mg II 2	43.0 ± 1.2	16.05 ± 0.01
Mn II 1	30.6 ± 2.8	13.31 ± 0.04
Mn II 2	25.5 ± 1.7	13.45 ± 0.03
Mn II 3	...	13.59 ± 0.05
Ge II	17.7 ± 1.4	12.24 (+0.03, -0.04)
Kr I	5.4 ± 2.1	12.28 (+0.14, -0.21)
HD63005 M 8 to 57 km s ⁻¹		
H I	...	21.24 (+0.03, -0.06)
O I	13.4 ± 2.5	17.89 (+0.07, -0.08)
Mg II 1	57.8 ± 2.8	15.98 ± 0.02
Mg II 2	39.5 ± 2.8	16.02 ± 0.03
Mn II 1	54.0 ± 8.1	13.56 (+0.06, -0.07)
Mn II 2	23.1 ± 6.0	13.41 (+0.10, -0.12)
Ge II	32.3 ± 4.2	12.51 (+0.05, -0.06)
Kr I	7.0 ± 8.4	< 12.76

Table 7 continued on next page

Table 7 (*continued*)

Line ^b	W_λ (mÅ)	$\log N_a(\text{cm}^{-2})^c$
HD66788 M -1 to 52 km s ⁻¹		
H I	...	21.23 (+0.04, -0.02)
O I	11.4 ± 6.5	< 17.98
Mg II 1	76.0 ± 3.4	16.07 ± 0.02
Mg II 2	28.8 ± 3.8	15.85 (+0.05, -0.06)
Mn II 1	31.5 ± 8.0	13.30 (+0.10, -0.12)
Mn II 2	12.1 ± 21.0	< 13.55
Ge II	13.4 ± 8.2	< 12.27
Kr I	4.7 ± 4.0	< 12.49
HD69106 H 11 to 40 km s ⁻¹		
H I	...	21.07 ± 0.04
O I	7.2 ± 0.8	17.61 ± 0.05
Mg II 1	36.7 ± 0.5	15.79 ± 0.01
Mg II 2	25.6 ± 0.6	15.82 ± 0.01
Mg II 3	...	15.89 (+0.02, -0.01)
Mn II 1	33.0 ± 0.5	13.36 ± 0.01
Mn II 2	19.0 ± 0.7	13.32 ± 0.02
Ge II	17.8 ± 0.6	12.24 ± 0.02
Kr I	4.7 ± 0.4	12.23 (+0.03, -0.04)
HD72648 H 3 to 35 km s ⁻¹		
H I	...	21.19 (+0.07, -0.06)
O I	12.7 ± 4.0	17.89 (+0.12, -0.16)
Mg II 1	41.6 ± 1.9	15.83 ± 0.02
Mg II 2	30.1 ± 1.8	15.88 ± 0.03
Mg II 3	...	15.94 ± 0.03
Mn II 1	34.6 ± 3.0	13.43 (+0.03, -0.04)
Mn II 2	19.3 ± 7.3	13.37 (+0.13, -0.18)
Ge II	26.4 ± 1.7	12.45 ± 0.03
Kr I	6.0 ± 2.2	12.36 (+0.13, -0.19)

Table 7 continued on next page

Table 7 (*continued*)

Line ^b	W_λ (mÅ)	$\log N_a(\text{cm}^{-2})^c$
HD75309 H 0 to 43 km s ⁻¹		
H I	...	21.10 (+0.03, -0.06)
O I	8.9 ± 2.3	17.72 (+0.09, -0.12)
Mg II 1	50.4 ± 1.5	15.94 ± 0.01
Mg II 2	33.0 ± 1.7	15.94 ± 0.02
Mn II 1	35.5 ± 1.8	13.43 ± 0.02
Mn II 2	23.4 ± 4.1	13.45 (+0.06, -0.07)
Ge II	26.0 ± 1.6	12.43 ± 0.03
Kr I	3.2 ± 1.5	12.08 (+0.16, -0.26)
HD88115 H -29 to 23 km s ⁻¹		
H I	...	21.05 (+0.06, -0.08)
H I sc	...	21.03 (+0.06, -0.09)
O I	8.7 ± 3.4	17.69 (+0.14, -0.21)
Mg II 1	69.6 ± 1.7	16.04 ± 0.01
Mg II 2	46.0 ± 2.1	16.06 ± 0.02
Mn II 1	49.4 ± 2.7	13.53 ± 0.02
Mn II 2	38.6 ± 5.1	13.64 (+0.05, -0.06)
Mn II 3	...	13.76 (+0.07, -0.05)
Ge II	27.2 ± 2.1	12.42 ± 0.03
Kr I	3.4 ± 4.4	< 12.47
HD88115 M -26 to 23 km s ⁻¹		
H I	...	21.06 (+0.04, -0.10)
O I	5.6 ± 4.0	< 17.72
Mg II 1	53.4 ± 5.0	15.88 (+0.04, -0.05)
Mg II 2	37.3 ± 7.2	15.94 (+0.08, -0.10)
Mn II 1	49.6 ± 4.7	13.50 (+0.04, -0.05)
Mn II 2	38.0 ± 9.9	13.61 (+0.10, -0.14)
Ge II	17.0 ± 3.1	12.19 (+0.07, -0.09)
Kr I	-8.3 ± 8.3	< 12.44

Table 7 continued on next page

Table 7 (*continued*)

Line ^b	W_λ (mÅ)	$\log N_a(\text{cm}^{-2})^c$
HD89137 H -17 to 23 km s^{-1}		
H I	...	$21.03 (+0.07, -0.02)$
O I	8.5 ± 1.8	$17.70 (+0.08, -0.10)$
Mg II 1	60.2 ± 1.3	16.02 ± 0.01
Mg II 2	40.4 ± 1.3	16.03 ± 0.01
Mn II 1	42.5 ± 1.8	13.50 ± 0.02
Mn II 2	33.2 ± 2.3	13.60 ± 0.03
Mn II 3	...	13.71 ± 0.04
Ge II	19.8 ± 1.7	$12.29 (+0.03, -0.04)$
Kr I	9.6 ± 7.1	< 12.77
HD90087 H -11 to 31 km s^{-1}		
H I	...	$21.19 (+0.05, -0.09)$
O I	13.8 ± 1.5	$17.90 (+0.04, -0.05)$
Mg II 1	68.7 ± 0.8	16.13 ± 0.01
Mg II 2	50.7 ± 1.0	16.16 ± 0.01
Mg II 3	...	16.19 ± 0.02
Mn II 1	58.1 ± 1.3	13.67 ± 0.01
Mn II 2	40.3 ± 2.0	13.69 ± 0.02
Ge II	30.4 ± 1.7	12.50 ± 0.02
Kr I	9.2 ± 3.6	$12.53 (+0.14, -0.22)$
HD91824 H -22 to 24 km s^{-1}		
H I	...	21.12 ± 0.04
O I	4.0 ± 4.8	< 17.70
Mg II 1	74.2 ± 1.1	16.13 ± 0.01
Mg II 2	52.3 ± 1.9	16.16 ± 0.02
Mg II 3	...	16.20 ± 0.02
Mn II 1	56.1 ± 2.8	13.61 ± 0.02
Mn II 2	32.5 ± 2.8	13.56 ± 0.04
Ge II	30.3 ± 1.1	12.48 ± 0.02
Kr I	8.2 ± 1.7	$12.47 (+0.08, -0.10)$

Table 7 continued on next page

Table 7 (*continued*)

Line ^b	W_λ (mÅ)	$\log N_a(\text{cm}^{-2})^c$
HD91983 H -26 to 25 km s^{-1}		
H I	...	21.15 (+0.06, -0.05)
O I	16.0 ± 2.6	17.97 (+0.06, -0.08)
Mg II 1	78.0 ± 1.7	16.14 ± 0.01
Mg II 2	57.6 ± 2.6	16.20 ± 0.02
Mg II 3	...	16.28 (+0.03, -0.02)
Mn II 1	61.1 ± 4.9	13.64 (+0.03, -0.04)
Mn II 2	38.7 ± 6.6	13.65 (+0.07, -0.08)
Ge II	31.4 ± 2.0	12.50 ± 0.03
Kr I	0.3 ± 2.7	< 12.14
HD92554 M -31 to 34 km s^{-1}		
H I	...	21.34 (+0.09, -0.11)
O I	13.6 ± 5.9	17.89 (+0.15, -0.24)
Mg II 1	102.0 ± 4.0	16.29 ± 0.02
Mg II 2	83.1 ± 3.9	16.38 ± 0.02
Mg II 3	...	16.48 ± 0.03
Mn II 1	85.1 ± 4.2	13.80 ± 0.03
Mn II 2	68.5 ± 17.4	13.92 (+0.10, -0.12)
Ge II	47.9 ± 5.2	12.67 ± 0.05
Kr I	-5.1 ± 5.9	< 12.31
HD93129 M -54 to 24 km s^{-1}		
H I	...	21.47 (+0.07, -0.04)
O I	26.5 ± 2.6	18.18 (+0.04, -0.05)
Mg II 1	134.2 ± 3.0	16.37 ± 0.01
Mg II 2	92.5 ± 3.0	16.39 (+0.01, -0.02)
Mn II 2	60.2 ± 7.1	13.85 ± 0.05
Ge II	56.8 ± 2.6	12.76 ± 0.02
Kr I	-2.8 ± 5.9	< 12.38

Table 7 continued on next page

Table 7 (*continued*)

Line ^b	W_λ (mÅ)	$\log N_a(\text{cm}^{-2})^c$
HD93205 H -49 to 23 km s^{-1}		
H I	...	21.36 ± 0.05
Mg II 1	113.4 ± 2.0	16.30 ± 0.01
Mg II 2	80.3 ± 1.9	16.33 ± 0.01
Mg II 3	...	16.40 ± 0.02
Mn II 2	93.6 ± 3.8	14.07 ± 0.02
Ge II	45.0 ± 3.6	$12.65 (+0.03, -0.04)$
Kr I	8.5 ± 5.3	< 12.68
HD93222 H -34 to 24 km s^{-1}		
H I	...	$21.47 (+0.03, -0.04)$
Mg II 1	113.7 ± 1.8	16.36 ± 0.01
Mg II 2	85.4 ± 1.9	16.41 ± 0.01
Mg II 3	...	16.50 ± 0.02
Mn II 1	101.9 ± 3.3	13.95 ± 0.02
Mn II 2	85.7 ± 5.6	14.07 ± 0.03
Mn II 3	...	14.22 ± 0.07
Ge II	48.1 ± 2.3	12.71 ± 0.02
Kr I	10.3 ± 5.4	< 12.74
HD93843 H -41 to 24 km s^{-1}		
H I	...	$21.30 (+0.05, -0.04)$
O I	15.3 ± 3.7	$17.93 (+0.09, -0.12)$
Mg II 1	107.7 ± 1.5	16.25 ± 0.01
Mg II 2	71.1 ± 1.6	16.26 ± 0.01
Mn II 1	104.7 ± 1.8	13.88 ± 0.01
Mn II 2	58.0 ± 2.5	13.82 ± 0.02
Ge II	37.2 ± 2.1	$12.55 (+0.02, -0.03)$
Kr I	3.8 ± 2.6	< 12.35

Table 7 continued on next page

Table 7 (*continued*)

Line ^b	W_λ (mÅ)	$\log N_a(\text{cm}^{-2})^c$
HD94493 H -22 to 21 km s^{-1}		
H I	...	21.10 (+0.06, -0.05)
O I	9.0 ± 2.9	17.71 (+0.12, -0.16)
Mg II 1	73.9 ± 0.8	16.12 ± 0.01
Mg II 2	54.8 ± 1.4	16.17 ± 0.01
Mg II 3	...	16.22 ± 0.02
Mn II 1	63.8 ± 3.1	13.68 ± 0.02
Ge II	28.2 ± 5.5	12.45 (+0.08, -0.09)
Kr I	5.1 ± 2.0	12.27 (+0.14, -0.21)
HD97175 H -34 to 24 km s^{-1}		
H I	...	20.96 (+0.06, -0.05)
O I	12.7 ± 3.2	17.87 (+0.09, -0.12)
Mg II 1	57.4 ± 2.5	15.93 ± 0.02
Mg II 2	34.2 ± 2.2	15.91 ± 0.03
Mn II 1	36.0 ± 3.9	13.38 (+0.04, -0.05)
Mn II 2	26.7 ± 4.6	13.48 (+0.07, -0.08)
Mn II 3	...	13.62 ± 0.09
Ge II	16.8 ± 2.7	12.20 (+0.06, -0.07)
Kr I	9.7 ± 2.9	12.54 (+0.11, -0.15)
HD99857 H -40 to 26 km s^{-1}		
H I	...	21.27 (+0.07, -0.03)
O I	12.7 ± 3.2	17.90 (+0.09, -0.11)
Mg II 1	76.5 ± 2.0	16.16 ± 0.01
Mg II 2	55.7 ± 2.0	16.20 ± 0.01
Mg II 3	...	16.26 ± 0.02
Mn II 1	64.3 ± 3.3	13.70 ± 0.02
Mn II 2	42.9 ± 7.8	13.74 (+0.07, -0.08)
Ge II	30.8 ± 2.3	12.54 ± 0.03
Kr I	10.2 ± 2.4	12.58 (+0.09, -0.11)

Table 7 continued on next page

Table 7 (*continued*)

Line ^b	W_λ (mÅ)	$\log N_a(\text{cm}^{-2})^c$
HD99890 H -35 to 19 km s^{-1}		
H I	...	$21.12 (+0.05, -0.07)$
O I	14.4 ± 3.6	$17.92 (+0.09, -0.12)$
Mg II 1	84.6 ± 0.6	16.19 ± 0.01
Mg II 2	54.5 ± 1.3	16.17 ± 0.01
Mn II 1	60.7 ± 0.7	13.63 ± 0.01
Mn II 2	36.1 ± 1.3	$13.60 (+0.01, -0.02)$
Ge II	26.4 ± 2.0	12.41 ± 0.03
Kr I	4.8 ± 1.9	$12.23 (+0.14, -0.22)$
HD99953 H -24 to 20 km s^{-1}		
H I	...	21.45 ± 0.07
O I	19.6 ± 5.5	$18.07 (+0.11, -0.14)$
Mg II 1	88.4 ± 3.0	16.24 ± 0.02
Mg II 2	63.6 ± 3.0	16.27 ± 0.02
Mn II 1	71.5 ± 7.2	$13.78 (+0.04, -0.05)$
Mn II 2	49.8 ± 3.9	$13.81 (+0.03, -0.04)$
Ge II	48.4 ± 1.9	12.73 ± 0.02
Kr I	10.6 ± 5.7	< 12.75
HD100199 M -27 to 20 km s^{-1}		
H I	...	$21.18 (+0.06, -0.13)$
O I	14.8 ± 3.8	$17.92 (+0.10, -0.13)$
Mg II 1	68.2 ± 3.8	16.04 ± 0.03
Mg II 2	52.6 ± 3.8	$16.13 (+0.03, -0.04)$
Mg II 3	...	16.23 ± 0.04
Mn II 1	59.9 ± 3.8	13.61 ± 0.03
Mn II 2	40.2 ± 7.4	$13.67 (+0.07, -0.09)$
Ge II	41.0 ± 4.6	$12.61 (+0.05, -0.06)$
Kr I	3.7 ± 5.9	< 12.57

Table 7 continued on next page

Table 7 (*continued*)

Line ^b	W_λ (mÅ)	$\log N_a(\text{cm}^{-2})^c$
HD101190 M -34 to 22 km s^{-1}		
H I	...	$21.24 (+0.03, -0.06)$
O I	17.5 ± 2.6	$18.00 (+0.06, -0.07)$
Mg II 1	77.6 ± 1.9	16.09 ± 0.01
Mg II 2	57.4 ± 1.7	16.17 ± 0.01
Mg II 3	...	16.29 ± 0.04
Mn II 1	62.7 ± 3.8	13.64 ± 0.03
Mn II 2	39.8 ± 3.1	13.65 ± 0.03
Ge II	31.5 ± 2.3	12.49 ± 0.03
Kr I	7.7 ± 3.8	$12.45 (+0.17, -0.28)$
HD103779 H -29 to 17 km s^{-1}		
H I	...	21.17 ± 0.05
O I	11.2 ± 3.4	$17.80 (+0.11, -0.16)$
Mg II 1	78.9 ± 1.4	16.14 ± 0.01
Mg II 2	57.5 ± 1.6	16.19 ± 0.01
Mg II 3	...	16.27 ± 0.02
Mn II 1	56.3 ± 4.3	$13.62 (+0.03, -0.04)$
Mn II 2	32.3 ± 6.4	$13.59 (+0.07, -0.09)$
Ge II	27.7 ± 3.7	$12.44 (+0.05, -0.06)$
Kr I	11.4 ± 2.9	$12.62 (+0.10, -0.13)$
HD104705 H -40 to 19 km s^{-1}		
H I	...	$21.15 (+0.06, -0.05)$
O I	12.0 ± 2.0	$17.84 (+0.07, -0.08)$
Mg II 1	83.1 ± 1.1	16.15 ± 0.01
Mg II 2	56.0 ± 1.1	16.17 ± 0.01
Mn II 1	65.4 ± 2.3	13.67 ± 0.02
Mn II 2	44.6 ± 3.9	13.71 ± 0.04
Ge II	36.2 ± 6.2	$12.56 (+0.07, -0.08)$
Kr I	4.7 ± 2.2	$12.24 (+0.16, -0.26)$

Table 7 continued on next page

Table 7 (*continued*)

Line ^b	W_λ (mÅ)	$\log N_a(\text{cm}^{-2})^c$
HD108639 H -32 to 17 km s^{-1}		
H I	...	21.36 (+0.04, -0.03)
O I	22.2 ± 2.2	18.11 (+0.04, -0.05)
Mg II 1	102.6 ± 0.8	16.34 ± 0.01
Mg II 2	75.9 ± 1.1	16.37 ± 0.01
Mg II 3	...	16.41 ± 0.02
Mn II 1	80.6 ± 1.8	13.82 ± 0.01
Mn II 2	61.8 ± 5.3	13.88 ± 0.04
Mn II 3	...	13.97 ± 0.05
Ge II	43.9 ± 1.8	12.66 ± 0.02
Kr I	8.5 ± 1.4	12.49 (+0.07, -0.08)
HD109399 H -32 to 27 km s^{-1}		
H I	...	21.11 (+0.05, -0.06)
O I	8.4 ± 2.9	17.69 (+0.12, -0.17)
Mg II 1	58.1 ± 1.6	15.95 ± 0.01
Mg II 2	41.8 ± 2.3	16.01 ± 0.02
Mg II 3	...	16.09 ± 0.02
Mn II 1	49.8 ± 2.9	13.54 (+0.02, -0.03)
Ge II	22.2 ± 2.9	12.34 (+0.05, -0.06)
Kr I	6.6 ± 3.0	12.38 (+0.16, -0.25)
HD111934 H -34 to 16 km s^{-1}		
H I	...	21.32 (+0.06, -0.14)
O I	15.5 ± 6.4	17.96 (+0.14, -0.22)
Mg II 1	87.7 ± 3.8	16.23 ± 0.02
Mg II 2	73.0 ± 3.7	16.33 ± 0.02
Mg II 3	...	16.45 (+0.05, -0.04)
Mn II 1	83.7 ± 11.5	13.82 (+0.06, -0.07)
Mn II 2	54.0 ± 12.2	13.83 (+0.09, -0.11)
Ge II	43.9 ± 2.3	12.67 ± 0.02
Kr I	11.1 ± 8.2	< 12.84

Table 7 continued on next page

Table 7 (*continued*)

Line ^b	W_λ (mÅ)	$\log N_a(\text{cm}^{-2})^c$
HD114886 H -45 to 17 km s^{-1}		
H I	...	21.34 (+0.06, -0.05)
O I	19.0 ± 5.4	18.05 (+0.11, -0.14)
Mg II 1	102.6 ± 3.3	16.28 (+0.01, -0.02)
Mg II 2	66.8 ± 2.6	16.28 ± 0.02
Mn II 1	77.2 ± 3.7	13.76 ± 0.02
Mn II 2	50.9 ± 4.8	13.78 ± 0.04
Ge II	50.6 ± 2.4	12.72 ± 0.02
Kr I	8.3 ± 4.0	12.49 (+0.16, -0.26)
HD115071 H -40 to 17 km s^{-1}		
H I	...	21.39 (+0.04, -0.09)
O I	26.0 ± 3.3	18.20 (+0.05, -0.06)
Mg II 1	90.6 ± 1.4	16.27 ± 0.01
Mg II 2	67.5 ± 1.3	16.31 ± 0.01
Mg II 3	...	16.36 ± 0.02
Mn II 1	64.3 ± 2.1	13.73 (+0.01, -0.02)
Mn II 2	56.3 ± 3.1	13.85 (+0.02, -0.03)
Mn II 3	...	13.96 ± 0.04
Ge II	49.7 ± 1.7	12.74 ± 0.01
Kr I	9.8 ± 2.0	12.56 (+0.08, -0.10)
HD115455 H -46 to 17 km s^{-1}		
H I	...	21.38 (+0.05, -0.09)
O I	29.2 ± 6.9	18.24 (+0.09, -0.12)
Mg II 1	96.5 ± 2.3	16.29 ± 0.01
Mg II 2	70.4 ± 2.2	16.32 ± 0.01
Mg II 3	...	16.44 (+0.03, -0.02)
Mn II 1	75.0 ± 7.0	13.77 ± 0.04
Mn II 2	41.7 ± 4.9	13.73 (+0.04, -0.05)
Ge II	44.3 ± 2.5	12.70 ± 0.02
Kr I	18.8 ± 12.0	< 13.03

Table 7 continued on next page

Table 7 (*continued*)

Line ^b	W_λ (mÅ)	$\log N_a(\text{cm}^{-2})^c$
HD116781 H -35 to 17 km s^{-1}		
H I	...	21.21 ± 0.05
O I	17.8 ± 3.3	$18.01 (+0.07, -0.09)$
Mg II 1	74.1 ± 2.5	$16.11 (+0.01, -0.02)$
Mg II 2	49.4 ± 2.8	$16.12 (+0.02, -0.03)$
Mn II 1	60.7 ± 2.8	13.65 ± 0.02
Mn II 2	40.0 ± 4.6	13.66 ± 0.05
Ge II	31.1 ± 2.7	12.49 ± 0.04
Kr I	3.7 ± 5.1	< 12.52
HD116852 H -47 to 27 km s^{-1}		
H I	...	20.96 ± 0.04
O I	9.9 ± 2.7	$17.74 (+0.10, -0.13)$
Mg II 1	54.6 ± 1.1	15.90 ± 0.01
Mg II 2	35.1 ± 1.2	15.92 ± 0.01
Mn II 1	42.1 ± 2.2	13.45 ± 0.02
Mn II 2	29.1 ± 1.6	13.50 ± 0.02
Mn II 3	...	13.59 ± 0.03
Ge II	15.2 ± 1.4	12.17 ± 0.04
Kr I	3.7 ± 2.4	< 12.33
HD122879 H -36 to 18 km s^{-1}		
H I	...	$21.31 (+0.06, -0.05)$
O I	19.0 ± 2.2	18.04 ± 0.05
Mg II 1	89.2 ± 0.4	16.20 ± 0.01
Mg II 2	60.8 ± 0.7	16.22 ± 0.01
Mn II 1	70.6 ± 1.6	13.73 ± 0.01
Mn II 2	45.7 ± 15.4	$13.75 (+0.12, -0.17)$
Ge II	40.4 ± 2.1	12.62 ± 0.02
Kr I	9.8 ± 1.5	$12.55 (+0.06, -0.07)$

Table 7 continued on next page

Table 7 (*continued*)

Line ^b	W_λ (mÅ)	$\log N_a(\text{cm}^{-2})^c$
HD124314 H -30 to 17 km s^{-1}		
H I	...	$21.41 (+0.06, -0.04)$
O I	26.5 ± 1.4	18.21 ± 0.02
Mg II 1	96.8 ± 1.2	16.29 ± 0.01
Mg II 2	70.6 ± 1.2	16.32 ± 0.01
Mg II 3	...	$16.37 (+0.02, -0.01)$
Mn II 1	78.7 ± 1.9	13.81 ± 0.01
Mn II 2	55.5 ± 2.1	13.85 ± 0.02
Mn II 3	...	13.93 ± 0.03
Ge II	51.0 ± 1.7	12.74 ± 0.02
Kr I	20.0 ± 2.8	$12.87 (+0.06, -0.07)$
HD124979 H -32 to 16 km s^{-1}		
H I	...	21.27 ± 0.09
O I	15.0 ± 3.2	$17.94 (+0.08, -0.10)$
Mg II 1	93.7 ± 1.8	16.30 ± 0.01
Mg II 2	67.4 ± 1.9	16.32 ± 0.01
Mn II 1	89.3 ± 2.9	13.88 ± 0.02
Mn II 2	56.6 ± 3.6	13.87 ± 0.03
Ge II	43.0 ± 3.7	12.67 ± 0.04
Kr I	6.6 ± 4.6	< 12.60
HD137595 H -45 to 16 km s^{-1}		
H I	...	$21.00 (+0.06, -0.07)$
H I sc	...	$20.97 (+0.06, -0.08)$
O I	13.7 ± 1.9	$17.91 (+0.05, -0.06)$
Mg II 1	39.3 ± 2.2	15.74 ± 0.02
Mg II 2	22.2 ± 3.8	$15.71 (+0.07, -0.08)$
Mn II 1	36.2 ± 2.7	13.38 ± 0.03
Mn II 2	26.5 ± 2.6	13.46 ± 0.04
Mn II 3	...	13.56 ± 0.05
Ge II	18.3 ± 1.9	12.28 ± 0.04
Kr I	4.5 ± 1.1	$12.23 (+0.09, -0.11)$

Table 7 continued on next page

Table 7 (*continued*)

Line ^b	W_λ (mÅ)	$\log N_a(\text{cm}^{-2})^c$
HD144965 H -14 to 16 km s^{-1}		
H I	...	21.07 (+0.05, -0.13)
H I sc	...	20.97 (+0.09, -0.30)
O I	12.1 ± 2.1	17.89 (+0.06, -0.08)
Mg II 1	22.8 ± 1.2	15.57 ± 0.02
Mg II 2	16.0 ± 1.5	15.61 ± 0.04
Mn II 1	17.3 ± 2.4	13.10 (+0.05, -0.06)
Mn II 2	13.9 ± 4.1	13.20 (+0.11, -0.14)
Ge II	14.9 ± 1.6	12.22 ± 0.04
Kr I	6.3 ± 1.4	12.38 (+0.08, -0.10)
HD147888 H -33 to -1 km s^{-1}		
H I	...	21.73 (+0.06, -0.05)
H I sc	...	21.68 (+0.08, -0.19)
O I	20.5 ± 1.1	18.21 ± 0.02
Mg II 1	27.8 ± 0.6	15.72 ± 0.01
Mg II 2	21.0 ± 0.5	15.82 ± 0.01
Mg II 3	...	16.00 (+0.03, -0.02)
Mn II 1	33.2 ± 1.3	13.45 ± 0.02
Mn II 2	22.3 ± 1.5	13.53 (+0.02, -0.03)
Mn II 3	...	13.77 (+0.06, -0.04)
Ge II	28.3 ± 1.4	12.85 ± 0.07
Kr I	10.4 ± 0.7	12.66 (+0.08, -0.03)
HD148422 M -66 to 22 km s^{-1}		
H I	...	21.24 (+0.09, -0.06)
O I	2.8 ± 21.5	< 18.23
Mg II 1	98.8 ± 7.7	16.23 ± 0.03
Mg II 2	81.4 ± 10.3	16.34 (+0.05, -0.06)
Mg II 3	...	16.47 ± 0.06
Mn II 1	105.8 ± 24.9	13.88 (+0.10, -0.12)
Ge II	27.3 ± 13.9	< 12.54
Kr I	-20.8 ± 13.9	< 12.59

Table 7 continued on next page

Table 7 (*continued*)

Line ^b	W_λ (mÅ)	$\log N_a(\text{cm}^{-2})^c$
HD148937 H -38 to 11 km s^{-1}		
H I	...	$21.48 (+0.06, -0.11)$
O I	41.2 ± 2.9	18.40 ± 0.03
Mg II 1	99.6 ± 2.0	16.29 ± 0.01
Mg II 2	73.4 ± 2.0	16.32 ± 0.01
Mg II 3	...	16.40 ± 0.02
Mn II 1	83.3 ± 5.9	$13.89 (+0.05, -0.06)$
Mn II 2	72.0 ± 7.8	13.99 ± 0.05
Mn II 3	...	14.12 ± 0.07
Ge II	65.3 ± 3.1	12.87 ± 0.02
Kr I	7.5 ± 5.0	< 12.64
HD151805 M -65 to 9 km s^{-1}		
H I	...	21.33 ± 0.05
O I	19.8 ± 3.9	$18.06 (+0.08, -0.09)$
Mg II 1	105.0 ± 4.6	16.22 ± 0.02
Mg II 2	64.9 ± 6.5	$16.21 (+0.04, -0.05)$
Mn II 1	92.9 ± 8.4	13.85 ± 0.04
Mn II 2	60.8 ± 22.2	$13.84 (+0.13, -0.20)$
Ge II	49.2 ± 3.6	12.69 ± 0.03
Kr I	11.2 ± 4.2	$12.62 (+0.13, -0.19)$
HD152249 H -50 to 10 km s^{-1}		
H I	...	21.38 ± 0.07
O I	21.0 ± 4.1	$18.09 (+0.08, -0.09)$
Mg II 1	97.7 ± 2.3	16.26 ± 0.01
Mg II 2	69.3 ± 2.0	16.29 ± 0.01
Mg II 3	...	16.35 ± 0.02
Mn II 1	70.5 ± 7.5	$13.75 (+0.20, -0.05)$
Ge II	47.4 ± 2.4	12.70 ± 0.02
Kr I	12.9 ± 5.1	$12.68 (+0.14, -0.21)$

Table 7 continued on next page

Table 7 (*continued*)

Line ^b	W_λ (mÅ)	$\log N_a(\text{cm}^{-2})^c$
HD152424 H -57 to 14 km s^{-1}		
H I	...	$21.48 (+0.06, -0.07)$
O I	26.1 ± 5.2	$18.21 (+0.08, -0.09)$
Mg II 1	100.9 ± 2.1	16.31 ± 0.01
Mg II 2	71.4 ± 2.6	$16.33 (+0.01, -0.02)$
Mn II 1	102.2 ± 6.8	13.96 ± 0.03
Ge II	51.7 ± 5.1	$12.81 (+0.03, -0.04)$
Kr I	15.7 ± 7.7	$12.78 (+0.17, -0.27)$
HD152590 H -51 to 19 km s^{-1}		
H I	...	$21.37 (+0.07, -0.03)$
O I	19.7 ± 6.5	$18.08 (+0.12, -0.16)$
Mg II 1	82.3 ± 1.4	16.22 ± 0.01
Mg II 2	60.1 ± 1.6	16.25 ± 0.01
Mg II 3	...	16.30 ± 0.02
Mn II 1	61.0 ± 6.6	$13.72 (+0.04, -0.05)$
Mn II 2	44.0 ± 5.7	13.76 ± 0.05
Ge II	35.2 ± 1.2	12.60 ± 0.01
Kr I	11.8 ± 3.8	$12.64 (+0.12, -0.16)$
HD152590 M -63 to 15 km s^{-1}		
H I	...	21.39 ± 0.05
O I	16.2 ± 13.6	< 18.22
Mg II 1	75.9 ± 7.6	16.12 ± 0.04
Mg II 2	54.7 ± 5.7	16.19 ± 0.04
Mg II 3	...	$16.36 (+0.05, -0.04)$
Mn II 1	64.6 ± 19.9	$13.68 (+0.11, -0.14)$
Mn II 2	40.2 ± 10.8	$13.69 (+0.10, -0.13)$
Ge II	49.1 ± 5.8	12.70 ± 0.05
Kr I	13.6 ± 9.6	< 12.91

Table 7 continued on next page

Table 7 (*continued*)

Line ^b	W_λ (mÅ)	$\log N_a(\text{cm}^{-2})^c$
HD156359 M -19 to 24 km s^{-1}		
H I	...	$20.80 (+0.10, -0.06)$
O I	6.6 ± 4.7	< 17.79
Mg II 1	34.1 ± 3.9	15.67 ± 0.05
Mg II 2	27.7 ± 2.9	$15.81 (+0.04, -0.05)$
Mg II 3	...	15.92 ± 0.05
Mn II 1	24.7 ± 9.4	$13.17 (+0.14, -0.21)$
Mn II 2	13.8 ± 9.7	< 13.35
Ge II	11.6 ± 5.0	$12.02 (+0.15, -0.24)$
Kr I	3.3 ± 8.7	< 12.69
HD163522 M -31 to 42 km s^{-1}		
H I	...	$21.14 (+0.08, -0.07)$
O I	8.5 ± 9.1	< 18.00
Mg II 1	92.3 ± 6.2	16.18 ± 0.03
Mg II 2	62.2 ± 5.6	16.21 ± 0.04
Mn II 1	46.0 ± 19.8	$13.50 (+0.14, -0.21)$
Mn II 2	2.4 ± 34.2	< 13.67
Ge II	34.1 ± 5.3	$12.50 (+0.06, -0.07)$
Kr I	6.2 ± 16.1	< 12.96
HD165246 H -59 to 5 km s^{-1}		
H I	...	$21.41 (+0.03, -0.04)$
O I	16.1 ± 1.8	$18.01 (+0.04, -0.05)$
Mg II 1	60.5 ± 1.9	16.05 ± 0.01
Mg II 2	39.9 ± 2.1	16.07 ± 0.02
Mn II 1	41.9 ± 1.8	13.56 ± 0.01
Mn II 2	32.5 ± 0.9	13.65 ± 0.01
Mn II 3	...	13.80 ± 0.03
Ge II	30.4 ± 4.4	$12.55 (+0.05, -0.06)$
Kr I	5.5 ± 1.0	$12.34 (+0.07, -0.08)$

Table 7 continued on next page

Table 7 (*continued*)

Line ^b	W_λ (mÅ)	$\log N_a(\text{cm}^{-2})^c$
HD167402 M -32 to 46 km s^{-1}		
H I	...	$21.13 (+0.05, -0.04)$
O I	8.3 ± 10.8	< 18.04
Mg II 1	88.0 ± 8.8	$16.14 (+0.04, -0.05)$
Mg II 2	66.2 ± 8.2	$16.22 (+0.05, -0.06)$
Mg II 3	...	16.34 ± 0.06
Mn II 1	75.7 ± 15.8	$13.72 (+0.08, -0.10)$
Ge II	33.4 ± 8.6	$12.51 (+0.10, -0.12)$
Kr I	-3.1 ± 13.0	< 12.76
HD168941 M -26 to 37 km s^{-1}		
H I	...	$21.18 (+0.05, -0.07)$
O I	12.2 ± 2.6	$17.84 (+0.08, -0.10)$
Mg II 1	57.2 ± 5.5	15.92 ± 0.04
Mg II 2	40.5 ± 6.2	$15.99 (+0.06, -0.07)$
Mn II 1	47.4 ± 8.2	$13.51 (+0.06, -0.08)$
Mn II 2	25.3 ± 14.0	< 13.57
Ge II	31.7 ± 5.3	$12.50 (+0.06, -0.08)$
Kr I	-2.6 ± 9.5	< 12.62
HD170740 H -26 to 0 km s^{-1}		
H I	...	$21.20 (+0.04, -0.11)$
H I sc	...	$21.09 (+0.06, -0.17)$
O I	15.9 ± 2.1	$18.01 (+0.05, -0.06)$
Mg II 1	31.6 ± 1.7	15.75 ± 0.02
Mg II 2	23.7 ± 1.5	15.82 ± 0.03
Mg II 3	...	15.91 ± 0.04
Mn II 1	23.9 ± 4.3	$13.29 (+0.06, -0.07)$
Mn II 2	11.5 ± 5.8	< 13.21
Ge II	19.2 ± 1.9	12.36 ± 0.04
Kr I	6.9 ± 2.7	$12.43 (+0.14, -0.20)$

Table 7 continued on next page

Table 7 (*continued*)

Line ^b	W_λ (mÅ)	$\log N_a(\text{cm}^{-2})^c$
HD177989 H -23 to 12 km s^{-1}		
H I	...	$20.99 (+0.05, -0.06)$
O I	9.6 ± 1.1	17.75 ± 0.05
Mg II 1	42.1 ± 1.3	15.84 ± 0.01
Mg II 2	26.8 ± 1.2	15.83 ± 0.02
Mn II 1	39.4 ± 1.3	13.44 ± 0.01
Ge II	17.8 ± 1.2	12.24 ± 0.03
Kr I	4.8 ± 0.9	$12.24 (+0.07, -0.09)$
HD178487 M -33 to 23 km s^{-1}		
H I	...	$21.22 (+0.04, -0.10)$
O I	6.2 ± 5.9	< 17.83
Mg II 1	59.2 ± 5.4	15.97 ± 0.04
Mg II 2	40.8 ± 7.8	$16.03 (+0.07, -0.09)$
Mn II 1	54.2 ± 14.6	$13.59 (+0.10, -0.13)$
Ge II	21.4 ± 7.5	$12.38 (+0.11, -0.15)$
Kr I	5.8 ± 7.2	< 12.69
HD179407 M -29 to 22 km s^{-1}		
H I	...	$21.20 (+0.06, -0.10)$
O I	11.3 ± 5.1	$17.82 (+0.15, -0.24)$
Mg II 1	59.4 ± 11.6	$15.98 (+0.07, -0.09)$
Mg II 2	36.9 ± 7.4	$15.99 (+0.08, -0.09)$
Mn II 1	54.6 ± 8.5	$13.60 (+0.06, -0.08)$
Ge II	28.6 ± 10.6	$12.46 (+0.13, -0.19)$
Kr I	7.9 ± 8.5	< 12.78

Table 7 continued on next page

Table 7 (*continued*)

Line ^b	W_λ (mÅ)	$\log N_a(\text{cm}^{-2})^c$
HD185418 H -26 to 6 km s^{-1}		
H I	...	$21.19 (+0.05, -0.04)$
O I	15.6 ± 1.1	18.00 ± 0.03
Mg II 1	43.0 ± 0.8	15.92 ± 0.01
Mg II 2	31.6 ± 1.1	15.96 ± 0.01
Mg II 3	...	$16.03 (+0.02, -0.01)$
Mn II 1	40.2 ± 1.2	13.57 ± 0.01
Mn II 2	30.2 ± 1.8	13.62 ± 0.02
Mn II 3	...	13.72 ± 0.03
Ge II	25.9 ± 0.8	12.49 ± 0.01
Kr I	10.8 ± 0.7	12.61 ± 0.03
HD191877 H -28 to 14 km s^{-1}		
H I	...	21.03 ± 0.05
O I	11.0 ± 2.0	$17.80 (+0.07, -0.09)$
Mg II 1	48.4 ± 1.4	15.92 ± 0.01
Mg II 2	33.5 ± 1.5	15.94 ± 0.02
Mn II 1	39.9 ± 2.2	13.46 ± 0.02
Mn II 2	24.4 ± 4.6	$13.45 (+0.07, -0.09)$
Ge II	20.4 ± 1.9	12.31 ± 0.04
Kr I	2.9 ± 1.0	$12.02 (+0.13, -0.19)$
HD192035 M -40 to 7 km s^{-1}		
H I	...	$21.20 (+0.04, -0.10)$
O I	17.5 ± 2.3	$18.01 (+0.05, -0.06)$
Mg II 1	50.8 ± 3.4	15.90 ± 0.03
Mg II 2	38.7 ± 3.3	15.98 ± 0.04
Mg II 3	...	$16.07 (+0.05, -0.04)$
Mn II 1	39.9 ± 4.7	$13.40 (+0.05, -0.06)$
Mn II 2	23.8 ± 8.6	$13.43 (+0.13, -0.18)$
Ge II	31.1 ± 2.7	12.49 ± 0.04
Kr I	6.1 ± 3.2	< 12.51

Table 7 continued on next page

Table 7 (*continued*)

Line ^b	W_λ (mÅ)	$\log N_a(\text{cm}^{-2})^c$
HD195455 H -28 to 27 km s^{-1}		
H I	...	$20.61 (+0.04, -0.09)$
O I	7.6 ± 2.1	$17.62 (+0.10, -0.14)$
Mg II 1	29.4 ± 1.5	15.58 ± 0.02
Mg II 2	16.9 ± 2.1	$15.57 (+0.05, -0.06)$
Mn II 1	21.6 ± 2.6	$13.10 (+0.05, -0.06)$
Mn II 2	15.0 ± 4.9	$13.18 (+0.12, -0.17)$
Ge II	5.7 ± 1.6	$11.70 (+0.11, -0.14)$
Kr I	6.0 ± 2.3	$12.33 (+0.14, -0.21)$
HD195965 H -29 to 1 km s^{-1}		
H I	...	20.92 ± 0.05
O I	9.5 ± 1.3	$17.74 (+0.05, -0.06)$
Mg II 1	44.5 ± 1.4	$15.86 (+0.01, -0.02)$
Mg II 2	31.6 ± 1.4	15.91 ± 0.02
Mg II 3	...	$16.00 (+0.03, -0.02)$
Mn II 1	36.1 ± 4.5	$13.43 (+0.05, -0.06)$
Mn II 2	27.1 ± 3.8	$13.49 (+0.06, -0.07)$
Ge II	22.1 ± 1.4	12.35 ± 0.03
Kr I	-0.9 ± 1.5	< 11.76
HD198478 H -35 to 5 km s^{-1}		
H I	...	$21.33 (+0.12, -0.13)$
H I sc	...	$21.32 (+0.12, -0.13)$
O I	24.9 ± 7.1	$18.19 (+0.11, -0.15)$
Mg II 1	53.2 ± 4.2	15.99 ± 0.03
Mg II 2	42.7 ± 5.0	16.06 ± 0.05
Mg II 3	...	16.13 ± 0.05
Mn II 1	46.2 ± 5.2	13.62 ± 0.04
Mn II 2	44.8 ± 7.4	$13.77 (+0.07, -0.08)$
Mn II 3	...	$13.83 (+0.09, -0.08)$
Ge II	40.3 ± 3.5	$12.68 (+0.03, -0.04)$
Kr I	6.7 ± 3.6	< 12.56

Table 7 continued on next page

Table 7 (*continued*)

Line ^b	W_λ (mÅ)	$\log N_a(\text{cm}^{-2})^c$
HD198781 H -49 to 0 km s^{-1}		
H I	...	20.93 (+0.07, -0.03)
O I	12.8 ± 1.3	17.87 (+0.04, -0.05)
Mg II 1	40.1 ± 1.0	15.74 ± 0.01
Mg II 2	26.9 ± 2.6	15.79 (+0.04, -0.05)
Mn II 1	36.0 ± 2.0	13.35 ± 0.02
Mn II 2	27.0 ± 3.5	13.45 (+0.05, -0.06)
Ge II	23.0 ± 1.0	12.34 ± 0.02
Kr I	7.3 ± 1.2	12.42 (+0.07, -0.08)
HD201345 H -34 to 8 km s^{-1}		
H I	...	21.00 (+0.05, -0.06)
O I	9.4 ± 1.5	17.72 (+0.06, -0.07)
Mg II 1	56.4 ± 1.0	15.95 ± 0.01
Mg II 2	38.4 ± 0.9	15.98 ± 0.01
Mg II 3	...	16.02 ± 0.02
Mn II 1	42.9 ± 0.9	13.47 ± 0.01
Mn II 2	28.1 ± 1.4	13.49 ± 0.02
Ge II	29.3 ± 3.0	12.44 (+0.04, -0.05)
Kr I	2.9 ± 0.8	12.00 (+0.11, -0.15)
HD202347 H -27 to 7 km s^{-1}		
H I	...	20.94 (+0.06, -0.05)
H I sc	...	20.83 (+0.08, -0.10)
O I	4.6 ± 1.9	17.43 (+0.14, -0.22)
Mg II 1	28.6 ± 1.3	15.63 ± 0.02
Mg II 2	17.3 ± 1.4	15.62 (+0.03, -0.04)
Mn II 1	21.9 ± 3.6	13.18 (+0.06, -0.07)
Mn II 2	15.9 ± 2.3	13.23 (+0.06, -0.07)
Ge II	15.0 ± 1.4	12.16 ± 0.04
Kr I	6.8 ± 1.2	12.38 (+0.07, -0.09)

Table 7 continued on next page

Table 7 (*continued*)

Line ^b	W_λ (mÅ)	$\log N_a(\text{cm}^{-2})^c$
HD203374 H -36 to 14 km s^{-1}		
H I	...	$21.20 (+0.05, -0.04)$
O I	11.8 ± 1.5	17.87 ± 0.05
Mg II 1	67.3 ± 1.3	16.09 ± 0.01
Mg II 2	45.4 ± 2.0	16.09 ± 0.02
Mn II 1	54.6 ± 2.0	13.62 ± 0.02
Mn II 2	33.4 ± 2.2	13.60 ± 0.03
Ge II	36.3 ± 1.3	12.59 ± 0.02
Kr I	8.5 ± 1.1	$12.50 (+0.05, -0.06)$
HD203374 M -40 to 12 km s^{-1}		
H I	...	21.20 ± 0.06
O I	19.7 ± 2.8	$18.06 (+0.06, -0.07)$
Mg II 1	66.9 ± 2.7	16.04 ± 0.02
Mg II 2	43.5 ± 3.0	16.05 ± 0.03
Mn II 1	47.7 ± 4.2	13.54 ± 0.04
Mn II 2	44.9 ± 4.6	$13.70 (+0.04, -0.05)$
Ge II	31.6 ± 2.9	12.50 ± 0.04
Kr I	2.8 ± 3.2	< 12.35
HD206267 H -37 to 4 km s^{-1}		
H I	...	$21.22 (+0.06, -0.04)$
O I	19.7 ± 1.4	18.10 ± 0.03
Mg II 1	57.6 ± 2.3	16.04 ± 0.02
Mg II 2	38.5 ± 1.8	16.03 ± 0.02
Mn II 1	50.9 ± 2.8	13.62 ± 0.02
Mn II 2	31.7 ± 2.3	13.61 ± 0.03
Ge II	33.0 ± 2.2	12.58 ± 0.03
Kr I	10.1 ± 2.1	$12.59 (+0.08, -0.10)$

Table 7 continued on next page

Table 7 (*continued*)

Line ^b	W_λ (mÅ)	$\log N_a(\text{cm}^{-2})^c$
HD206773 H -36 to 4 km s^{-1}		
H I	...	21.09 (+0.07, -0.03)
O I	13.0 ± 1.0	17.89 ± 0.03
Mg II 1	52.9 ± 1.1	15.98 ± 0.01
Mg II 2	35.1 ± 1.2	15.97 ± 0.01
Mn II 1	42.8 ± 1.5	13.53 (+0.01, -0.02)
Ge II	25.9 ± 1.9	12.45 ± 0.03
Kr I	8.3 ± 2.1	12.49 (+0.10, -0.12)
HD207198 H -38 to 0 km s^{-1}		
H I	...	21.28 (+0.07, -0.09)
O I	22.5 ± 1.6	18.15 ± 0.03
Mg II 1	57.7 ± 1.1	16.06 ± 0.01
Mg II 2	41.4 ± 1.0	16.08 ± 0.01
Mn II 1	54.1 ± 2.8	13.66 ± 0.02
Mn II 2	26.4 ± 3.8	13.53 (+0.05, -0.06)
Ge II	34.2 ± 1.3	12.61 ± 0.02
Kr I	12.5 ± 2.3	12.67 (+0.07, -0.09)
HD207308 M -38 to -4 km s^{-1}		
H I	...	21.20 (+0.06, -0.05)
O I	15.2 ± 3.2	17.97 (+0.08, -0.10)
Mg II 1	46.2 ± 2.3	15.88 ± 0.02
Mg II 2	35.3 ± 2.9	15.95 ± 0.04
Mg II 3	...	16.01 ± 0.04
Mn II 1	45.8 ± 3.7	13.55 ± 0.04
Mn II 2	27.3 ± 5.6	13.50 (+0.08, -0.10)
Ge II	30.2 ± 1.9	12.51 ± 0.03
Kr I	5.4 ± 2.6	12.33 (+0.16, -0.25)

Table 7 continued on next page

Table 7 (*continued*)

Line ^b	W_λ (mÅ)	$\log N_a(\text{cm}^{-2})^c$
HD207538 M -36 to 2 km s^{-1}		
H I	...	$21.27 (+0.06, -0.07)$
O I	23.7 ± 2.6	$18.17 (+0.04, -0.05)$
Mg II 1	58.6 ± 3.1	16.02 ± 0.02
Mg II 2	40.7 ± 2.3	$16.05 (+0.02, -0.03)$
Mn II 1	47.6 ± 11.7	$13.56 (+0.09, -0.12)$
Mn II 2	24.7 ± 9.3	$13.48 (+0.13, -0.18)$
Ge II	34.1 ± 4.6	$12.58 (+0.05, -0.06)$
Kr I	7.0 ± 6.9	< 12.70
HD208440 H -37 to 3 km s^{-1}		
H I	...	$21.24 (+0.06, -0.04)$
O I	16.1 ± 1.5	17.98 ± 0.04
Mg II 1	59.9 ± 1.8	16.04 ± 0.01
Mg II 2	35.7 ± 2.7	15.99 ± 0.03
Mn II 1	42.4 ± 2.7	13.50 ± 0.03
Mn II 2	34.8 ± 2.3	13.60 ± 0.03
Mn II 3	...	13.69 ± 0.04
Ge II	31.4 ± 1.3	12.51 ± 0.02
Kr I	5.9 ± 1.5	$12.34 (+0.10, -0.12)$
HD209339 H -32 to 4 km s^{-1}		
H I	...	21.20 ± 0.04
O I	10.9 ± 1.4	17.82 ± 0.05
Mg II 1	52.9 ± 1.1	16.01 ± 0.01
Mg II 2	38.7 ± 1.6	16.05 ± 0.02
Mg II 3	...	$16.11 (+0.03, -0.02)$
Mn II 1	43.6 ± 2.6	$13.55 (+0.02, -0.03)$
Mn II 2	33.5 ± 3.2	13.62 ± 0.04
Mn II 3	...	13.73 ± 0.05
Ge II	28.0 ± 1.4	12.49 ± 0.02
Kr I	7.1 ± 1.3	$12.41 (+0.07, -0.09)$

Table 7 continued on next page

Table 7 (*continued*)

Line ^b	W_λ (mÅ)	$\log N_a(\text{cm}^{-2})^c$
HD210809 H -59 to 9 km s^{-1}		
H I	...	$21.31 (+0.06, -0.05)$
O I	13.4 ± 2.7	$17.88 (+0.08, -0.10)$
Mg II 1	107.3 ± 1.4	16.25 ± 0.01
Mg II 2	80.2 ± 1.3	16.31 ± 0.01
Mg II 3	...	16.39 ± 0.03
Mn II 1	75.5 ± 2.7	13.71 ± 0.02
Mn II 2	53.3 ± 4.1	13.80 ± 0.03
Mn II 3	...	13.96 ± 0.06
Ge II	41.0 ± 3.5	12.59 ± 0.04
Kr I	1.3 ± 5.1	< 12.44
HD210809 M -66 to 9 km s^{-1}		
H I	...	21.30 ± 0.07
O I	14.4 ± 3.9	$17.90 (+0.10, -0.14)$
Mg II 1	105.1 ± 3.8	16.21 ± 0.02
Mg II 2	67.3 ± 3.8	16.21 ± 0.03
Mn II 1	85.7 ± 8.5	$13.76 (+0.04, -0.05)$
Mn II 2	55.6 ± 13.1	$13.79 (+0.09, -0.12)$
Ge II	36.1 ± 6.8	$12.53 (+0.08, -0.09)$
Kr I	13.5 ± 23.2	< 13.16
HD210839 H -44 to 4 km s^{-1}		
H I	...	21.24 ± 0.05
O I	23.7 ± 1.6	18.17 ± 0.03
Mg II 1	61.7 ± 1.1	16.04 ± 0.01
Mg II 2	42.4 ± 1.2	16.05 ± 0.01
Mn II 1	50.4 ± 2.0	13.59 ± 0.02
Mn II 2	31.6 ± 1.8	13.58 ± 0.02
Ge II	39.7 ± 2.7	12.64 ± 0.03
Kr I	-0.2 ± 5.8	< 12.45

Table 7 continued on next page

Table 7 (*continued*)

Line ^b	W_λ (mÅ)	$\log N_a(\text{cm}^{-2})^c$
HD218915 H -69 to 10 km s^{-1}		
H I	...	21.20 (+0.07, -0.06)
O I	8.8 ± 2.8	17.72 (+0.11, -0.15)
Mg II 1	82.6 ± 1.6	16.12 ± 0.01
Mg II 2	57.7 ± 1.5	16.16 ± 0.01
Mg II 3	...	16.22 ± 0.02
Mn II 1	60.2 ± 4.3	13.60 ± 0.03
Mn II 2	36.4 ± 4.4	13.59 ± 0.05
Ge II	27.6 ± 3.3	12.43 ± 0.05
Kr I	-2.0 ± 7.7	< 12.53
HD219188 H -20 to 10 km s^{-1}		
H I	...	20.72 (+0.07, -0.05)
O I	3.6 ± 0.7	17.30 (+0.08, -0.10)
Mg II 1	25.8 ± 0.4	15.59 ± 0.01
Mg II 2	18.4 ± 0.6	15.65 ± 0.01
Mg II 3	...	15.72 ± 0.02
Mn II 1	20.1 ± 0.9	13.10 ± 0.02
Ge II	11.2 ± 1.0	12.02 ± 0.04
Kr I	2.5 ± 0.7	11.95 (+0.10, -0.13)
HD220057 H -20 to 1 km s^{-1}		
H I	...	21.12 (+0.09, -0.10)
H I sc	...	20.95 (+0.14, -0.23)
O I	9.5 ± 1.2	17.76 (+0.05, -0.06)
Mg II 1	25.8 ± 1.0	15.62 ± 0.02
Mg II 2	18.5 ± 0.9	15.68 ± 0.02
Mg II 3	...	15.80 (+0.04, -0.02)
Mn II 1	22.4 ± 1.6	13.21 ± 0.03
Mn II 2	19.5 ± 1.8	13.35 ± 0.04
Mn II 3	...	13.44 ± 0.05
Ge II	15.0 ± 1.1	12.22 ± 0.03
Kr I	4.9 ± 1.2	12.26 (+0.09, -0.12)

Table 7 continued on next page

Table 7 (*continued*)

Line ^b	W_λ (mÅ)	$\log N_a(\text{cm}^{-2})^c$
HD224151 H -61 to 6 km s^{-1}		
H I	...	21.35 (+0.05, -0.08)
O I	19.2 ± 3.6	18.06 (+0.07, -0.09)
Mg II 1	106.6 ± 2.5	16.30 ± 0.01
Mg II 2	70.8 ± 3.0	16.29 ± 0.02
Mn II 1	75.3 ± 4.5	13.75 ± 0.03
Mn II 2	48.1 ± 9.3	13.76 (+0.07, -0.09)
Ge II	40.7 ± 3.8	12.65 ± 0.04
Kr I	9.0 ± 5.7	< 12.71
HDE232522 H -72 to 9 km s^{-1}		
H I	...	21.12 (+0.04, -0.05)
O I	18.1 ± 6.5	18.02 (+0.13, -0.19)
Mg II 1	77.9 ± 3.1	16.15 (+0.01, -0.02)
Mg II 2	52.9 ± 2.8	16.16 ± 0.02
Mn II 1	58.3 ± 5.6	13.61 ± 0.04
Ge II	28.2 ± 2.0	12.45 ± 0.03
Kr I	4.4 ± 2.7	< 12.40
HDE303308 H -51 to 24 km s^{-1}		
H I	...	21.41 (+0.03, -0.08)
Mg II 1	105.7 ± 3.1	16.31 ± 0.01
Mg II 2	76.6 ± 2.6	16.34 ± 0.01
Mg II 3	...	16.39 ± 0.02
Mn II 1	143.5 ± 2.3	14.13 ± 0.01
Ge II	48.3 ± 3.7	12.70 ± 0.03
Kr I	9.1 ± 3.8	12.53 (+0.14, -0.22)

Table 7 continued on next page

Table 7 (*continued*)

Line ^b	W_λ (mÅ)	$\log N_a(\text{cm}^{-2})^c$
HDE308813 M -70 to 28 km s^{-1}		
H I	...	21.20 (+0.06, -0.04)
O I	11.2 ± 3.7	17.81 (+0.12, -0.16)
Mg II 1	87.3 ± 7.0	16.12 (+0.03, -0.04)
Mg II 2	58.5 ± 8.5	16.16 (+0.06, -0.07)
Mn II 1	63.7 ± 6.5	13.62 (+0.04, -0.05)
Mn II 2	41.0 ± 8.8	13.67 (+0.08, -0.10)
Ge II	35.5 ± 3.3	12.53 ± 0.04
Kr I	15.4 ± 5.0	12.74 (+0.12, -0.17)

^aThe subheadings list the name of the star, the observation mode [H = high-resolution mode (E140H), M = medium-resolution mode (E140M)], and the endpoints v_1 and v_2 for the heliocentric velocities that span the integration intervals for equivalent widths W_λ and apparent column densities N_a .

^bFor the heavy elements, the transitions that match the entries here are listed in Table 3. If the numeral 3 follows an ion, it means that a correction for line saturation needed to be applied. See Section 3.1 for details. The entry “H I” refers to a direct measurement of the Ly α absorption, whereas for the few cases that needed a correction for stellar Ly α absorption “H I sc” shows the modified value for $\log N(\text{H I})$.

^cSee Eq. 5.

^dNot included in the study of element abundance behaviors because no *FUSE* observations that revealed H₂ column densities are available for this star. The outcomes for H I and heavy elements are shown for the benefit of other investigations that could make use of these results.